ISSN 2320 - 9569

International Journal of Emerging Trends in Electrical and Electronics (IJETEE)

Volume 4, June Issue.

(Online Journal)

Published by

Institute of Research in Engineering & Technology (IRET)

Nagulapalli, Visakhapatnam, Andhrapradesh, India-531001

(www.iieee.co.in)

Computer-Aided Noise modeling, analysis and optimization of a SiGe HBT based Input Buffer

Santosh Kumar Patnaik

Abstract: This article presents the computer aided noise modeling, analysis and optimization of an Input Buffer designed using SiGe heterojunction bipolar transistor (HBT), intended to be used in a high speed Track and Hold Amplifier (THA). This is done by noise matrix manipulation using MATLAB programme. This helps in better understanding the noise involvement with the circuit. Direct parameter extraction technique is used to obtain all the extrinsic and intrinsic parameters of the SiGe HBT. Extracted parameters are then used in the MATLAB programme to obtain the input referred noise voltage of the Input Buffer. The programming involves in breaking the small-signal equivalent circuit of the Input Buffer including the noise sources into many smaller blocks. These smaller blocks may either contain a voltage control current source (VCCS), a resistor, or a capacitor. To get the final output, these blocks are combined either in parallel, or in series, or in cascade (chain) configuration depending on how these parameters are connected in the circuit. Here Z, Y, and ABCD-parameters are used to do the matrix operation. Also, parameter conversions are required when two blocks of different configurations are combined. The validity of the results obtained from the MATLAB programme is done after comparing them with the simulated results obtained through SPICE. Both the results are in good agreement with each other.

Keywords: SiGe, HBT, ADC, SNDR, THA, Input Buffer, SEF

I. INTRODUCTION

The study of noise in electronic circuit is important because it represents a lower limit to the size of the electrical signal that can be processed by a circuit without significant deterioration in signal quality. Noise also results in an upper limit to the useful gain of an amplifier. In an electronic circuit, resistors, transistors, conductors etc. are the prime cause of noise. There are many types of noise which are involved with the electronic components out of which shot noise and thermal noise are the predominant noises [1].

For any electronic circuit, noise calculation can be done using either nodal analysis or mesh analysis with the help of Kirchhoff's voltage law or current law respectively. This method is very simple as long as the circuit is small. With the increase in the number of nodes or meshes in the circuit, this method becomes complicated and a tedious process is required to get a mathematical noise model of the circuit [1]. Noise matrix is used to overcome this problem and to calculate the overall noise of the electronic circuit in terms of input referred noise voltage considering the noise associated with each component present inside the electronic circuit.

Santosh Kumar Patnaik is working as an Associative Professor in the Department of ECE, National Institute of Science and Technology, Berhampur, Odisha, India. Email:skpatnaik@rediffmail.com.

A specific architecture along with Signal-to-Noise and Distortion Ratio (SNDR) plays an important role in determining the speed and resolution of an Analog-to-Digital Converter (ADC)[2]. High speed and moderate resolution ADCs are essential in the areas of data acquisition, satellite communication, radar processing, sampling oscilloscopes, high-density disk drives etc. For designing high speed ADCs, HBTs are preferred because of its high f_t and linearity [3] [4]. On the other hand, to improve the resolution, it is important to increase the SNDR of the ADC [2]. This improvement in SNDR can be started at the very first block of an ADC which is a THA. So, if the SNDR of a THA is improved, its resolution will also improve. This improvement in resolution of THA improves the resolution of the ADC.

A THA consists of three main blocks: an Input Buffer, a Switch and an Output Buffer [2] [5] [6] as shown in Fig. 1.

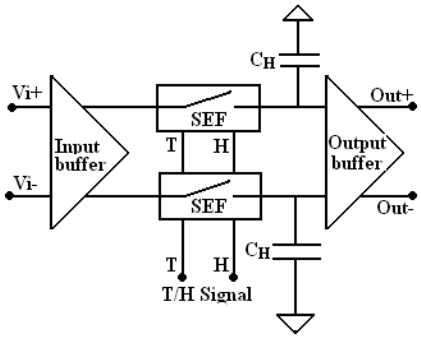

Figure 1: Block diagram of a THA

A Switch is used to do the sampling. It can be implemented using an emitter follower, popularly known as Switched Emitter Follower (SEF). Input Buffer is used to keep the SEF isolated from the input signal and Output Buffer acts as an intermediate block between THA and rest of the ADC. The Input Buffer used for our THA is a differential amplifier having unity gain. To improve the resolution of the THA, its SNDR must be kept as low as possible. Out of these three blocks the noise and distortion level of Input Buffer has to be minimized to allow the THA to have a good resolution as it is exposed directly to the input signal.

In this article, the noise behavior of an Input Buffer has been explored using computer-aided noise modeling. Noise analysis has been done to find out the input referred noise voltage of the Input Buffer designed with SiGe HBT with a view to use it in our designed THA which will operate at 3 GSample/s and the resolution should not be less than 10-bit. Intrinsic and extrinsic parameters of SiGe HBT required in the noise modeling are obtained through direct parameter extraction method from the measured S-parameters [7]-[20].

The extraction of parameters has been done in a frequency range of 1-50 GHz. Further, the input referred noise voltage level has been optimized using mathematical noise modeling.

This article has been arranged in the following manner. Section II presents the steps to obtain the input referred noise voltage of the Input Buffer. Section III describes the extraction of intrinsic and extrinsic parameters of SiGe HBT. In Section VI, computer-aided noise modeling is illustrated. Results and discussion are given in Section V. Finally Section VI concludes the article.

II. STEPS TO CALCULATE INPUT REFERRED NOISE VOLTAGE OF INPUT BUFFER

1. A schematic of THA circuit using SiGe HBT is implemented using SPICE [2] [5] [6].
2. Intrinsic and extrinsic parameters for SiGe HBT involved in the circuit are extracted using S-parameters [7]-[20].
3. Small-signal noise model by using noise voltages and currents for the differential Input Buffer is considered [1] [21]-[23].
4. Noise model is separated into discrete components and the electrical noise matrix is formed for each component [24]-[26].
5. Noise matrix of discrete components are combined as per the small-signal noise model given in step 4, using MATLAB programme [24]-[26].
6. Final output of MATLAB programme is multiplied with √2 to get the input referred noise voltage of the Input Buffer [1].
7. With this input referred noise voltage Fourier analysis is done to get the SNDR of the THA [2].
8. Optimization of the noise is done using mathematical noise modeling [27].
9. After optimization of the noise, steps 3 to 6 are repeated to obtain SNDR of the THA.
10. Resolution of the THA is calculated by comparing the results of steps 6 and 8 [2].

III. EXTRACTION OF INTRINSIC AND EXTRINSIC PARAMETERS OF SIGE HBT

For extracting the parameters of SiGe HBT direct parameter extraction method is preferred over numerical optimization because of its uniqueness and efficiency. For this purpose, hybrid-π equivalent model is used. The small-signal equivalent model of the SiGe HBT is shown in Fig. 2 [7]-[20].

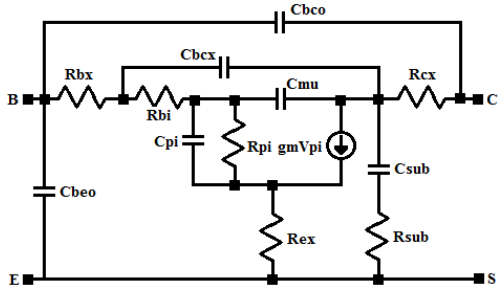

Figure 2: Small-signal equivalent circuit model for a SiGe HBT

To extract the extrinsic resistances, HBT must be operated in over driven I_B bias condition. Under this condition the equivalent small-signal circuit reduces to a resistive network. The extrinsic resistances can be described by the Z-parameter of the circuit employing following equations [12];

$$R_{bx} = real(Z_{11} - Z_{12}) \quad (1)$$

$$R_{ex} = real(Z_{12}) \quad (2)$$

$$R_{cx} = real(Z_{22} - Z_{21}) \quad (3)$$

The parasitic capacitance extraction is done under cold mode operation [12]. The equivalent circuit under this condition reduces to a capacitive network. The Y-parameters for this equivalent circuit are;

$$\omega\left(C_{pi} + C_{beo}\right) = \mathrm{Im}(Y_{11} + Y_{12}) \quad (4)$$

$$\omega\left(C_{mu} + C_{bcx} + C_{bco}\right) = \mathrm{Im}(-Y_{12}) \quad (5)$$

To extract the intrinsic resistors and capacitors, the SiGe HBT ($0.21\text{x}0.84\mu m^2$) should be connected in cutoff mode (V_{BE} = 0 V with forward collector voltage V_{CE} = 3 V). With this mode the small-signal equivalent model of the HBT looks as shown in Fig. 3.

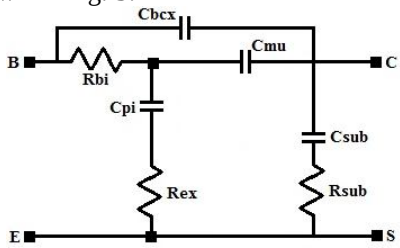

Figure 3: Small-signal equivalent circuit model for SiGe HBT biased in the cut off mode

The Y-parameters, obtained from the reduced equivalent circuit shown in Fig. 3, are given below [13];

$$Y_{11} = j\omega C_{bcx} + \frac{j\omega(C_{mu} + C_{pi})}{1 + j\omega R_{bi}(C_{mu} + C_{pi})} \quad (6)$$

$$Y_{12} = Y_{21} = -j\omega C_{bcx} - \frac{j\omega C_{mu}}{1 + j\omega R_{bi}(C_{mu} + C_{pi})} \quad (7)$$

$$Y_{22} = Y_{sub} + j\omega C_{bcx} + \frac{j\omega C_{mu}(1 + j\omega R_{bi} C_{pi})}{1 + j\omega R_{bi}(C_{mu} + C_{pi})} \quad (8)$$

From (6) and (7), R_{bi} and C_{pi} can be obtained as

$$R_{bi} = \mathrm{Re}\left[\frac{1}{Y_{11} + Y_{12}}\right] \frac{\mathrm{Re}(Y_{11} + Y_{12})}{\mathrm{Re}(Y_{11})} \quad (9)$$

$$\omega C_{pi} = -\mathrm{Im}\left(\frac{1}{Y_{11} + Y_{12}}\right)^{-1} \quad (10)$$

Fig. 4 shows the plot of extracted R_{bi} and C_{pi} with respect to frequency.

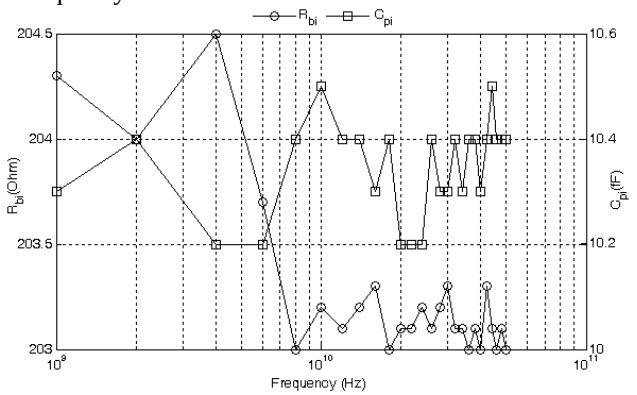

Figure 4: Plot of R_{bi} and C_{pi} vs. frequency

To extract the rest of the intrinsic parameters, HBT should operate in forward bias mode. Fig. 5 shows S-parameter data from the forward mode SiGe HBT in the frequency range of 1-50 GHz.

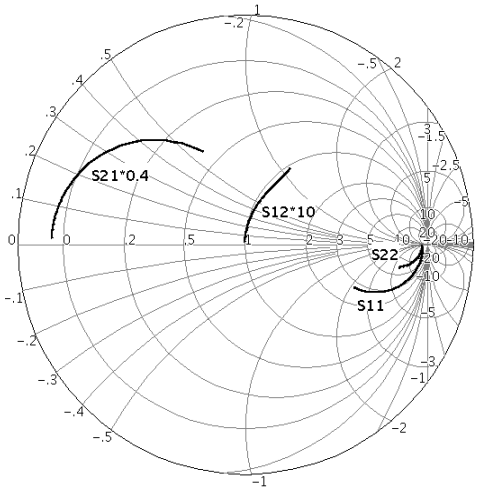

Figure 5: S-parameter data from the forward bias mode SiGe HBT in the frequency range of 1-50 GHz (V_{CE} = 3 V, I_C = 1.29 mA, V_{BE} = 450 mV)

The small-signal equivalent circuit of SiGe HBT under this forward bias mode is shown in Fig. 6 [13].

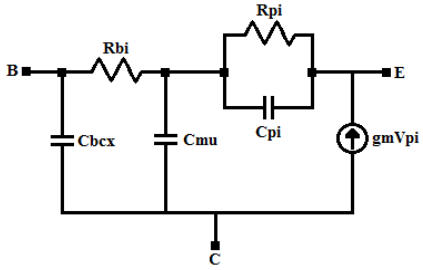

Figure 6: Small-signal equivalent circuit of SiGe HBT in forward bias mode

The ABCD-parameters for this equivalent circuit are;

$$A_{11} = 1 + R_{bi} Y_{bc} \quad (11)$$

$$A_{12} = \frac{1}{g_m + Y_{pi}}(1 + R_{bi} Y_{bc} + R_{bi} Y_{pi}) \quad (12)$$

$$A_{21} = Y_{bc} + Y_{ex} + R_{bi} Y_{bc} Y_{ex} \quad (13)$$

$$A_{22} = \frac{1}{g_m + Y_{pi}}\left(Y_{ex}\left(1 + R_{bi} Y_{bc} + R_{bi} Y_{pi}\right) + Y_{bc} + Y_{pi}\right) \quad (14)$$

where $g_m = g_{mo} \exp(-j\omega\tau)$, $Y_{pi} = \frac{1}{R_{pi}} + j\omega C_{pi}$,

$Y_{bc} = j\omega C_{mu}$, $Y_{ex} = j\omega C_{bcx}$

Utilizing (11)-(14), one can obtain;

$$\mathrm{Re}\left(\frac{A_{12}}{A_D}\right) = \sim R_{bi}\left(1 + \frac{C_{mu}}{C_{pi}}\right) \quad (15)$$

where $A_D = \left(A_{11} A_{22} - A_{12} A_{21}\right)$

Using the ABCD-parameters presented in (11)-(15), the intrinsic parameters of the SiGe HBT are calculated as given below;

$$\mathrm{Im}\left(A_{11}\right) = \omega R_{bi} C_{mu} \quad (16)$$

$$\mathrm{Im}\left(\frac{A_{11}}{A_{21}}\right) \sim \frac{-1}{\omega\left(C_{mu} + C_{bcx}\right)} \quad (17)$$

$$\frac{1}{R_{pi}} = \mathrm{Re}\left(\frac{A_{11}A_D}{A_{12} - A_D R_{bi}}\right) \tag{18}$$

$$g_m = \left(\frac{1 - A_D}{A_D}\right) Y_{pi} \tag{19}$$

$$g_{mo} = \sqrt{\mathrm{Re}(g_m)^2 + \mathrm{Im}(g_m)^2} \tag{20}$$

$$\tau = -\tan^{-1}\left(\frac{\mathrm{Im}(g_m)}{\mathrm{Re}(g_m)}\right) \times \frac{1}{\omega} \tag{21}$$

Fig. 7 shows the plot of R_{pi} and g_{mo} versus frequency.

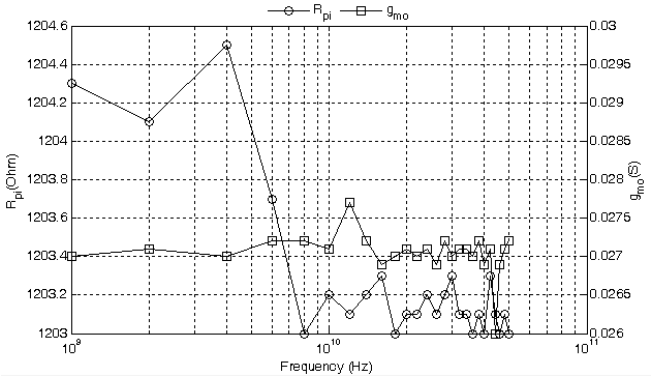

Figure 7: Plot of R_{pi} and g_{mo} vs. frequency

The extracted parameters with values are listed in Table 1.

Table 1: Extracted parameters of the SiGe HBT

Extracted Bias-Independent Parameters		Extracted Bias-Dependent Parameters (V_{CE} = 3V, I_C = 1.29mA, V_{BE} = 450mV)	
Parameter	Extracted Value	Parameter	Extracted Value
R_{bx}	54Ω	R_{bi}	203.2Ω
R_{cx}	6Ω	R_{pi}	1203.3Ω
R_{ex}	20Ω	C_{pi}	10.4fF
C_{beo}	0.34fF	C_{mu}	70fF
C_{bco}	0.62fF	C_{bcx}	97fF
		g_{mo}	28mS
		C_{sub}	29.31fF
		R_{sub}	2.31KΩ

IV. COMPUTER-AIDED NOISE MODELING

Fig. 8 shows the circuit schematic of the Input Buffer which is a differential amplifier with unity gain. Transistors Q1 and Q2 are the driver transistors and transistors Q3 and Q4 are used in diode configuration to overcome the V_{BE} modulation in the driver transistors Q1 and Q2, hence improves the linearity of the Input Buffer. In a differential amplifier, if both sides are considered symmetrical then the total input referred noise voltage of one side will be $\sqrt{2}$ times the input referred noise voltage of the differential amplifier [1].

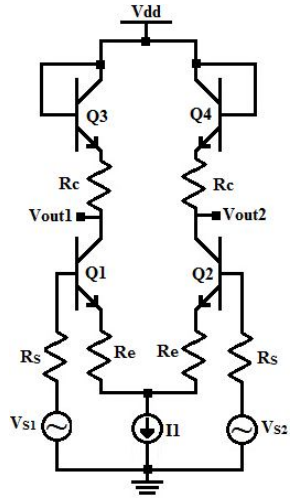

Figure 8: Circuit schematic of an Input Buffer

Using this concept, the electrical noise model for one side of the Input Buffer is drawn in Fig. 9 [1] [21]-[23].

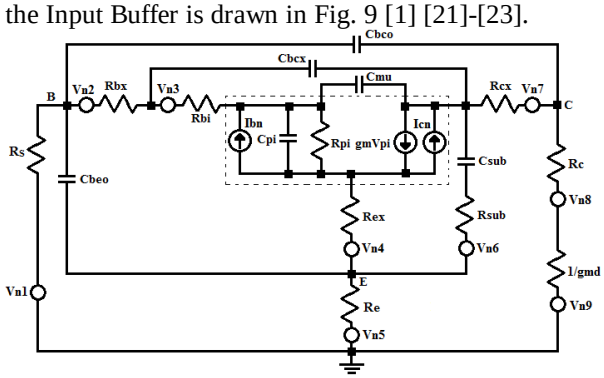

Figure 9: Electrical noise model representation of one side of Input Buffer

Voltages V_{n1}-V_{n9} are the thermal noise voltages associated with all the resistors. Currents I_{bn} and I_{cn} are the shot noise currents present in the HBT. The block present inside the dashed box shown in Fig. 9 is a VCCS.

Now, using noise correlation matrix, total input referred noise voltage of the electrical noise model, shown in Fig. 9, can be calculated. For obtaining the noise matrix, the electrical noise model is separated into several blocks containing VCCS, resistors and capacitors. In the noise matrix, the series, parallel and cascade combinations are written by using Z, Y and ABCD-parameter, respectively. All the combinations, conversion between parameters and matrix operations are done using MATLAB [24]-[26].

Tables 2(a)-(c) indicate the noise matrices used in MATLAB to determine the input referred noise voltage of the Input Buffer.

Table 2(a) Y-matrix for VCCS

VCCS_11 = (j.*omega.*Cpi)+(1/Rpi);	C_VCCS_11 = q*I_B.*ones(size(f));
VCCS_12 = zeros(size(f));	C_VCCS_12 = zeros(size(f));

VCCS_21 = g_{mo}.*ones(size(f));	C_VCCS_21 = zeros(size(f));
VCCS_22 = zeros(size(f));	C_VCCS_22 = q*I_C.*ones(size(f));

where "omega" is the angular frequency, "f" is the frequency of operation, "q" is the charge of an electron, "g_{mo}" is the transconductance of the circuit, "I_B" is the current flowing through the base of HBT, "I_C" is the current flowing through the collector of HBT. In Table 2(a), the content of the second column represents the noise correlation matrix associated with the matrix of the first column.

Table 2(b) Y-matrix for a Resistor

R_11 = (1/R).*ones(size(f));	C_R_11 = 2.*K.*T.*real(R_11);
R_12 = -(1/R).*ones(size(f));	C_R_12 = 2.*K.*T.*real(R_12);
R_21 = -(1/R).*ones(size(f));	C_R_21 = 2.*K.*T.*real(R_21);
R_22 = (1/R).*ones(size(f));	C_R_22 = 2.*K.*T.*real(R_22);

where "K" is the Boltzmann's constant and "T" is the temperature of operation.

Similarly for a Z-matrix of a resistor, R_11-R_22 will be "R" multiplied with "ones(size(f))" and the correlation matrix is the same as in Y-matrix.

Table 2(c) Y-matrix for a Capacitor

C_11 = j.*omega.*C;	C_C_11 = zeros(size(f));
C_12 = -j.*omega.*C;	C_C_12 = zeros(size(f));
C_21 = -j.*omega.*C;	C_C_21 = zeros(size(f));
C_22 = j.*omega.*C;	C_C_22 = zeros(size(f));

In case of a Z-matrix for a capacitor, C_11-C_22 will be "1/j.*omega.*C" and the correlation matrix is the same as in Y-matrix. Contents of the second column of Tables 2(b) and 2(c) represent the noise correlation component associated with the content of the first column. Using the matrices given in Table 2, a MATLAB programme has been written to find out the input referred noise voltage of half circuit of the Input Buffer. Multiplying the final output of MATLAB programme with a factor of $\sqrt{2}$, the total input referred noise voltage of the Input Buffer can be obtained. The MATLAB programme flow is given below;

1. Xa = VCCS [Y] + C_{mu} [Y] - Parallel Combination [No conversion]

2. Xb = Xa [Y] + R_{ex} [Z] - Series Combination [Xa is converted from Y to Z]

3. Xc = Xb [Z] + R_{bi} [Y] - Chain Combination [Xb is converted from Z to A and R_{bi} is converted from Y to A]

4. Xd = Xc [A] + Xy [Z] - Chain Combination [Xy is converted from Z to A]

   4.1. Xy = C_{sub} [Z] + R_{sub} [Z] - Series Combination [No conversion]

5. Xe = Xd [A] + C_{bcx} [Y] - Parallel Combination [Xd is converted from A to Y]

6. Xf = R_{bx} [Y] + Xe [Y] - Chain Combination [R_{bx} and Xe both are converted from Y to A]

7. Xg = Xf [A] + R_{cx} [Y] - Chain Combination [R_{cx} is converted from Y to A]

8. Xh = Xg [A] + C_{bco} [Y] – Parallel Combination [Xg is converted from A to Y]

9. Xi = C_{beo} [Z] + Xh [Y] – Chain Combination [C_{beo} is converted from Z to A]

10. Xj = Xi [A] + R_e [Z] – Series Combination [Xi is converted from A to Z]

11. Xk = R_S [Y] + Xj [Z] – Chain Combination [R_S is converted from Y to A and Xj is converted from Z to A]

    11.1. Xz = R_c [Z] + 1/g_{md} [Z] – Series Combination [No conversion]

12. Xout = Xk [A] + Xz [Z] – Chain Combination [Xz is converted from Z to A]

13. Xirn = $\sqrt{2}$ * Xout.

[Y – Admittance Parameter, Z – Impedance Parameter, A – ABCD parameter]

Xout is the input referred noise voltage of one side of the Input Buffer and Xirn is the input referred noise voltage of the complete Input Buffer.

V. RESULTS AND DISCUSSION

Fig. 10 shows the simulated input referred noise voltage of the Input Buffer.

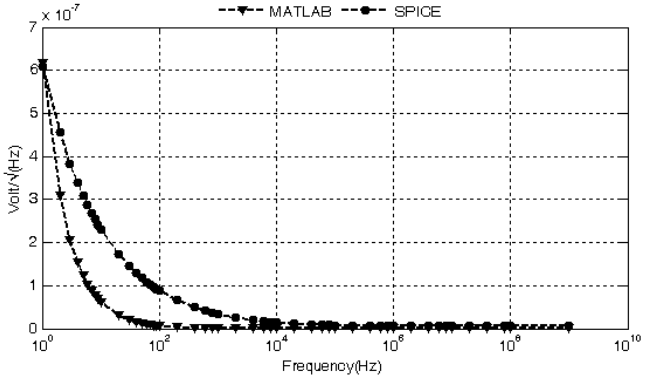

Figure 10: Input referred noise voltage of the Input Buffer

From Fig. 10 it is evident that both SPICE simulated and MATLAB simulated results are nearly equal and it is

approximately 621 nV/sqrt(Hz) at low frequency and decreases with the increase in frequency. With this value of input referred noise voltage the total SNDR of THA is 58.23 dB at 3 GHz sampling frequency. Therefore, the effective number of bits (ENOB) is 9.38 (resolution is 9-bit). This is 1 bit less than the desired 10-bit resolution.

To improve the resolution of the THA, the input referred noise voltage of the Input Buffer has to be reduced. This is done with the help of Noise Figure (NF). The overall NF of one side of the Input Buffer can be calculated by considering it as a series feedback amplifier as shown in Fig. 11 [27].

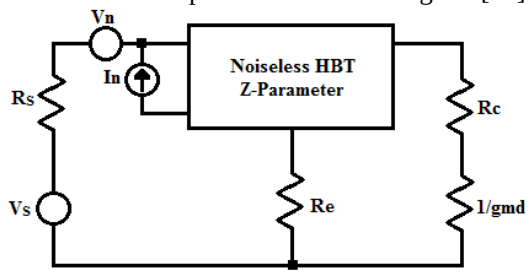

Figure 11: Series feedback amplifier with noise source

Considering the HBT as s noiseless block represented by Z-parameters, (22) and (23) represent the input referred noise voltage and current of HBT respectively and (24) is the noise voltage of source resistance R_S.

$$V_n = \sqrt{4KTA\Delta f} \tag{22}$$

$$I_n = \sqrt{4KTB\Delta f} \tag{23}$$

$$V_s = \sqrt{4KTR_S\Delta f} \tag{24}$$

The NF of the one side of the Input Buffer is;

$$NF = 1 + \frac{A}{R_S} + \frac{B}{R_S}\left|\frac{R_S Z_{21} + R_e(Z_{21} - Z_{11})}{Z_{21} + R_e}\right|^2 + \frac{R_e}{R_S}\left|\frac{Z_{21} - R_S - Z_{11}}{Z_{21} + R_e}\right|^2 \tag{25}$$

where R_e is the resistance connected to the emitter of transistors Q1 and Q2 as shown in Fig. 8 and Z_{11} - Z_{22} are the Z-parameters of the HBT.

From (25) the optimum value of R_S is obtained as;

$$R_{Sopt} = \sqrt{\frac{A + \left(BR_e^2 + R_e\right)\left|\frac{Z_{21} - Z_{11}}{Z_{21} - R_e}\right|^2}{B\left|\frac{Z_{21}}{R_e + Z_{21}}\right|^2 + \frac{R_e}{\left|R_e + Z_{21}\right|^2}}} \tag{26}$$

Fig. 12 shows the reduction in the input referred noise voltage of the Input Buffer with the optimized source resistance.

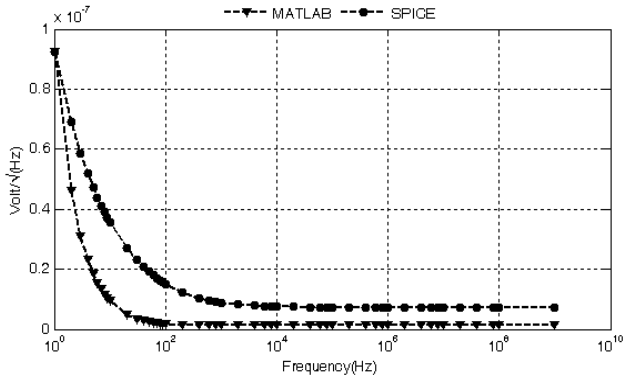

Figure 12: Reduction in input referred noise voltage after optimization

Fig. 12 clearly indicates that both the SPICE simulated and the MATLAB results are almost equal and the low frequency input referred noise voltage is approximately 93 nV/sqrt(Hz). This reduction in the input referred noise voltage improves the SNDR of the THA to 68.34 dB at 3GHz sampling frequency. So, the ENOB is now changed to 11.06 and hence, the resolution is 11-bit which is one bit more than the required resolution of our THA.

Fig. 13 shows the SNDR of the THA both for non-optimized and optimized input referred noise voltage of the Input Buffer. This result is obtained using SPICE at five different sampling frequencies of the THA. It is evident from Fig. 10 and Fig. 12 that with the increase in frequency the input referred noise voltage is getting reduced while Fig. 13 indicates that the SNDR is also getting reduced with increasing frequency. This is because of the parasitic capacitance present in each stage of the THA circuit. To improve the SNDR of the THA with sampling frequency, we have included an inductor in series with R_c of the Input Buffer shown in Fig. 8 to compensate the parasitic capacitive effect.

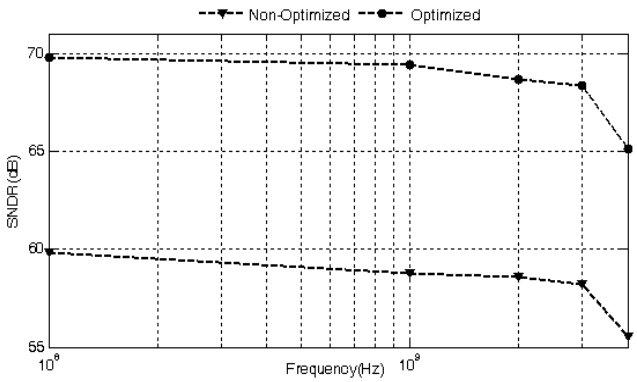

Figure 13: Plot of SNDR of the THA vs. frequency

Fig. 14 indicates the improvement in the SNDR of the THA after inclusion of the inductor. The noise level is not affected much because an inductor is a noiseless component.

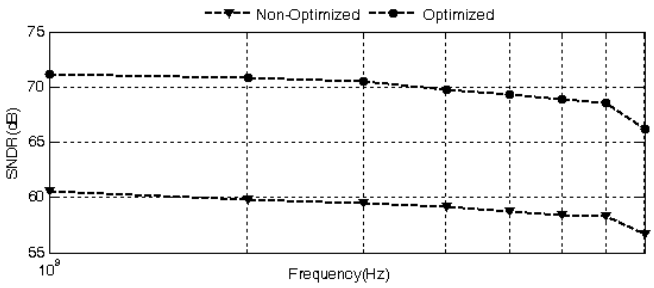

Figure 14: Improved SNDR of the THA vs. frequency

From Fig. 14 it is clear that the SNDR of the THA at 7GHz is 58.31 for non-optimized input referred noise voltage and 68.57 for optimized input referred noise voltage of the Input Buffer and hence an improvement is obtained in the speed of the THA for desired resolution.

VI. CONCLUSION

In this article a computer aided noise analysis technique has been proposed for an Input Buffer which is intended to be used in a THA having a sampling speed of 3GHz and a resolution of 10-bit. Without any noise optimization, it has been seen that the resolution is only 9-bit which is less than one bit from the required resolution of the THA. After the noise optimization of the Input Buffer, the resolution of the THA has been improved by one bit which satisfies our initial consideration of 10-bit resolution. With the inclusion of an inductor in series with the resistor R_c of the Input Buffer, the SNDR and hence the sampling speed of the THA for the required resolution is improved. This computer-aided noise modeling and analysis method can also be applied to other electronic circuits for calculating the input referred noise voltage.

REFERENCES

[1] P. R. Gray, P. J. Hurst, S. H. Lewis, and R. G. Meyer, "Analysis and Design of Analog Integrated Circuits," New York: Wiley, 2001.

[2] Behzad Razavi, "Principles of data Conversion SystemDesign," AT & T Bell laboratories, IEEE Press.

[3] John. D. Cressler, Guofu Niu, " Silicon-Germanium Heterojunction Bipolar Transistors," Norwood, Artech House, 2003.

[4] Peter Ashburn, "SiGe Heterojunction Bipolar Transistor," John Wiley & Sons, Ltd. 2003.

[5] F. Vessal and C. A. T. Salama, "A Bipolar 2-GSample/s track-and-hold amplifier (THA) in 0.35 um SiGe technology", *Proc. IEEE Int. Symp. Circuits and Systems*, vol. 5, pp. 573-576, 2002.

[6] C. Fiocchi, U. Gatti and F. Maloberti, "Design Issues on High-Speed High-Resolution Track-and-Hold in BiCMOS Technology", *IEE Circuits Devices Systems*, vol. 147, pp. 100-106, 2000.

[7] R. Uscola and M. Tutt, "Direct extraction of equivalent circuit model parameters for HBTs,". *In Proc. IEEE Int. Conf. Microelectronics Test Structures, 2001*, pp.83-87.

[8] D. Costa, W. U. Liu, and J. S. Harris, "Direct extraction of the Al-GaAs/GaAs heterojunction bipolar transistor small-signal equivalent circuit," *IEEE Trans. Electron Devices*, vol. 38, no.9, pp. 2018-2024, Sep. 1991.

[9] D. R. Pehlke and D. Pavlidis, "Evaluation of the factors determining HBT high-frequencY-performance by direct analysis of S-parameter data," *IEEE Trans. Microw. Theory Tech.*, vol. 40, no. 12, pp.1139-1151, Dec. 1992.

[10] C.-J. Wei and J. C. M. Hwang, "Direct extraction of equivalent circuit parameters for heterojunction bipolar transistors," *IEEE Trans. Microw. Theory Tech.*, vol. 43, no.9, pp. 2035-2040, sep. 1995.

[11] M. Rudolph, R. Doerner, and P. Heymann, "Direct extraction of HBT equivalent-circuit elements," *IEEE Trans. Microw. Theory Tech*., vol. 47, no.1, pp. 82-84, Jan. 1999.

[12] K. Lee, K. Choi, S.-H. Kook, D.-H. Cho, K.-W. Park, and B. Kim, "Direct parameter extraction of SiGe HBTs for the VBIC bipolar compact model," *IEEE Trans. Electron Devices*, vol. 52, no. 3, pp.375-384, Mar. 2005.

[13] H.-Y. Chen, K.-M. Chen, G.-W. Huang, and C.-Y. Chang, "Small-Signal Modelling of SiGe HBTs Using Direct Parameter-Extraction Method," *IEEE Trans. Electron Devices*, vol. 53, no. 9, pp.2287-2295, Sep. 2006.

[14] H. Cho and D. E. Burk, "A three-step method for the de-embedding of high-frequency S-parameters," *IEEE Trans. Electron Devices*, vol. 38, no. 6, pp. 1371-1375, Jun. 1991.

[15] Y. Govert, P. J. Tasker, and K. H. Bachem, "A physical, yet simple, small-signal equivalent circuit for the heterojunction bipolar transistor," *IEEE Trans. Microw. Theory Tech*., vol. 45, no. 1, pp. 149-153, Jan. 1997.

[16] H.-Y. Chen, K.-M. Chen, G.-W. Huang, and C.-Y. Chang, "A novel approach for parameter determination of HBT small-signal equivalent circuit," *IEICE Trans. Electron*., vol. E88-C, no. 6, pp. 1133-1141, Jun. 2005.

[17] C. J. Wei and J. C. M. Hwang, "Direct extraction of equivalent circuit parameters for heterojunction bipolar transistors," *IEEE Trans. Microw. Theory Tech*., vol. 43, no. 9, pp. 2035-2040, Sep. 1995.

[18] H. C. Wu, S. Mijalkovic, J. N. Burghartz, "Extraction of collector resistances for device characterization and compact models," *Solid-State Electronics*, vol. 50, pp. 1475-1478, Aug. 2006.

[19] L. Degachi and F. M. Ghannouchi, "An Augmented Small-Signal HBT Model With Its Analytical Based Parameter Extraction Technique," *IEEE Trans. Electron Devices*, vol. 55, no. 4, pp. 968-972, April. 2008.

[20] Fu Jun, "Small-signal model parameter extraction for microwave SiGe HBTs based on Y- and Z-parameter characterization," *J. Semicond*. vol. 30, issue 8, Aug 2009.

[21] U. Basaran, N. Wieser, G. Feiler, and M. Berroth, "Small-signal and high-frequency noise modeling of Sige HBTs," *IEEE Trans. Microw. Theory Tech*., vol. 53, no. 3, pp. 919-928, Mar. 2005.

[22] U. Basaran and M. Berroth, "High frequency noise modeling of SiGe HBTs using direct parameter extraction technique," *in Proc. EDMO*, 2002, pp. 189-195.

[23] A. Penarier, S. G. Jarrix, M. Perotin, F. Pascal, and C. Delseny, "Parameter extraction of heterojunction bipolar transistor from low-frequency noise and S-parameter measurements," *Semicond. Sci. Technol*. vol. 22, pp. 492-496, Mar. 2007.

[24] L. Moura and I. Darwazeh, "Introduction to Linear Circuit Analysis and Modelling," Newnes: An imprint of Elsevier, 2005.

[25] G. D. Vendelin, A. M. Pavio, U. L. Rohde, "Microwave Circuit Design Using Linear and Nonlinear Techniques," 2nd Edition, Wiley, 2005

[26] G. Vasilescu, "Signals and Communication Technology: Electronic Noise and Interfering Signals Principles and Applications," Berlin Heidelberg: Springer, 2005.

[27] A. F. Bellomo, "Gain and Noise Considerations in RF Feedback Amplifier," *IEEE J. Solid-state circuits*, vol. sc-3, no. 3. Sept. 1968.

Santosh Kumar Patnaik received the B.E and M.Tech degree in Electronics and Communication Engineering from Utkal University and Biju Patnaik University of Technology, Orissa, in the year of 1999 and 2003, respectively and submitted the Ph.D thesis in the department of E and ECE, IIT Kharagpur. He is currently working as an Associate Professor in the Department of Electronics and Communication Engineering, National Institute of Science and Technology, Berhampur, India. His current research areas are high speed ADC design and noise modelling and analysis of analog circuits.

Review On: Design of Low Complexity LDPC Decoding Algorithm in LDPC Coded BICM-OFDM Systems

Tarannum Shaikh and Prof. Devichand P. Rathod

Abstract : Digital Video Broadcasting-Terrestrial (DVB-T) is the most widely deployed digital terrestrial television system worldwide with services on air in over thirty countries. In order to increase its spectral efficiency and to enable new services the DVB consortium has developed a new standard named DVB-T2. Latest and next-generation wireless broadcasting standards, such as DVB-T2 or DVB-NGH, are considering distributed multi-antenna transmission in order to increase bandwidth efficiency and signal quality. Full-rate full-diversity (FRFD) space-time codes (STC) such as the Golden code and LDPC code are studied for that purpose. Bit-interleaved coded modulation (BICM) schemes based on low-density parity check (LDPC) codes have been used to enhance the detection complexity. A novel low-complexity soft detection algorithm for the reception of Golden codes in LDPC based orthogonal frequency-division multiplexing (OFDM) systems is presented in this paper. Computational complexity investigation as well as simulation results indicate that this algorithm has significant performance and complexity advantages over existing optimal detection in the various DVB-T2 broadcasting scenario.

Keywords –Bit Interleaved Coded Modulation (BICM), Low-density parity check (LDPC) codes, MAP detection, MIMO systems, Orthogonal frequency division multiplexing (OFDM).

I. INTRODUCTION

Since the invention of Information Theory by Shannon in 1948, coding theorists have been trying to come up with coding schemes that will achieve capacity dictated by Shannon's Theorem. The most successful two coding schemes among many are the LDPCs and Turbo codes. This article presents LDPC codes and in particular their usage by the second generation terrestrial digital video broadcasting (DVB-T2) [1], DVB-T2 specification makes use of LDPC (Low density parity-check) codes in combination with BCH (Bose-Chaudhuri- Hocquengham) to protect against high noise levels and interference. The second generation of the terrestrial digital video broadcasting standard (DVB-T2) [1] has adopted a space-frequency block code (SFBC) based on the well-known Alamouti technique. In order to increase the capacity and reach the full multiple-input multiple-output (MIMO) diversity-multiplexing frontier, the proposals for the future generations of terrestrial, portable and mobile digital video broadcasting standards, such as DVB-NGH, focus on the combination of both diversity and spatial multiplexing [2, 3] through full-rate full diversity (FRFD) codes such as the Golden code.

The main advantage of LDPC codes is that they provide a performance which approaches the channel capacity for many different scenarios, as well as the linear algorithms that can be used for decoding. Actually, the efficiency improvement provided by DVB-T2 in comparison with DVB-T is mainly based on these new coding and interleaving schemes. LDPC codes are commonly decoded by a soft-input soft- output (SISO) algorithm. When iterative decoders, such as turbo or low-density parity check (LDPC) codes, are included in the reception chain, soft information on the conditional probabilities for all possible transmitted symbols is required in the form of log-likelihood ratios (LLR). Several algorithms that serve this purpose can be found in the literature for spatial multiplexing MIMO systems, mostly based on list sphere detection (LSD) [4].
This paper presents the design of a low-complexity soft detection algorithm for Golden codes in bit-interleaved coded modulation (BICM) OFDM systems based on LDPC coding. We design the tree search algorithm in order to find the best balance between complexity and performance, by analyzing different tree configuration. Results based on a the DVB-T2 transmission scheme show how the proposed receiver design and algorithms can make the processing of Golden codes feasible for close-to-optimal soft decoding.

II. BLOCK DIAGRAM

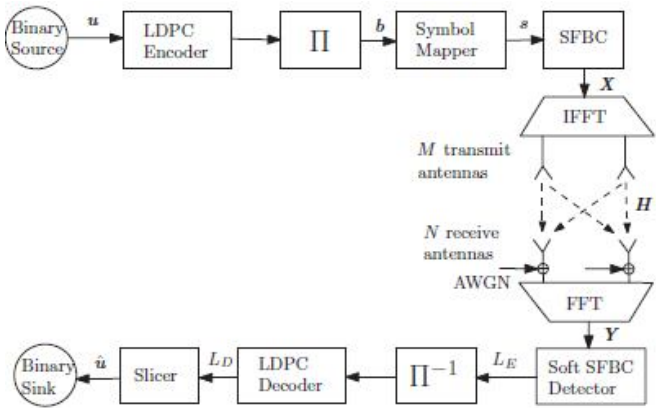

Fig. 1. Simplified diagram of a LDPC-based MIMO transmission and reception scheme based on DVB-T2.

Tarannum Shaikh and Prof. Devichand P. Rathod are with Department of Electrical Engineering, V.J.T.I, Mumbai, Email:tanu99@gmail.com, dprathod@vjti.org.in)

Fig. 1 shows the basic structure of LDPC-coded BICM-OFDM scheme with two transmit (M = 2) and two receive (N = 2) antennas. As can be seen, the bit stream is coded, interleaved and mapped onto a complex constellation which is spread across the transmit antennas and consecutive subcarriers through the Golden code. If subcarriers are grouped according to the chosen space-frequency mapping, a frequency-domain received symbol block $\boldsymbol{Y}$ of dimensions $N \times T$ can be represented mathematically as

$$\boldsymbol{Y} = \boldsymbol{HX} + \boldsymbol{Z}, \qquad (1)$$

where $\boldsymbol{H}$ denotes the $N \times M$ complex channel matrix, $\boldsymbol{X}$ is any $M \times T$ codeword matrix and $\boldsymbol{Z}$ represents the $N \times T$ zero-mean additive white Gaussian noise (AWGN) matrix whose complex coefficients fulfill $CN(0, 2\sigma^{2})$ being σ^2 the noise variance per real component. Note that T = 2is the frequency depth of the considered codewords $\boldsymbol{X}$. The Golden code is the 2 × 2 FRFD scheme which achieves the maximal coding gain [6]. A data symbol vector $\boldsymbol{s}$ = ($s1$, $s2$, $s3$, $s4$) is transformed into the transmitted codeword as follows:

$$\boldsymbol{X} = \frac{1}{\sqrt{5}} \begin{bmatrix} \alpha(s_1 + \theta s_3) & \alpha(s_2 + \theta s_4) \\ i\bar{\alpha}(s_2 + \bar{\theta} s_4) & \bar{\alpha}(s_1 + \bar{\theta} s_3) \end{bmatrix}, \qquad (2)$$

with $\theta = \frac{1+\sqrt{5}}{2}$ (the golden number), $\bar{\theta} = \frac{1-\sqrt{5}}{2}$, $\alpha = 1 + i - i\theta$ and $\bar{\alpha} = 1 + i - i\bar{\theta}$. However, the symbols are not dispersed with equal energy in all spatial and temporal directions in such a way that the symbol power within each of the pairs, ($s1$, $s3$) and ($s2$, $s4$), are always unbalanced.

The main drawback of the Golden code lies on the decoding complexity, which is exponential in the length of the symbol vector s, i.e. $O(P^4)$, becoming prohibitive for large constellation sizes P.

III. SOFT DETECTION

The aim of a soft-output detector is to calculate or approximate the *a posteriori* probability (APP) for each of the coded bits cj in a given signaling interval, where $j \in \{1, \ldots \omega Nt\}$ is the bit index. This probability is conveniently represented by the so-called a posteriori log-likelihood ratio (LLR):

$$L_D(b_k|\boldsymbol{Y}) = \ln \frac{\Pr[b_k = +1|\boldsymbol{Y}]}{\Pr[b_k = -1|\boldsymbol{Y}]} = L_A(b_k) + L_E(b_k|\boldsymbol{Y}), \quad (3)$$

The sign of $L_D(b_k|\mathbf{y})$ is the maximum a posteriori (MAP) estimate for b_k, and the magnitude represents the reliability of the estimate. Larger magnitudes correspond to higher reliability, and smaller magnitudes indicate low reliability. In particular, the extreme case of L = 0 indicates that b_k is equally likely to be +1 and −1.where Pr [b_k = +1] and Pr [b_k = −1] are the *a priori* probabilities that bit b_k is 1 or −1, respectively, and where

$$LA(bk) = \ln \frac{\Pr[bk = +1]}{\Pr[bk = -1]}$$

is the a priori LLR for the k-th bit. The second term LE in (3) represents the extrinsic contribution to the a posteriori LLR [4]. Using the law of total probability, it can be written as

$$L_E(b_k|\boldsymbol{Y}) = \ln \frac{\sum_{\boldsymbol{b} \in \mathbb{B}_{k,+1}} p(\boldsymbol{Y}|b) \exp\left(\sum_{j \in \mathbb{J}_{k,\boldsymbol{b}}} L_A(b_j)\right)}{\sum_{\boldsymbol{b} \in \mathbb{B}_{k,-1}} p(\boldsymbol{Y}|b) \exp\left(\sum_{j \in \mathbb{J}_{k,\boldsymbol{b}}} L_A(b_j)\right)}, \qquad (4)$$

where $LD(bk)$, $LA(bk)$ and $LE(bk|\boldsymbol{Y})$ denote the *a posteriori*, *a priori* and *extrinsic* information, respectively. The extrinsic information conditioned to the received vector $\boldsymbol{Y}$ is written in (4).

where $p(\boldsymbol{Y}|\boldsymbol{b})$ represents the likelihood function. Defining $K_b = MT \log 2\, P$, B_k, +1 represent the set of $2^{Kb}-1$ bit vectors $\boldsymbol{b}$ having b_k = +1.

The most important part of the calculation of LD in (3) is the likelihood function $p(\boldsymbol{Y}|\boldsymbol{b})$. Considering our system in (1), we can rewrite it as an equivalent 4 × 4 MIMO channel where there is no channel interference between the sets of transmit antennas {1, 2}, {3, 4} and the sets of receive antennas {3, 4}, {1, 2}, respectively.

Thus, the equivalent channel can be expressed as

$$\breve{\boldsymbol{H}} = \begin{bmatrix} \boldsymbol{H}^1 & \boldsymbol{0} \\ \boldsymbol{0} & \boldsymbol{H}^2 \end{bmatrix} = \begin{bmatrix} h_{11}^1 & h_{12}^1 & 0 & 0 \\ h_{21}^1 & h_{22}^1 & 0 & 0 \\ 0 & 0 & h_{11}^2 & h_{12}^2 \\ 0 & 0 & h_{21}^2 & h_{22}^2 \end{bmatrix}, \qquad (5)$$

where h_{ij}^{k} is the complex channel coefficient from transmit antenna j to receive antenna i at the k-th carrier. Note that we have distinguished between $\boldsymbol{H}^1$ and $\boldsymbol{H}^2$ since they are equal if and only if the channel does not vary in adjacent carriers.

By taking the elements column-wise from matrices $\boldsymbol{X}$ and $\boldsymbol{Y}$, the column vectors $\boldsymbol{x}$ = [$x11$, $x21$, $x12$, $x22$]T and $\boldsymbol{y}$ = [$y11$, $y21$, $y12$, $y22$]T can be defined, respectively.

On the other hand, if we define a generator matrix $\boldsymbol{G}$ for the Golden code as

$$\boldsymbol{G} = \begin{bmatrix} 1 + i\bar{\theta} & 0 & \theta - i & 0 \\ 0 & -\theta + i & 0 & 1 - i\bar{\theta} \\ 0 & 1 + i\bar{\theta} & 0 & \theta - i \\ 1 + i\theta & 0 & \bar{\theta} - i & 0 \end{bmatrix}, \qquad (6)$$

the codeword $\boldsymbol{X}$ can be expressed as $\boldsymbol{x} = \boldsymbol{Gs}$, where $\boldsymbol{s}$ corresponds to the symbol column vector [$s1$, $s2$, $s3$, $s4$]T . Using the new notation, the likelihood function $p(\boldsymbol{Y}|\boldsymbol{b})$ can be rewritten as

$$p(\boldsymbol{Y}|s = map(\boldsymbol{b})) = \frac{\exp\left(-\frac{\|\boldsymbol{y} - \breve{\boldsymbol{H}}\boldsymbol{G}\boldsymbol{s}\|^2}{2\sigma^2}\right)}{(2\pi\sigma^2)^{NT}}, \qquad (7)$$

where $\boldsymbol{s} = map(\boldsymbol{b})$ is the mapping of the vector $\boldsymbol{b}$ into the symbols of column vector $\boldsymbol{s}$. Only the term inside the exponent in (7) is relevant for the calculation of LE, and the constant factor outside the exponent can be omitted.

The main difficulty in the calculation of (4) arises from the computation of the ML metrics since a calculation of $P4$

metrics is necessary for the considered 2 × 2 code. This becomes unfeasible for high modulation orders unless the calculation of (4) can be reduced.

This detection approach results in a good system performance and its complexity depends on the method to obtain the candidate list *L*. The LSD is the most common approach, but its complexity order will be upper-bounded by *O*(*P*4) in the same way as the SD [4]. In the next section, we propose a fixed-complexity detection algorithm and its design for FRFD codes such as (2).

IV. FIXED-COMPLEXITY DETECTION

The proposed fixed-complexity tree-search-style algorithm is based on the functionality of list fixed-complexity sphere decoder (LFSD) presented in [7] for spatial multiplexing schemes with soft symbol information requirements. The main feature of the LFSD is that, instead of constraining the search to those nodes whose accumulated Euclidean distances are within a certain radius from the received signal, the search is performed in an unconstrained fashion. The tree search is defined instead by a tree configuration vector $\boldsymbol{n} = [n1, \ldots, nMT]$, which determines the number of child nodes (ni) to be considered at each level. At the end of the process, a list of *Ncand* candidate symbol vectors is retrieved from the last-level nodes that have been reached. It is worth noting that the set G composed of the *Ncand* selected symbol vectors may not correspond to the vectors of the *L* set with the smallest metrics given by the LSD, but provides sufficiently small metrics and diversity of bit values to obtain accurate soft information. A representation of an LFSD tree search is depicted in Figure 2 for a QPSK modulation and a tree configuration vector of $\boldsymbol{n} = [1, 1, 2, 4]$.

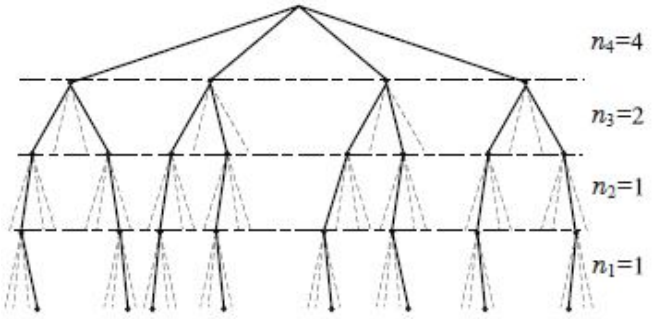

Fig. 2. Fixed-complexity tree search of a QPSK-modulated signal using a tree configuration vector of $\boldsymbol{n} = [1, 1, 2, 4]$.

The basic idea behind the Fixed Sphere Decoder is to perform a search over only a fixed number of possible transmitted signals, generated by a small subset of all possible signals located around the received signal vector. This ensures that the detector complexity is fixed over time, a major advantage for hardware implementation. In order for such a search to operate efficiently, a key point is to order the antennas in such a way that most of the points considered relate to transmit antennas with the poorest signal to noise (SNR) conditions.

4.1 Ordering algorithm

A simple ordering algorithm is used that exploits the golden code's structure to ensure that the overall algorithm performs well. Our detector has computational complexity O($q2$) when the list length $\ell = q2$. However, for $\ell << q2$, our algorithm achieves comparable performance at much lower complexity.

The first step in the proposed algorithm is to determine which pair of information symbols should be detected first, and to furthermore determine the order in which the remaining pair of symbols is to be detected. The pseudo code for an efficient ordering algorithm, is shown below

Ordering Algorithm.

Input: H Output: P

if $\|\mathbf{h}_1\| > \|\mathbf{h}_2\|$ **then**
  $k_1 = 1$
  $C_2 = [2, 3, 4], C_3 = [4, 4, 2], C_4 = [3, 2, 3]$
else
  $k_1 = 2$
  $C_2 = [1, 3, 4], C_3 = [3, 1, 3], C_4 = [4, 4, 1]$
end
$\delta_{min} = \infty$
for *i from* 1 *to* 3 **do**
  $k_2 = C_2[i], k_3 = C_3[i], k_4 = C_4[i]$
  $\delta = |\mathbf{h}_{k_1}^* \mathbf{h}_{k_2}| / (\|\mathbf{h}_{k_1}\| \|\mathbf{h}_{k_2}\|)$
  if $\delta < \delta_{min}$ **then**
    $\delta_{min} = \delta$
    $\mathbf{P} = [\mathbf{e}_{k_1}, \mathbf{e}_{k_2}, \mathbf{e}_{k_3}, \mathbf{e}_{k_4}]$
  end
end

The performance of the LFSD soft-detector in uncoded scenarios is strongly dependent on the ordering algorithm of the channel matrix and the choice of the tree configuration vector [8]. However, in the specific case of space-frequency-coded systems the effect of the ordering algorithm on the overall performance relies on the symbol power distribution in spatial and frequency directions. The structure of the Golden code generates a difference in the norms of the equivalent subchannels of each symbol in a pair, which allows for the implementation of an ordering procedure in order to improve the overall system's performance. The proposed ordering approach yields close-to-optimum performance when combined with the suggested tree configuration vector. Moreover, the matrix ordering process only requires the computation of *MT* vector norms as opposed to other ordering algorithms such as FSD [7] which need to perform $MT - 1$ matrix inversion operations.

V. SIMULATION RESULTS

The performance of the overall system has been assessed by means of the bit error rate (BER) after the LDPC decoder. The DVB-T2 parameters used in the simulations are: 64800 bits of length of the LDPC block, code rate R =2/3, 16-QAM

modulation, OFDM symbol of 2048 carriers (2K) and 1/4 of guard interval. The simulations have been carried out over a Rayleigh channel (Typical Urban of six path, TU6), commonly used as the simulation environment for terrestrial digital television systems. Perfect CSI and non-iterative detection has been considered at the receiver.

5.1. Performance comparison over DVB-T2 BICM system

This section presents the performance assessment and the complexity analysis of the new list fixed-complexity soft detector of the LDPC code over a SFBC DVB-T2 broadcasting scenario. Fig. 3 shows the BER curves versus SNR for different configurations of the proposed algorithm. for the LFSD configuration $k = 1$, $p = P$ and $Ncand = 25$. However, this grows up to 1.3 dB with a less complex configuration, i.e. $k = 2$, $p = 8$. On the other hand, one should note that the LSD performance difference between $Ncand = 25$ and 50 is negligible resulting advantageous in the complexity degree of the algorithm.

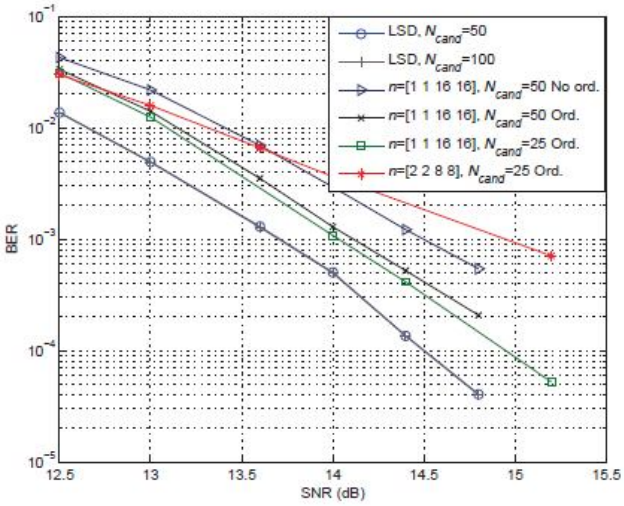

Fig. 3. BER performance comparison between LSD and LFSD detection of LDPC codes in the 2 × 2 DVB-T2 system with 16-QAM modulation over TU6 channel.

The BER performances of the proposed algorithm, the LFSD of [8] and the LSD solution are depicted in Fig. 4 for $Ncand = 50$. One can observe that the proposed fixed complexity detection algorithm achieves a similar performance result as the LSD with a substantial reduction in the detection complexity. Moreover, the new ordering design and the proposed tree search configuration vector $\boldsymbol{n}$ outperform the LFSD solution of [8] in about 0.7 and 1 dB for Golden and SS codes, respectively. If we observe the behavior of the proposed fixed-complexity algorithm for the SS code, we can see that it obtains the same BER performance as the algorithm proposed in [7], which has a complexity of $O(P^3)$, with complexity P^2. For the Golden code, if the fixed-complexity tree of P^2 branches is considered, the performance is 0.4 dB worse than the LSD with complexity $O(P^4)$. However, if the complexity is increased to $4P^2$, the performance difference is negligible.

In order to analyze the complexity of the detection algorithms, the cumulative distribution functions of the overall visited nodes have been depicted in Fig. 4. We see that the reduction of *Ncand* decreases the complexity of the LSD decoder compared to the LFSD. For $Ncand = 50$, 75 % of the LSD solutions are obtained visiting lower number of nodes than the LFSD algorithm.

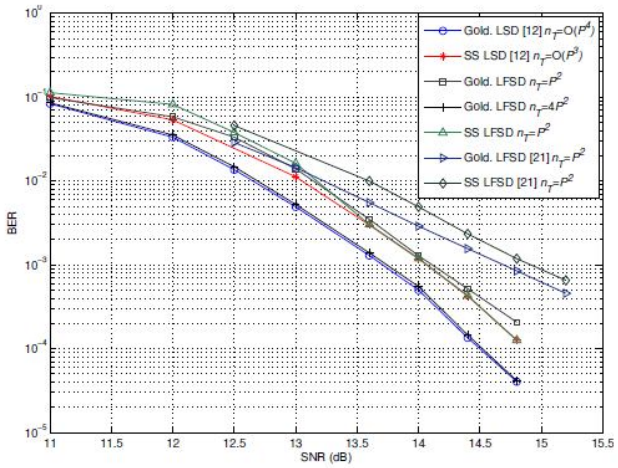

Fig . 4. BER performance comparison of FRFD SFBC codes detection with LSD [9], LFSD of [11] and the proposed ordered LFSD for DVB-T2 transmission.

If *Ncand* is reduced up to 25, this value rises to 95 %. Despite these differences, the sequential nature of the LSD tree search and its variable complexity results in a problem for real hardware implementations. Nevertheless, the design of LFSD makes it possible a parallel architecture of the algorithm that can be fully pipelined and maintains fixed the search complexity.

VI. Conclusion

In this paper, a fixed-complexity detector for Golden codes and the analysis of its implementation on future digital TV broadcasting systems based on LDPC-coded BICM-OFDM is presented. The main drawback of the LSD detection is its variable complexity that is strongly dependent on the noise and channel conditions, which leads to a complexity order upper-bounded by $O(P^4)$. A list fixed-complexity detector with a novel ordering algorithm is proposed in this paper with the aim of approaching the performance of the LSD using fixed complexity.BER simulation results show the close-to-optimal performance of the proposed low-complexity detector in a typical LDPC-based DVB-T2 broadcasting scenario. The proposed detection algorithm can enable the realistic implementation and the inclusion of LDPC codes in the forthcoming digital video broadcasting standards or in any similar BICM-OFDM system. BER simulation results show the close-to-optimal performance of the proposed low-complexity detector for both Golden and SS SFBC codes in a typical LDPC-based DVB-T2 broadcasting scenario. The performance is clearly improved when the proposed channel and candidate ordering algorithm is applied with Golden codes, though its effects are negligible for the SS code. In any case, the proposed detection algorithm can enable the realistic implementation and the inclusion of any FRFD SFBC code in any

BICM-OFDM system such as the forthcoming digital video broadcasting standards or in any similar BICM-OFDM system.

ACKNOWLEDGMENT

I would like to express my deepest gratitude to my guide Prof. D.P.Rathod for his support and guidance. It was his enthusiastic encouragement that led me to work with him, then his appreciation led me to further successes in my academic career. I also would like to thank him for his suggestion and support to write this Paper.

REFERENCES

[1] *ETSI*, "Digital Video Broadcasting (DVB); Frame structure channel coding and modulation for a second generation digital terrestrial television broadcasting system (DVB-T2). *ETSI EN302 755 V1.1.1*," September 2009.

[2] Y. Nasser, J.F. Helard, and M. Crussire, "System Level Evaluation of Innovative Coded MIMO-OFDM Systems for Broadcasting Digital TV," *International Journal of Digital Multimedia Broadcasting*, vol. 2008, pp. 1–12, 2008.

[3] I. Sobron, M. Mendicute, and J. Altuna, "Full-rate full-diversity space-frequency block coding for digital TV broadcasting," in *Proc. European Signal Processing Conf. (EUSIPCO-2010)*, Aalborg, Denmark, August 2010.

[4] B.M. Hochwald and S. ten Brink, "Achieving near-capacity on a multiple-antenna channel," *IEEE Trans. on Commun.*, vol. 51, no. 3, pp. 389–399, 2003.

[5] L. G. Barbero and J.S. Thompson, "A fixed-complexity MIMO detector based on the complex sphere decoder," in *Proc. IEEE International Workshop on Signal Processing Advances in Wireless Communications (SPAWC '06)*, Cannes, France, July 2006.

[6] JC Belfiore, G Rekaya, and E Viterbo, "The golden code: A 2 x 2 full-rate space-time code with non-vanishing determinants," in *2004 IEEE International Symposium on Information Theory, Proceedings*. 2004, p. 308, IEEE.

[7] J. Paredes, A. B. Gershman, and M. Gharavi-Alkhansari, "A 2 x 2 spacetime code with non-vanishing determinants and fast maximum likelihood decoding," in *Proc. 2007 IEEE ICASSP*, vol. 2, pp. 877–880.

[8] P.W. Wolniansky, G. J. Foschini, G.D. Golden, and R.A. Valenzuela, "V-BLAST: An architecture for realizing very high data rates over the rich-scattering wirelss channel," in *Proc. URSI International Symposium on Signals, Systems and Electronics (ISSSE'98)*, September 1998, pp. 295–300.

[9] B. Hochwald and S. ten Brink, "Achieving near-capacity on a multiple antenna channel," *IEEE Trans. Commun.*, vol. 51, no. 3, pp. 389–399, 2003.

[10] D.P.Rathod and " An efficient heuristic approach for irregular LDPC codes with low error floor" in *International Journal of advances in engineering science and technology* ISSN:2319-1120/IJAEST/V1N2:Pg.53-58.

[11] L. Barbero, "Rapid prototyping of a fixed-complexity sphere decoder and its application to iterative decoding of turbo-MIMO systems," Ph.D. dissertation, University of Edinburgh, 2006.

[12] D.P.Rathod and " An efficient algorithm for irregular LDPC codes with reduced computational complexity and error floor" in *International Conference on Communication, Information and Computing Technologies* ISBN: 978-1-4577-2077-2. Pg1-4 available on IEEExplore digital library year 2012.

[13] D.P.Rathod and " An efficient Genetic based algorithm for an irregular LDPC codes with low computational complexity and low error floor" in *International Conference on Computing, Communication &Control (ICAC3). communication in computer and information science.volume 361,2013pp249-258.available on springerlink digital library*. ISBN:978-3-642-36320-7.\

[14] Iker Sobrón, Maitane Barrenechea, Pello Ochandiano, Lorena Martínez,Mikel Mendicute, and Jon Altuna, "Low-Complexity Detection of Full-Rate SFBC in BICM-OFDM Systems" in *IEEE Transactions on Communications, VOL. 60, no. 3,* pp. 626–631, *MARCH 2012*

A Novel Optical Sensing Technique for Detection of Fluoride in Ground Water of Guwahati

Tridiv Medhi, Tipu Kumar Prithani, Parismita Das, Bikramjit Goswami and Shakuntala Laskar

Abstract: This paper presents the design of a novel optical sensor for detection of anions such as Fluoride present in ground water of Guwahati city of the North Eastern India. The penetrating property of laser is taken as the base to perform the experiments for designing of the sensor. The experimental set up is made with a laser source, detector and the sample of ground water used in between the source and the detector. The partially absorbed light from the sample is detected using a photo detector and simulated using labVIEW. The complete setup is based on the intensity-voltage relationship obtained at the photo detector.

Keywords: Fluoride, laser, optical sensing, photo detector.

I. INTRODUCTION

Approximately half of the world's population lives in urban areas and by the year 2025 will have risen to 60 per cent, comprising some 5 billion people. Rapid urban population growth and industrialization are putting severe strains on the water resources and environmental protection capabilities of many cities particularly in developing nations. The lack of source of clean drinking water is giving birth to public health concern worldwide. Waterborne diseases are a consequence. Access to safe drinking water is essential to health, a basic human right and a component of effective policy for health protection. Human use of fresh water has registered a 35 fold increase in the last 300 years.

Ground water is generally considered as a safe source of fresh drinking water. But the contamination of ground water is not away from the evils of modernization. Ground water is assumed to be of higher quality unlike surface water sources as it remains unexposed but with the increase in domestic sewage and agricultural and other industrial wastes the natural sources are getting contaminated every now and then.

Tridiv Medhi is pursuing B.Tech degree in Electrical and Electronics Engineering, DBCET, Assam. Email: tridiv.medhi@gmail.com
Tipu Kumar Prithani is pursuing B.Tech degree in Electrical and Electronics Engineering, DBCET, Assam. Email: prithani.tipu@gmail.com
Parismita Das is pursuing B.Tech degree in Electrical and Electronics Engineering, DBCET, Assam.
Shakuntala Laskar is working as the H.O.D. of Department of Electrical and Electronics Engineering, DBCET, Assam.
Bikramjit Goswami is working as assistant professor in Department of Electrical and Electronics Engineering, DBCET, Assam.

The chronic impact of these chemical contaminants of drinking water is dreadful. They cause very serious health problems, whether the chemicals are naturally occurring or derived from source of pollution [11].

India is currently facing critical water supply and drinking water quality problems. There is evidence of prevailing contamination of water resources in many areas of India. Although information on drinking water quality of Northeastern India is very little, results reported by various agencies have been alarming. Available literature shows that groundwater in Assam are highly contaminated with iron. The occurrence of fluoride contamination in Darrang, Karbi Anglong, and Nagoan districts of Assam in the form of fluorosis were already reported. High level of fluoride and iron distribution in groundwater sources of certain districts of Assam has also been observed. The health problems arising as a result of fluoride contamination are far more widespread in India. Nearly 177 districts have been confirmed as fluoride-affected areas [11].

A recent survey showed that 18 districts in Assam have become prone to arsenic and fluoride contamination triggering alarm. But it's not the only area where we found ground water contaminated. Almost 16 per cent of city areas and suburbs were also affected. Fluoride and arsenic contamination can cause serious health problems, as reported by United Nations International Children Emergency Fund during its fluoride and arsenic mitigation programme recently [12].

Accurate measurement of chemicals such as heavy metal ions and anions in water has acquired great practical significance because of the toxic effects these chemicals may cause in humans. Development of simple, sensitive, low-cost, light weight sensors capable of direct measurement of water pollution is of considerable interest to all. The main focus is on designing a sensor based on all these attributes in the project. The paper emanates out of that focussed project endeavour [6].

Fluoride compounds present in water causes a major health disease and hence their detection is very important in the process of pollution monitoring. The safe level of Fluoride concentration in ground water is between 0.5 and 1.0 mg/L (according to World Health Organisation standards). Fluoride concentration above 1.5 ppm level is unsafe and can cause diseases like Fluorosis and dental disorders. So, it is

desirable to have a simple, handy and layman's sensor for measurement of Fluoride content in water, as it is found in many parts of the North East India's ground water [9].

A recent study shows 28,181 water sources located in Assam have been contaminated with fluoride and inorganic materials, followed by 2,931 in Tripura, 566 in Arunachal Pradesh, 136 in Nagaland, 124 in Meghalaya, 76 in Sikkim, 37 in Manipur and 26 in Mizoram [10].

The sensor designed for measurement of fluoride is based on the principle of intensity modulation through light interruption. A laser of certain wavelength is used as the source and a photo detector form the basic optical sensor system. Amount of light reaching the detector gives the measure of the pollutant content in the pre-calibrated sensor set-up. The amount of photons i.e. light falling on the photo detector is converted to change into analog voltage. The analog voltage signals from the sensors are converted to equivalent digital signals by analog to digital converter [8].

For Fluoride the wavelength of maximum absorption is 570 nm. The presence of fluorine in solution is detected when laser beam at the wavelength of 570 nm results in a decrease in the intensity of the light propagating in the sample medium. For small concentration levels of fluoride, the loss of the power of light is proportional to the amount of fluoride in the solution. That is, a change in the sensor output signal level is a linear function of the amount of fluoride. Similarly the same can be said for arsenic operated at 330 nm. To determine the sensitivity of the results and accuracy of the analysis the whole process can be simulated using the tools like labVIEW. The preliminary results establish the feasibility of detecting low concentration fluoride in water. Also it is found from the existing literatures that the optical sensing techniques are simple, low cost, acurate and user friendly. The main motivation of designing optical sensor for detection of water pollutants came from the definite merits seen from the existing literatures on the field and the urge to overcome the limitations found in some of the related existing chemical techniques [9], [10].

In this paper the design of the sensor system is discussed, the relation between light intensity and absorbance in the section II. The experimental details are presented in section III and the results are discussed and analysed in section IV.The paper is concluded in section V.

II. LIGHT INTENSITY, ABSORBANCE AND WAVELENGTH

The background principle behind the experimental work is dependent on the principles of laser i.e its wavelength and penetration and absorption in the media of air and water sample and the changes taking place in those parameters due to change in the concentration of the pollutant materials [7]. The most important parameter in this experiment is the wavelength of light source at which maximum absorption by fluoride takes place.

According to Beer-Lambart law, there is logarithmic dependence between the transmission (and or transmissivity), T of light through a substance and the product of the absorption coefficient of the substance, α, and the distance the light travels through the material (i.e., the path length), ℓ [1].

$$T = 10^{-\ell\alpha} \quad (1)$$

Also the transmittivity is related to

$$T = I/I_0 \quad (2)$$

where,I and I_o are the power transmitted with and without an absorbing medium, respectively.

The absorption coefficient, α can, in turn, be written as a product of either a molar absorptivity (extinction coefficient) of the absorber, ε, and the molar concentration c of absorbing species in a sample,

$$\alpha = c\varepsilon \quad (3)$$

Hence the power incident at the detector is givenas below.

$$I = I_0 . e^{\alpha\ell} \quad (4)$$

Finally the absorbance

$$A = -\log_{10} I/Io \quad (5)$$

The ever increasing demand for in situ monitoring of health, environment and security has created a need for reliable, miniaturised sensing devices. To achieve this, appropriate analytical devices are required. The use of light emitting diodes (LEDs) as light sources is one strategy, which has been successfully applied in chemical sensing. The same principle is applicable to detect pollutants such as fluoride in water.

III. EXPERIMENTAL DETAILS

The primary aim of the experimental set-up for detecting the level of fluoride in ground water is the optimization of the sensor design for making it portable and achieving higher sensitivities with greater accuracy. The design can be further upgraded to make it user friendly so that it is accessible to all at ease.

The penetrating property of laser is utilized in the detection process in the experiment. An experimental set up is made with a laser Light Emitting Diodes as source and the light ray is passed through the collected samples of ground water. Air is taken as the medium for transmitting light before and after it passes the sample. The partially transmitted light from the sample is utilized and detected using a photo detector which acts as photo-sensor.

In order to exploit the modulation of intensity characteristic of the light ray, the source, the sample and the detector are kept as close as possible; the point where detector output is maximum when light passes an empty glass

container. The distance of the sample from the source is 10 cm. A test tube of 1cm diameter is taken to hold the sample and it is used throughout the experiment to maintain uniformity in results. After every test this tube is washed with distilled water. The test tube selected, is of good quality glass so that it absorbs minimum light and has good transmitting property. To hold the test tube in a fixed position and keep its alignment right a clamp stand is used. The experimental set-up used for the present investigation is shown schematically in figure 1. The light from a laser of wavelength 570 nm, is transmitted through air medium (neglecting losses). After getting passed through the sample, the light falls onto the detector, which digitally displays the obtained output voltage when connected to a multimeter. Depending on the chemical ions for analysis, the required wavelength of the source will vary.

For the experimental setup considered presently, the amount of absorbed light would depend on the concentrations of fluoride present in water. Due to absorbance, a part of light will be absorbed by the sample, and the remaining will fall on the photo-transducer. This is due to the absorptivity of fluoride particles. In the case of fluoride the absorbance is maximum when the light source is of 570 nm wavelength.

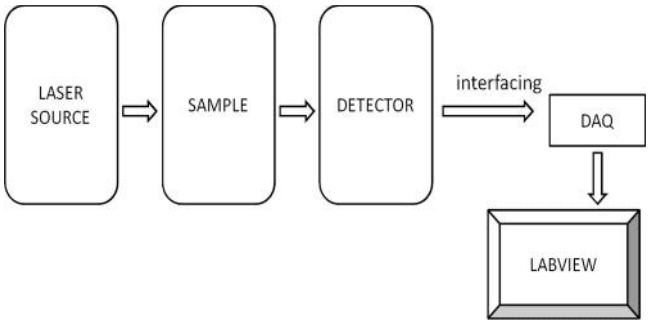

Fig 1. The experimental set-up used for measuring the fluoride concentration in ground water.

Standard test samples having chemical concentrations ranging from 0.001mg/l to 2mg/l are prepared by dissolving sodium fluoride in pure water. The reason for taking salt of sodium fluoride is that it gets fully dissolved in water. The samples are then allowed to mix uniformly for 4-5 hours, after which the measurements are carried out. When added to water, the NaF salt dissolute into sodium and fluoride ions. Since the wavelengths of light used is close to the peak absorption wavelength of the fluoride in the solutions, majority of the absorption are due to fluoride ions and it increases with the increase in chemicals' concentration.

After observing the outputs of the photo detector for all concentrations of the samples using a digital multimeter, the setup is then interfaced with LabVIEW through the DAQ for realtime monitoring of the voltage values with respect to time. A set was drawn beforehand in the workspace of LabVIEW where a filter has been used to filter out the noise and a numeric knob and a scope to observe the numeric value and the graph of voltage output respectively. The results were plotted for each concentration to obtain a standard curve. The basic slope equation obtained from the concentration (mg/l) versus detected voltage (mV) graph has been made use of to form the equation for concentration. This equation is applied in the LabVIEW to get real time value of concentration for any test sample. The same test procedure is performed for collected water samples from various water sources, first with predetermined quantity of the fluoride pollutants to check the sensitivity of the setup. These predetermined values were obtained by chemically testing the collected samples. When the sensitivity and accuracy of the method was set, the same test was performed for unknown quantity of any sample to determine the amount of pollutants i.e. fluoride in the given sample.

IV. RESULTS AND DISCUSSION

From the experimental result it is observed that the amount of absorption of light passing through the solution increases linearly with the increase in concentration of fluoride and arsenic in the solutions and accordingly the output voltage decreases. The readings of the experiment are tabulated in Table I.

Table I. Detector voltages obtained practically and theoritically in millivolts against concentration of fluoride and the error; when reference voltage using distilled water is 490 mV

Conc. of fluoride in distilled water (in mg/ml)	Detector output for fluoride (in mV) Practical	Detector output for fluoride (in mV) Theoritical	Error %
0.001	484.0	483.2	-0.165
0.005	483.5	482.8	-0.140
0.01	482.5	482.4	-0.020
0.02	480.5	481.5	0.207
0.05	478.0	478.8	0.167
0.10	475.0	474.2	-0.147
0.13	471.0	471.5	0.106
0.16	469.0	468.8	0.042
0.18	467.0	466.9	-0.012
0.20	465.0	465.1	0.026
0.23	462.5	462.4	-0.022
0.26	460.0	459.6	-0.072
0.30	456.0	456	0.000

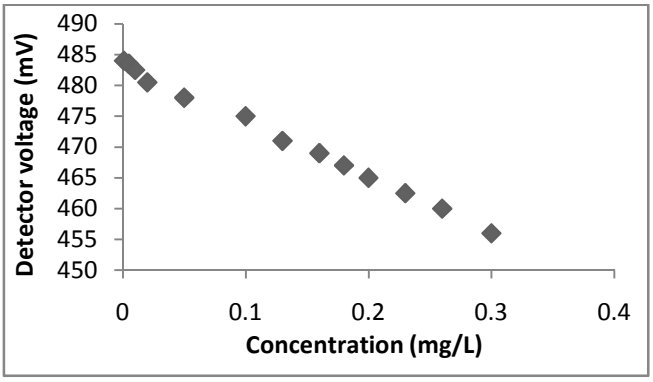

Fig. 2 Detector output (mV) versus concentration of absorbing species fluoride (mg/L)

Fig. 2 shows the output at the detector for different concentration of fluoride in water respectively. The graph for concentration (mg/L) versus detector voltage (mV) was plotted and a linear curve was obtained. From the relationship obtained, any unknown concentration of the absorbing species of fluoride in a sample of ground water from any source can be determined.

A water sample from the river Brahmaputra (at Kacharighat) was taken and tested to initialize the conclusive work. The sample was also chemically tested for validation of the results obtained by the optical sensing technique at Guwahati University chemical laboratory. Results showed that the value obtained in the optical sensor setup was 0.27 mg/l for a voltage of 459 mV approximately matched the value of 0.25 mg/l found by chemical analysis method. The values are tabulated in Table II.

Table II. Concentration obtained in the optical sensing technique and by chemical analysis for a water sample from river Brahmaputra

Concentration obtained from optical sensing technique (mg/L)	Concentration obtained by chemical analysis method (mg/L)	Percantage error
0.27	0.25	8.0

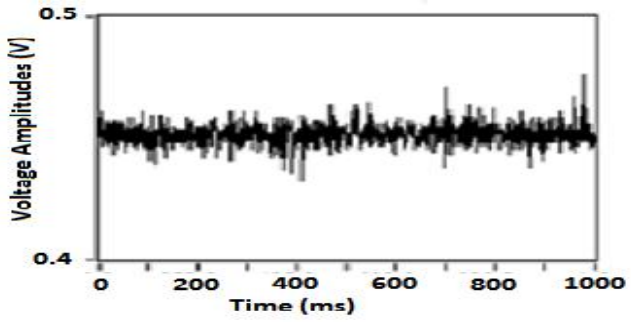

Fig. 3(a) Unfiltered detector voltage (V) obtained at labVIEW terminal versus time (ms).

The detector voltage curve at realtime obtained using Labview is shown in Fig. 3(a) while the filtered voltage for the same sample is shown in Fig. 3(b). The filtered voltage is obtained when the acquired signal by the DAQ is fed to a butterworth filter and then observed with a scope.

Results show that, the work plot produced a high degree of accuracy with the correlation coefficient R2 of 0.996 and a percentage error of 8%.

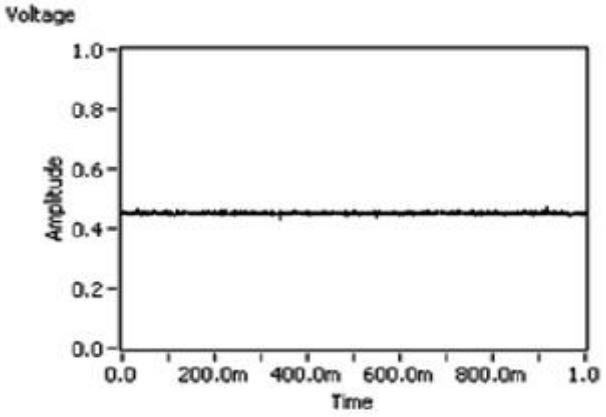

Fig. 3(b) Filtered detector voltage (V) obtained at LabVIEW terminal versus time (s).

V. CONCLUSION

The intensity of light from the source and the voltage obtained at the detector end forms a linear relationship as discussed in the paper for designing the sensor system for fluoride detection. Thus this is an intensity modulated optical sensor system with simple design and implementation. Unlike the conventional method that assesses ionic-strength and pH dependent fluoride ion activity in polluted water, the proposed sensors would directly measure fluoride levels.

It is also be possible to analyse and calculate the values of fluoride in water by interfacing the output of the transducer i.e., photodetector with computers. Smart detection processes using Artificial Neural Networks will be designed in the same project in the future work.

This newly developed optical sensor system produced a high degree of accuracy with the correlation coefficient (R^2) of 0.996. This study has proven that visible lasers are better for sensing water pollutants than the conventional chemical analysis methods. This new methodology is very useful for measuring the fluoride levels in water. The use of LabVIEW to acquire optical sensor data; and thus results obtained for real time monitoring of pollutants concentration using PC was encouraging.

The novel optical sensor can by optimally used for water pollution level information in Guwahati city and also equally at other places as it is versatile and one can test any heavy metal ion or any anion simply by varying the laser source rating. This sensor system can be used by many sectors such

as tourism, environmental department; public sectors and others related sectors. This can be of great help in estimating fluoride content of water bodies in both urban and rural areas. Moreover the accuracy of the system has been found to be of industry standard with less than 10% error.

ACKNOWLEDGMENT

The authors would like to show their gratitude to the Department of Electrical and Electronics Engineering, Assam Don Bosco University for providing the platform for all experimental works and specially to Prof. Manoranjan Kalita, Principal, Don Bosco College Of Engineering and Technology for his whole hearted support and inspirations. Finally, the authors offer their acknowledgment to the Chemistry departments of both Assam Don Bosco University and Guwahati University for providing the opportunity and assisting the authors in carrying out the chemical analysis of the data collected.

REFERENCES

[1] Eric Udd, "Fiber Optic Sensors: An Introduction for Engineers and Scientists", Wiley-Interscience, vol. ED-I, March 13, 1991

[2] L.S. Grattan, B.T. Meggitt, "Optical Fiber Sensor Technology: Volume 4: Chemical and Environmental Sensing", Kluwer Academic Publishers, 1998.

[3] Holst G., Mizaikoff B., "Fiber Optic Sensors for Environmental Sensing: Handbook of opticalfiber sensing technology",John Wiley & Sons Ltd., 2001.

[4] Fidanboylu, K and Efendioglu, H. S, "Fiber Optic Sensors And Their Applications", 5th International Advanced Technologies Symposium (IATS'09), Karabuk, Turkey, May 13-15, 2009.

[5] Radhakrishnan J, El-Sherif M. A., "Analysis on spatial intensity modulation for fiber optic sensorApplications", Optical Fiber Technology, Vol. 2, Number 1, 114-126, 1996.

[6] P. Suresh Kumar, C. P. G.Vallabhan, V. P. N.Nampoori, V. N.SivasankaraPillai and P.Radhakrishnan, "A fibre optic evanescent wave sensor used for the detection of trace nitrites in water", Journal Of Optics A: Pure And Applied Optics, Vol. 4, 247-250, 2002.

[7] M. O'Toole, D. Diamond, "Absorbance Based Light Emitting Diode Optical Sensors and Sensing Devices", Sensors 2008, 8, 2453-2479.

[8] A. B. Utkin et al, 'Optical methods for water pollution monitoring'.

[9] "Ground Water Quality in Greater Guwahati, Assam with reference to Trace Elements", *National* Institute of Hydrology, Roorkee.

[10] N.Linthoingambi Devi et al, "Recent Status of Arsenic Contamination in Groundwater of Northeastern India–A Review", School of Environmental Studies, China University of Geosciences,P.R. China.

[11] Sutapa Chakrabarty, Hari Prasad Sarma, "Fluoride, iron and nitrate contaminated drinking water in Kamrup district, Assam, India", Archives of Applied Science Research, 3(4):186-192 2011.

[12] Times of India, Guwahati Edition, June 2, 2011.

Tridiv Medhi was born in Golaghat, India, in 1989. At present, he is pursuing his B. Tech degree in Electrical and Electronics engineering from Assam Don Bosco University.

His research interest includes design of optimal sensor for level of water pollutant detection using labVIEW, comparative study on the techniques and equipments used in earlier day substations and modern day substations.

Tipu Kumar Prithani was born in Dibrugarh,India,in 1989. Presently, he is pursuing his B.Tech in Electrical and Electronics Department from Don Bosco College Of Engineering And Technology under Assam Don Bosco University.

His research interest is on Detection of water pollutants using Optical sensing technique and simulation using labVIEW which is a comparative study based on traditional and modern methods.

Parismita Das was born in 1990 at Barpeta. Presently,she is pursuing her B.Tech in Electrical And Electronics Department under Assam Don Bosco University.

Her research interest is on Detection of water pollutants using Optical sensing technique and simulation using labVIEW which is a comparative study based on traditional and modern methods of fiber optic sensors.

Bikramjit Goswami was born in Guwahati, India in 1981. He received his B.E. degree in Electrical Engineering from Assam Engineering College in 2003 and M.Tech degree in Electronics And Communication Engineering in 2012.He is currently pursuing his Ph.D under Assam Don Bosco University.

His Research interests includes developement of reconfigurable antenna design using ANN,optical sensing and detection of biomedical and environmental entities and microwave remote sensing**.**

Dr. Shakuntala Laskar obtained her graduation in Electrical Engineering from Assam Engineering College. She pursued M.Tech and Ph.d from IIT,Kharagpur in the year 1987 and 2002 respectively.Presently she is working as professor and head of EEE department in Don Bosco College Of Engineering And Technology.

Her research work includes-optoelectronics and optical communication, instrumentation design and simulation, electromechanical energy conversion and optimization, sensors and actuators.

A Low-Power Single-Phase Clock Multiband Flexible Divider

R.MAHESH KUMAR and PANEM.CHARAN ARUR

Abstract—In this paper, a low-power single-phase clock multiband flexible divider for Bluetooth,Zigbee and IEEE 802.15.4 and 802.11a/b/g WLAN frequency synthesizers is proposed based on pulse-swallow topology and is implemented using a 0.18- m CMOS technology. The multiband divider consists of a proposed wideband multimodulus 32/33/47/48 prescaler and an improved bit-cell for swallow (S) counter and can divide the frequencies in the three bands of 2.4–2.484 GHz, 5.15–5.35 GHz, and 5.725–5.825 GHz with a resolution selectable from 1 to 25MHz. The proposed multiband flexible divider is silicon verified and consumes power of 0.96 and 2.2mW in 2.4- and 5-GHz bands, respectively, when operated at 1.8-V power supply.

Index Terms—DFF, dual modulus prescaler, dynamic logic, E-TSPC, frequency synthesizer, high-speed digital circuits, true single-phase clock(TSPC), wireless LAN (WLAN).

I. INTRODUCTION

WirelessLAN (WLAN) in the multigigahertz bands, such as HiperLAN II and IEEE 802.11a/b/g, are recognized as leading standards for high-rate data transmissions, and standards like IEEE 802.15.4 are recognized for low-rate data transmissions. The demand for lower cost, lower power, and multiband RF circuits increased in conjunction with need of higher level of integration. The frequency synthesizer, usually implemented by a phase-locked loop (PLL), is one of the power-hungry blocks in the RF front-end and the first-stage frequency divider consumes a large portion of power in a frequency synthesizer. The integrated synthesizers for WLAN applications at 5 GHz CMOS realizations, where the first-stage divider is implemented using an injection-locked divider which consumes large chip area and has a narrow locking range. The best published frequency synthesizer at 5 GHz consumes 9.7mWat 1-V supply, where its complete divider consumes power around 6mW [3], where the first-stage divider is implemented using the source-coupled logic (SCL) circuit [4], which allows higher operating frequencies but uses more power. Dynamic latches are faster and consume less power compared to static dividers. The TSPC [5] and E-TSPC [6] designs are able to drive the dynamic latch with a single clock phase and avoid the skew problem [5]. However, the adoption of single-phase clock latches in frequency dividers has been limited to PLLs with applications below 5 GHz [7], [8].

R.MAHESH KUMAR, is working as Assistant Professor, Department of ECE, AITS Rajampet, e-Mail:r.mahesh.1021@gmail.com, PH.NO:+919885495443 and PANEM.CHARAN ARUR is a M.TECH Research Scholar, AITS Rajampet,e-Mail:panem.charan@gmail.com, PH.NO:+918008179453.

The frequency synthesizer reported in [6] uses an E-TSPC prescaler as the first-stage divider, but the divider consumes around 6.25mW. Most IEEE 802.11a/b/g frequency synthesizers employ SCL dividers as their first stage [3], [9], while dynamic latches are not yet adopted for multiband synthesizers. In this paper, a dyamic logic multiband flexible Fig. 1. Proposed dynamic logic multiband flexible divider integer-N divider based on pulse-swallow topology is proposed which uses a low-power wideband 2/3 prescaler [10] and a wideband multimodulus 32/33/47/48 prescaler as shown in Fig. 1. The divider also uses an improved low-power loadable bit-cell for the Swallow S-counter.

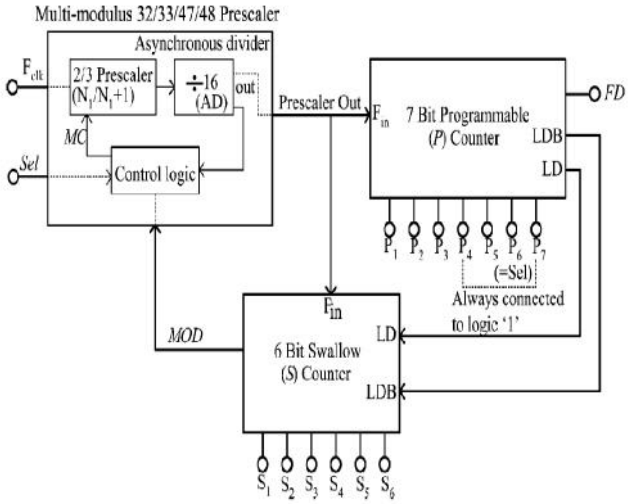

Fig.1. Proposed dynamic logic multiband flexible divider.

II. DESIGN CONSIDERATIONS

The key parameters of high-speed digital circuits are the propagation delay and power consumption. The maximum operating frequency of a digital circuit is calculated by the method described in [11] and is given by

$$F_{max} = \frac{1}{T_{plh} + T_{phl}} \quad (1)$$

where Tplh and Tphl are the propagation delays of the low-to-high and high-to-low transitions of the gates, respectively. The total power consumption of the CMOS digital circuits is determined by the switching and short circuit power.

The switching power is linearly proportional to the operating frequency and is given by the sum of switching power at each output node as in

$$P_{switch}=\sum_{I=1}^{n} F_{clk}\, C_{li}\, V_{dd}^2 \qquad (2)$$

Where n is the number of switching nodes, Fclk is the clock frequency, Cli is the load capacitance at the output node of the ith stage, and Vdd is the supply voltage. Normally, the short-circuit power occurs in dynamic circuits when there exists direct paths from the supply to ground which is given by

$$P_{sc} = I_{sc} * V_{dd} \qquad (3)$$

Where Isc is the short-circuit current. The analysis in [12] shows that the short-circuit power is much higher in E-TSPC logic circuits than in TSPC logic circuits. However, TSPC logic circuits exhibit higher switching power compared to that of E-TSPC logic circuits due to high load capacitance. For the E-TSPC logic circuit, the short-circuit power is the major problem. The E-TSPC cicuit has the merit of higher operating frequency than that of the TSPC circuit due to the reduction in load capacitance, but it consumes significantly more power than the TSPC circuit does for a given transistor size. The following analysis is based on the latest design using the popular and low-cost 0.18um CMOS process.

III. WIDEBAND E-TSPC 2/3PRESCALER

The E-TSPC 2/3 prescaler reported in [12] consumes large shortcircuit power and has a higher frequency of operation than that of TSPC 2/3 prescaler. The wideband single-phase clock 2/3 prescaler used in this design was reported in [10] which consists of two D-flip-flops and Fig. 2. Wideband single-phase clock 2/3 prescaler. Two NOR gates embedded in the flip-flops as in Fig. 2. The first NOR gate is embedded in the last stage of

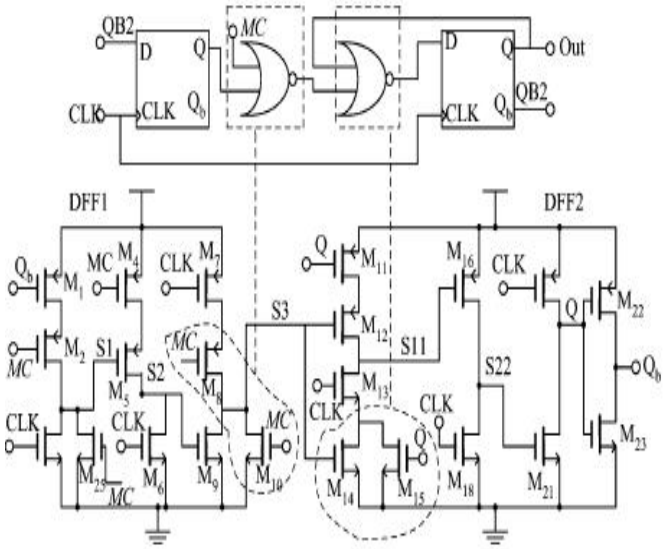

Fig.2. Wideband single phase clock 2/3 prescalar.

DFF1, and the second NOR gate is embedded in the first stage of DFF2 . Here, the transistors M2, M25, M4, andM8 in DFF1 helps to eliminate the short-circuit power during the divide-by-2 operation. The switching of division ratios between 2 and 3 is controlled by logic signal MC.

When MC switches from "0" to "1," transistors M2, M4, and M8 in DFF1 turns off and nodes S1, S2 and S3 switch to logic "0." Since node S3 is "0" and the other input to the NOR gate embedded in DFF2 is Qb, the wideband prescaler operates at the divide-by-2 mode. During this mode, nodes S1, S2 and S3 switch to logic "0" and remain at "0" for the entire divide-by-2 operation, thus removing the switching power contribution of DFF1. Since one of the transistors is always OFF in each stage of DFF1, the short-circuit power in DFF1 and the first stage of DFF2 is negligible. The total power consumption of the prescaler in the divide-by-2 mode is equal to the switching power in DFF2 and the short-circuit power in second and thirrd stages of DFF2 and is given by

$$P_{swittch\_divided\_by\_2}=\sum_{I=1}^{4} F_{clk}\, C_{Li}\, V_{dd}^{2} + P_{sc1} + P_{sc2}$$

Where CLi is the load capacitance at the output node of the ith stage of DFF2, and Psc1 and Psc2 are the short-circuit power in the second and third stages of DFF2. When logic signal MC switches from "1" to "0," the logic value at the input of DFF1 is transferred to the input of DFF2 as one of the input of the NOR gate embedded in DFF1 is "0" and the wideband prescaler operates at the divide-by-3 mode. During the divide-by-2 operation, only DFF2 actively participates in the operation and contributes to the total power consumption since all the switching activities are blocked in DFF1. Thus, the wideband 2/3 prescaler has benefit of saving more than 50% of power during the divide-by-2 operation. The measured results shows that the wideband 2/3 prescaler has the maximum operating frequency of 6.5 GHz. Fig. 3 shows the simulated and measured power consumption of the wideband 2/3 prescaler at different frequencies for a supply voltage of 1.8 V.

IV. MULTIMODULUS 32/33/47/48 PRESCALER

The proposed wideband multimodulus prescaler which can divide the input frequency by 32, 33, 47, and 48 is shown in Fig. 4. It is similar to the 32/33 prescaler used in [7], but with an additional inverter and a multiplexer. The proposed prescaler performs additional divisions (divide-by-47 and divide-by-48) without any extra flip-flop, thus saving a considerable amount of power and also reducing the complexity of Fig. 3. Post layout and measured power consumption results of 2/3 prescaler.

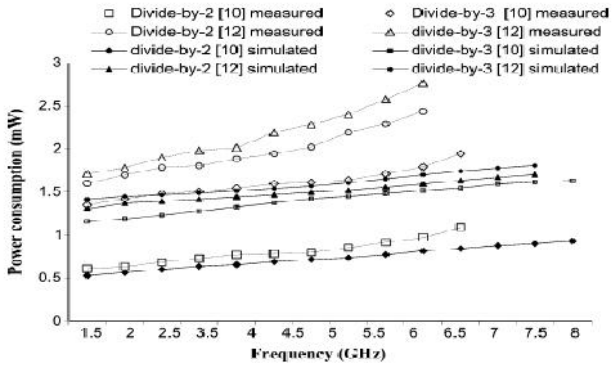

Fig.3. post layout and measured power consumption results of 2/3 prescaler.Fig. 4. Proposed multimodulus 32/33/47/48 Prescaler. Multiband divider which will be discussed in Section V. The multimodulus prescaler consists the wideband2/3(N1/(N1+1))prescaler[10],four asynchronous TSPC divide-by-2 circuits (AD=16) and combinational logic circuits to achieve multiple division ratios. Beside the usual MOD signal for controlling (N1/N1+1) divisions, the additional control signal Sel is used to switch the prescaler between 32/33 and 47/48 modes.

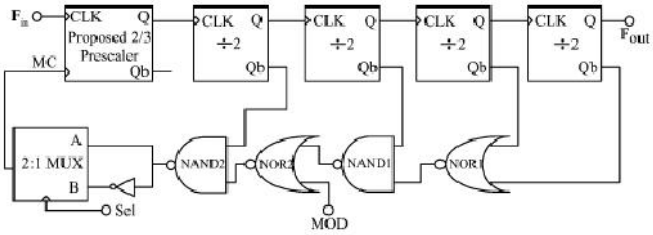

Fig.4.Proposed mltimodulus 32/33/47/48 prescaler.

A. Case 1: Sel='0'

When Sel=0 , the output from the NAND2 gate is directly transferred to the input of 2/3 prescaler and the multimodulus prescaler operates as the normal 32/33 prescaler, where the division ratio is controlled by the logic signal MOD. If MC=1, the 2/3 prescaler operates in the divide-by-2 mode and when MC=0 , the 2/3 prescaler operates in the divide-by-3 mode. If MOD=1, the NAND2 gate output switches to logic "1" (MC=1) and the wideband prescaler operates in the divide-by-2 mode for entire operation. The division ratio N performed by the multimodulus prescaler is

$$N=(AD*N1)+(0*(N1+1))=32 \quad (6)$$

Where N1=1 and AD=16 is fixed for the entire design. If MOD=0 , for 30 input clock cycles MC remains at logic "1", where wideband prescaler operates in divide-by-2 mode and, for three input clock cycles, MC remains at logic "0" where the wideband prescaler operates in the divide-by-3 mode. The division ratio N+1 performed by the multimodulus prescaler is

$$N+1=((AD-1)*N1)+(1*(N1+1))=33 \quad (7)$$

B. Case 2: Sel=1

When Sel=1, the inverted output of the NAND2 gate is directly transferred to the input of 2/3 prescaler and the multimodulus prescaler operates as a 47/48 prescaler, where the division ratio is controlled by the logic signal MOD. If MC=1, the 2/3 prescaler operates in divide-by-3 mode and when Sel=1, the 2/3 prescaler operates in divide-by-2 mode which is quite opposite to the operation performed when Sel=0. If MOD=1, the division ratio N+1 performed by the multimodulus prescaler is same as (6) except that the wideband prescaler operates in the divide-by-3 mode for the entire operation given by

$$N+1=(AD*(N1+1))+(0*N1)=48 \quad (8)$$

If MOD=1, the division ratio N performed by the multimodulus prescaler is

$$N=((AD-1)*(N1+1))+(1*N1)=47 \quad (9)$$

V. MULTIBAND FLEXIBLE DIVIDER

The single-phase clock multiband flexible divider which is shown in Fig. 1 consists of the multimodulus 32/33/47/48 prescaler, a 7-bit programmable P-counter and a 6-bit swallow S-counter. The multimodulus 32/33/47/48 prescaler is briefly discussed in Section IV. The control signal Sel decides whether the divider is operating in lower frequency band (2.4 GHz) or higher band (5–5.825 GHz).

A. Swallow ___ Counter

The 6-bit S-counter shown in Fig. 5 consists of six asynchronous loadable bit-cells, a NOR-embedded DFF and additional logic gates to allow it to be programmable from 0 to 31 for low-frequency band and from 0 to 47 for the high-frequency band. The asynchronous bit-cell used in this design shown in Fig. 6 is similar to the bit-cell reported in [13], except it uses two additional transistors M6 and M7 whose inputs are controlled by the logic signal MOD. If MOD is logically high, nodes S1 and S2 switch to logic "0" and the bit-cell does not perform any function. The MOD signal goes logically high only when the S-counter finishes counting down to zero. If MOD and LD are logically low, the bit-cell acts as a divide-by-2 unit. If MOD is logically low and LD is logically high, the input bit PI is transferred to the output.

In the initial state, MOD, the multimodulus prescaler selects the divide-by-(N+1) mode (divide-by-33 or divide-by-48) and P,S counters start down counting the input clock cycles. When the S-counter finishes counting, MOD switches to logic "1" and the prescaler changes to the divide-by-N mode (divide-by-32 or divide-47) for the remaining (P-S)clock cycles. During this mode, since S-counter is idle, transistors M6 and M7 which are controlled by MOD, keep the nodes S1 and S2 at logic "0," thus saving the switching power in S-counter for a period of (N*(P-S)) clock cycles. Here, the programmable input (PI) is used to load the counter to a specified value from 0 to 31 for the lower band and 0 to 48 for the higher band of operation.

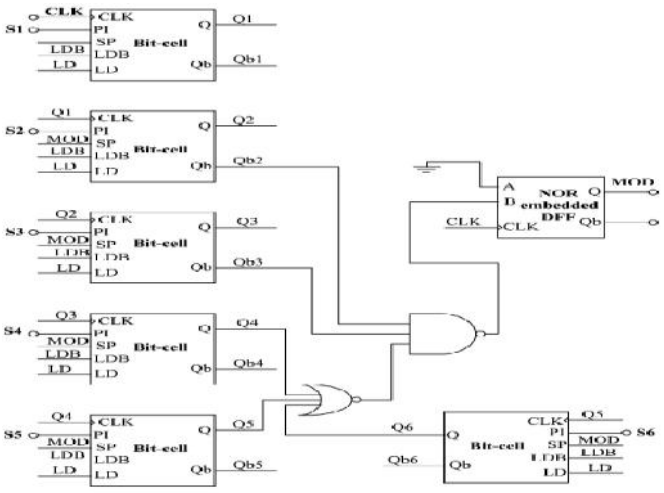

Fig.5. Asynchronous 6-bit S-counter.

B. Programmable (P) *Counter*

The programmable P-counter is a 7-bit asynchronous down counter which consists of 7 loadable bit-cells [13] and additional logic gates
as in [7]. Here, bit P7 is tied to the Sel signal of the multimodulus prescaler and bits P4 and P7 are always at logic "1." The remaining bits can be externally programmed from 75 to 78 for the lower
frequency band and from 105 to 122 for the upper frequency band. When the S-counter finishes counting down to zero, LD switches to logic "1" during which the output of all the bit-cells in S-counter switches to logic "1" and output of the NOR embedded DFF switches to logic "0" (MOD=0)where the programmable divider get reset to its initial state and thus a fixed division ratio is achieved. If a fixed dual-modulus prescaler is used, a 7-bit _-counter is needed for the low-frequency band (2.4 GHz) while an 8-bit P-counter would be needed for the high-frequency band (5–5.825 GHz) with a fixed 5-bit S-counter. Thus, the multimodulus 32/33/47/48 prescaler eases the design complexity of the P-counter.

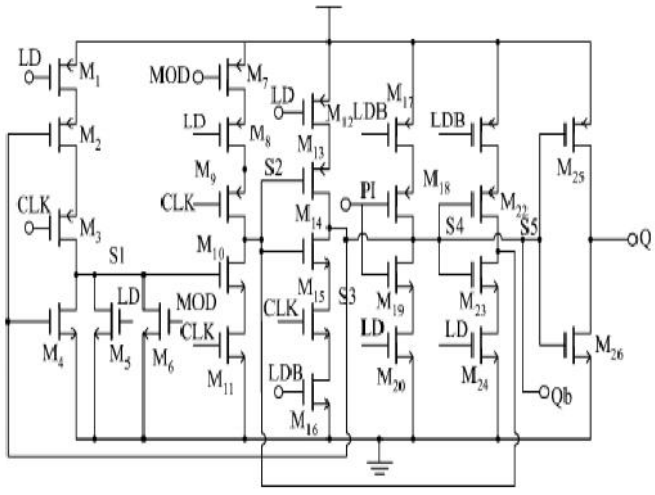

Fig.6. Asynchronous loadable bit-cell for S-counter.

1) Sel=0 *(2.4–2.484 GHz):* When logic signal Sel=0, the multimodulus prescaler acts as a 32/33 prescaler, the S-counter is programmable from 64 to 127 (bit Pt of the P-counter always remains at logic "1"), and the P-counter is programmable from 0 to 31 to accommodate division ratios from 2048 to 4095 with finest resolution of 1 MHz However, since we are interested in the 2.4-GHz band, bit Po of the P-counter always remains at logic "0," since it is tied to the logic signal Sel, allowing it to be programmable from 75 to 78. Bit S6 of the S-counter is kept at logic '0' (to satisfy the conditions N>S), allowing a programmable division from 0 to 31 for the low-frequency Fig. 7. Die photograph of the proposed multiband divider. band of operation to accommodate division ratios between 2400 and 2484 with a resolution of 1 MHz for Bluetooth and Zigbee applications [7] and 5 MHz for the IEEE 802.15.4 frequency synthesizer [8] with a fixed reference frequency of 1 MHz Since the finest resolution and reference frequency is 1 MHz; different channel spacing can be achieved by programming S-counter in steps of 1. For example, a 5-MHz channel spacing is achieved by programming S-counter in steps of "5" keeping the flexible divider resolution and reference frequency
to 1 MHz The frequency division (FD) ratio of the multiband divider in this mode is given by

$$FD=(N+1)*S+N*(P-S)=NP+S \quad (10)$$

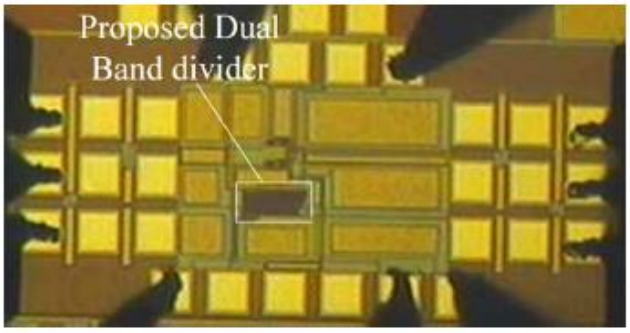

Fig.7.Die photograph of the proposed multiband divider.

*2) S*el= *(5–5.825 GHz):* When logic signal Sel=1 , the multimodulus prescaler acts as a 47/48(N/(N+1)) prescaler, the P-counter is programmable from 64 to 127 (bit P7 of the P-counter always remains at logic "1"), and the S-counter is programmable from 0 to 48 to accommodate division ratios from 3024 to 6096 with finest resolution of 1 MHz However, since we are interested in 5–5.825 GHz band, bit P6 of the P-counter always remains at logic "1," allowing it
to be programmable from 105 to 122. The S-counter is programmable from 0 to 48 for the high frequency band of operation to accommodate division ratios between 5000 and 5825 with a resolution of 5 MHz, 10 MHz or 20 MHz for IEEE 802.11a/b/g synthesizers [1]–[3], [6],[9].Since finest resolution and reference frequency is 1 MHz, S-counter is programmed in steps of '5', '10' or '20', and _-counter programmed from 105 to 122 in steps of '1' to provide channel spacing of 5 MHz, 10MHz or 20 MHz The frequency division (FD) ratio of the multiband divider in this mode is given by

$$FD=(N*S)+(N+1)*(P-S)=(N+1)P-S \quad (11)$$

VI.SIMULATIONS AND SILICON VERIFICATIONS

The simulations of the designs are performed using Cadence SPECTRE RF for a 0.18um CMOS process. The simulation results show that the wide band 2/3 prescaler has the maximum operating frequency of 8 GHz with a power consumption of 0.92 and 1.73 mW during the divide-by-2 and divide-by-3 modes, respectively. The proposed wide band multimodulus prescaler has the maximum operating frequency of 7.2 GHz (simulation) with power consumption of 1.52, 1.60, 2.10, and 2.13 mW during the divide-by-32, divide-by-33, divide-by-47 and divide-by-48, respectively. For silicon verification, the multiband divider is fabricated using the Global Foundries 1P6M 0.18-m CMOS process and the die photograph is shown in Fig. 7. On-wafer measurements are carried out using an 8 inch RF probe station. The input signal for the measurement is provided by the 83650B 10 MHz-50 GHz HP signal generator and the output signals are captured by the Lecroy Wavemaster 8600A 6G oscilloscope. The measurement results shows that the wideband 2/3 prescaler has a maximum operating frequency of 6.5 GHz [10] and the multimodulus.

Design Parameters	[6]	[12]	This work
Process (μm)	0.18	0.18	0.18
supply voltage (V)	1.8	1.8	1.8
Max.Frequency (GHz) (Sim/Measured)	6.7 / -	7.5 / 6	8 / 6.5
Power(mW) (sim/measured) Divide-by-2 mode	1.88 / -	1.63 / 2.2	0.82 / 0.97
Power(mW) (sim/measured) Divide-by-3 mode	2.18 / -	1.85 / 2.62	1.61 / 1.78

Table I Performance of different 2/3 prescalers at 2.5 GHz.

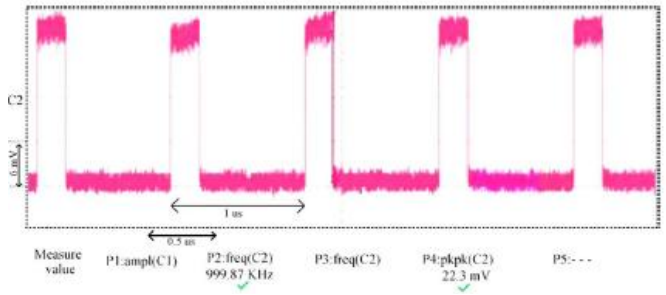

(a)

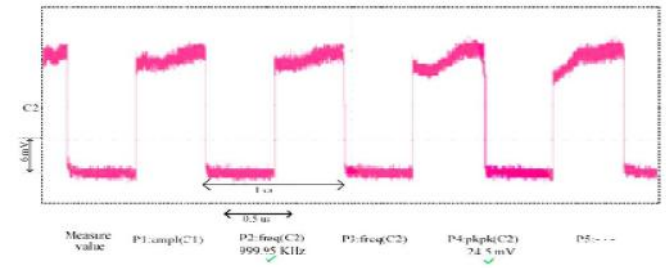

(b)

Fig. 8. Measured results of a dual-band divider. (a) 2.4-GHz band. (b) 5-GHz band.

32/33/47/48 prescaler designed using wideband 2/3 prescaler has maximum operating frequency of 6.2 GHz. However, the maximum operating frequency that can be achieved by the multimodulus 32/33/47/48 prescaler is limited by the wideband 2/3 prescaler. Table I shows the performance of proposed 2/3 prescaler and prescalers reported in [6] and [12] (resimulated). The performance of the multiband flexible divider is measured in both the lower frequency and higher frequency bands by programming the P- and S-counters. Fig. 8(a) shows the measured output waveform of the multiband divider at an input frequency of 2.47 GHz where P,S-counters are programmed to have values 77 and 6 respectively (FD=2470). Fig. 8(b) shows the measured output waveform of the multiband divider at an input frequency of 5.818 GHz where P-counters are programmed to have values 122 and 38, respectively (FD=5818). The proposed multiband flexible divider consumes an average power of 0.96 mW during lower frequency band (2.4–2.484 GHz), while it consumes 2.2 mW during the high-frequency band (5–5.825 GHz) of operation compared to the dual-band divider reported in [9], which consumes 2.7 mW at 1-V power supply. The proposed multiband divider has a variable resolution of K-MHz for lower frequency band (2.4–2.484 GHz) and for the higher frequency

Band (5–5.825 GHz), where K is integer from 1 to 5 for 2.4-GHz band and 5, 10, and 20 for WLAN applications. Table II shows the performance of different dividers.

Reference	[9]	[6]	This work
process (μm)	0.18	0.25	0.18
supply voltage (V)	1.0	1.8	1.8
Frequency range (GHz)	2.4-2.7 / 5.14-5.7	5.14-5.7	2.4-2.484 / 5-5.825
Resolution (MHz)	9.375 / 20	20	1,2,5,10,20
Power(mW)	2.7	6.25	0.96 / 2.2

Table. II. Performance of different dividers.

VII. CONCLUSION

In this paper, a wideband 2/3 prescaler is verified in the design of proposed wide band multimodulus 32/33/47/48 prescaler. A dynamic logic multiband flexible integer-N divider is designed which uses the wideband 2/3 prescaler, multimodulus 32/33/47/48 prescaler, and is silicon verified using the 0.18um CMOS technology. Since the multimodulus 32/33/47/48 prescaler has maximum operating frequency of 6.2 GHz, the values of P- and S-counters can actually be programmed to divide over the whole range of frequencies from 1 to 6.2 GHz with finest resolution of 1 MHz and variable channel spacing. However, since interest lies in the 2.4- and 5–5.825-GHz bands of operation, the P- and S-counters are programmed accordingly. The proposed multiband flexible divider also uses an improved loadable bit-cell for

Swallow _-counter and consumes a power of 0.96 and 2.2 mW in 2.4- and 5-GHz bands, respectively, and provides a solution to the low power PLL synthesizers for Bluetooth, Zigbee, IEEE 802.15.4, and IEEE 802.11a/b/g WLAN applications with variable channel spacing.

REFERENCES

[1] H. R. Rategh *et al.*, "A CMOS frequency synthesizer with an injected locked frequency divider for 5-GHz wirless LAN receiver," *IEEE J.Solid-State Circuits*, vol. 35, no. 5, pp. 780–787, May 2000.

[2] P. Y. Deng *et al.*, "A 5 GHz frequency synthesizer with an injection locked frequency divider and differential switched capacitors," *IEEE Trans. Circuits Syst. I, Reg. Papers*, vol. 56, no. 2, pp. 320–326, Feb. 2009.

[3] L. Lai Kan Leung *et al.*, "A 1-V 9.7-mW CMOS frequency synthesizer for IEEE 802.11a transceivers," *IEEE Trans. Microw. Theory Tech.*, vol. 56, no. 1, pp. 39–48, Jan. 2008.

[4] M. Alioto and G. Palumbo, *Model and Design of Bipolar and MOS Current-Mode Logic Digital Circuits*. New York: Springer, 2005. **Fir**.

[5] Y. Ji-ren *et al.*, "Atrue single-phase-clock dynamicCMOScircuit technique," *IEEE J. Solid-State Circuits*, vol. 24, no. 2, pp. 62–70, Feb.1989.

[6] S. Pellerano *et al.*, "A 13.5-mW 5 GHz frequency synthesizer with dynamic-logic frequency divider," *IEEE J. Solid-State Circuits*, vol. 39, no. 2, pp. 378–383, Feb. 2004.

[7] V. K. Manthena *et al.*, "A low power fully programmable 1 MHz resolution 2.4 GHz CMOS PLL frequency synthesizer," in *Proc. IEEE Biomed. Circuits Syst. Conf.*, Nov. 2007, pp. 187–190.

[8] S. Shin *et al.*, "4.2 mW frequency synthesizer for 2.4 GHz ZigBee application with fast settling time performance," in *IEEE MTT-S Int. Microw. Symp. Dig.* , Jun. 2006, pp. 411–414.

[9] S. Vikas *et al.*, "1 V 7-mW dual-band fast-locked frequency synthesizer," in *Proc. 15th ACM Symp. VLSI*, 2005, pp. 431–435.

[10] V. K. Manthena *et al.*, "A 1.8-V 6.5-GHz low power wide band singlephase clock CMOS 2/3 prescaler," in *IEEE 53rd Midwest Symp. Circuits Syst.*, Aug. 2010, pp. 149–152.

[11] J. M. Rabaey *et al.*, "Digital integrated circuits, a design perspective," in *Ser. Electron and VLSI*, 2nd ed. Upper Saddle River, NJ: Prentice- Hall, 2003.

[12] X. P. Yu *et al.*, "Design and optimization of the extended true singlephase clock-based prescaler," *IEEE Trans. Microw. Theory Tech.*, vol. 56, no. 11, pp. 3828–3835, Nov. 2006.

[13] X. P. Yu *et al.*, "Design of a low power wideband high resolution programmable frequency divider," *IEEE Trans. Very Large Scale Integr. (VLSI) Syst.*, vol. 13, no. 9, pp. 1098–1103, Sep. 2005.

R.MAHESH KUMAR, *Assistant Professor,* ***Department of ECE,*** Annamacharya Institute Of Technology And Science, Rajampet, YSRKadapa, Andhrapradesh, India. Attended Internatial and National level Conferences, Workshops, Faculty trainingprogrammes. Project review committee number in AITS. Published International Journals in Electronics and Communication,did the Research on Core Side.

PANEM CHARANARUR, M.TechIn VLSI System Design At Annamacharya Institute Of Technology AndScience, Rajampet, YSRKadapa,Andhrapradesh,India.PartcipatedNationalLevel Conference And Workshops On VLSI Current Trends.

An Integrated Model of Clustering and Routing in Wireless Sensor Networks

Arun Thangavel and Yuvarani B

Abstract: Nowadays, the applications of wireless sensor networks for industrial purpose have been rapidly increased. However, the main limitation is power consumption. As communication typically accounts for the major power consumption, the activity of the transceiver should be minimized, in order to prolong the network lifetime. To this end, this paper proposes an integration technique with sleep protocol for efficient power management along with an load balancing concept. This provides sleep schedules of nodes to match the network demands, even in time-varying operating conditions. In addition, it does not require any a-priority knowledge of the network topology or traffic pattern. Also the load balancing reduces the prolonged usage of a particular node. Additionally, the paper includes the efforts carried out on developing optimization techniques in the area of routing protocols for wireless sensor networks. Another approach to extend Wireless Sensors Networks (WSN) lifetime is to use mobile sinks to increase message delivery latency.

Keywords: **Data Acquisition, Energy, Load Balancing, Lifetime, Mobile Sinks, Message Delivery Latency, Sensor Nodes, Wireless Sensor Networks.**

I. INTRODUCTION

A wireless ad-hoc network is a decentralized type of network. The network is ad hoc because it is an backbone less network, such as routers in wired networks or access points in managed (infrastructure) wireless networks. Instead, each node participates in routing by forwarding data for other nodes, and so the determination of which nodes forward data is made dynamically based on the network connectivity. In addition to the classic routing, ad hoc networks can use flooding for forwarding the data. An ad hoc network typically refers to any set of networks where all devices have equal status on a network and are free to associate with any other ad hoc network devices in link range. Very often, ad hoc network refers to a mode of operation of IEEE 802.11 wireless networks. It also refers to a network device's ability to maintain link status information for any number of devices in a 1 link (aka "hop") range, and thus this is most often a Layer 2 activity.

This is only a Layer 2 activity; ad hoc networks alone may not support a routable IP network environment without additional Layer 2 or Layer 3 capabilities. The earliest wireless ad-hoc networks were the "packet radio" networks (PRNETs) from the 1970s, sponsored by DARPA after the ALOHA net project.

Arun Thangavel is with M.E- Applied Electronics, Department of Electrical Engineering, K. S. R. College of Engineering, Tiruchengode and Yuvarani B is working as Assistant Professor, Department of Electrical Engineering, K. S. R. College of Engineering, Tiruchengode. Emails: ecearun.india@gmail.com , yuvasasib@gmail.com

The decentralized nature of wireless ad-hoc networks makes them suitable for a variety of applications where central nodes can't be relied on, and may improve the scalability of wireless ad-hoc networks compared to wireless managed networks, though theoretical and practical limits to the overall capacity of such networks have been identified. The presence of dynamic and adaptive routing protocols enables ad-hoc networks to be formed quickly. Wireless ad hoc networks can be further classified by their application:

- Mobile ad-hoc networks (MANET)
- Wireless mesh networks (WMN)
- Wireless Sensor networks (WSN)

Wireless Sensor Network

A wireless sensor network (WSN) consists of spatially distributed autonomous sensors to monitor physical or environmental conditions, such as temperature, sound, pressure, etc. and to cooperatively pass their data through the network to a main location. The more modern networks are bi-directional, also enabling control of sensor activity. The development of wireless sensor networks was motivated by military applications such as battlefield surveillance; today such networks are used in many industrial and consumer applications, such as industrial process monitoring and control, machine health monitoring, and so on.

The WSN is built of "nodes"– from a few to several hundreds or even thousands, where each node is connected to one (or sometimes several) sensors. Each such sensor network node has typically several parts: a radio transceiver with an internal antenna or connection to an external antenna, a microcontroller, an electronic circuit for interfacing with the sensors and an energy source, usually a battery. A sensor node might vary in size from that of a shoebox down to the size of a grain of dust.

The cost of sensor nodes is similarly variable, ranging from a few to hundreds of dollars, depending on the complexity of the individual sensor nodes. Size and cost constraints on sensor nodes result in corresponding constraints on resources such as energy, memory, computational speed and communications bandwidth. The topology of the WSNs can vary from a simple star network to an advanced multi-hop wireless mesh network.

II.PROTOCOL DESCRIPTION

This section presents the description of ASLEEP protocol. After a general overview, we will describe the core components of the protocol, i.e., the sleep prediction algorithm (used by each node to dynamically estimate the length of its expected active period), and the sleep coordination algorithm (used to enforce the new sleep

schedule throughout the network).Finally, we will introduce two mechanisms to improve the robustness of the protocol.

A.Protocol Overview

In the following we will refer to a data collection scenario where data typically flow from source nodes to the sink, while data from the sink to the sources are much less frequent. We will assume that nodes are organized to form a logical routing tree (or data gathering tree) rooted at the sink, and use an underlying CSMA (Carrier Sense Multiple Access) MAC protocol for communication. These assumptions are quite realistic, as most MAC protocols commonly used in WSNs are CSMA-based , and many popular routing protocols for WSNs rely on a routing tree. In a real deployment the routing tree is re-computed periodically to cope with possible topology changes and better share the energy consumption among nodes. However, as nodes are supposed to be static, we can assume that the routing tree remains stable for a reasonable amount of time. The communication between a parent and its children occurs in communication periods which repeat periodically. Each communication period includes an active interval during which nodes communicate by using the underlying MAC protocol, and a silence interval during which nodes turn their radio off to save energy. As shown in Figure 1, active intervals are staggered so that nodes at the lower levels in the routing tree wake up earlier than their ancestors. The active interval of each (intermediate) sensor node consists of two adjacent talk intervals (TI), the first one with its children and the other one with its parent2. Throughout, we will refer to the talk interval shared by a generic node j and all its children, during the m-th communication period.

Figure 1. Parameters of the sleep scheduling protocol.

During each communication period every parent node estimates the duration of the talk interval to share with its children in the next communication period by means of the algorithm B. Although parent nodes can independently set their talk interval, a collective effort is needed for the schedule of the whole network to remain consistent and energy efficient. Hence, as a result of a change in the talk interval of a single parent node, the network-wide schedule must be rearranged. This is accomplished by appropriately shifting active intervals of a number of nodes, so as to ensure that (i) the active intervals of all nodes are properly staggered, and (ii) the two talk intervals of each node are contiguous.

Two special messages, direct beacons and reverse beacons, are used for propagating schedule parameters to downstream and upstream nodes, respectively. Direct beacons are broadcast by every parent node to all its children during each communication period. Instead, reverse beacons are sent in the opposite direction, i.e., from a child to its parent. As it will be shown below, direct beacons are critical for the correctness of the protocol. Hence, ASLEEP also includes mechanisms for (i) increasing the probability of successful delivery of direct beacons, and (ii) enforcing a correct (even if non-optimal) behaviour of nodes in case they miss a direct beacon. In particular, to increase the probability of successful delivery, direct beacons are transmitted at the end of each talk interval, in a reserved time period (Beacon Period).

B.Talk Interval Prediction

In the ASLEEP protocol a sleep schedule is basically defined by the communication period and the talk interval of each individual parent node. The length of the communication period is closely related to the specific application and, thus, it is a global parameter specified by the sink when distributing the query. A variation in the communication period corresponds to a modification of the query, i.e. the new interval for the periodic data acquisition.

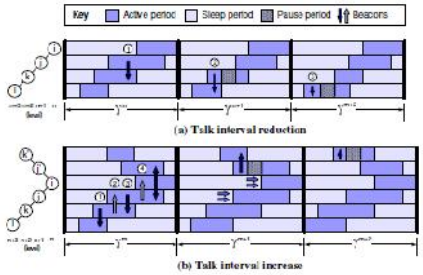

Figure 2.Examples of talk interval adaptation.

Choosing an appropriate talk interval is somewhat more involved. Ideally, each parent node should set the talk interval with its children to the minimum time needed to successfully receive all messages from all children. However, this time depends on a number of factors such as the underlying MAC protocol, channel conditions, degree of contention, and number of messages to be received, and so on. In its turn, the number of messages to be received by a sensor node depends on the number of its children, the message generation rate at source nodes, and the network topology. Therefore, computing the ideal talk interval would require the global knowledge of the network. Moreover this value should be continuously updated as the operating conditions change over time. Since such an approach is not practical, we propose here an adaptive technique that approximates this ideal scheme by letting every parent node to choose autonomously its own talk interval with its children. The decision involves only local information and, thus, it does not require knowing the network topology.

In principle, any algorithm can be used to estimate the expected talk interval in the next communication period. We used the simple algorithm discussed below. Each parent node measures and stores the following quantities.

• Message inter-reception time (Δ). This is the difference between the time instants at which two consecutive messages are correctly received.

• Number of received messages (npkt). The total number of messages correctly received in a single communication period.

A similar approach is employed also when a node increases the talk interval with its children. In this case, the node has to force its ancestors to defer their talk intervals, in order to accommodate the additional time required for communications. To this end, the node makes use of a reverse beacon, which is sent to its parent and forwarded up to the tree until the sink node is reached. Note that this step

is required to ensure the correctness of the protocol, i.e. that t he talk intervals of intermediate nodes do not overlap. As above, the example depicted in Figure 2-b will help understanding. Suppose that node k at the (n+2)-th level of the tree decides to increase the talk interval with its children, i.e., nodes at the (n+3)-th level (including node l). First, node k advertises the new talk interval to its children through the direct beacon (step 1). Second, in the same communication period, the node sends the reverse beacon (step 2) to its parent j at the (n+1)-th level, to force a talk interval shift ahead in time. Node j receives the reverse beacon, adjusts the parameters for the next communication period and advertises them, via the direct beacon (step 3), to its children. Because all ancestors have to shift their talk interval, node j also propagates the reverse beacon (step 4) up to its parent i at the n-th level. Note that in this case the schedule propagation impacts all nodes in the network. In fact, aside from the ancestors of the node which increases its talk interval, also other nodes can be involved in a transient phase which may require the introduction of a pause period. For instance, consider a node j' at the (n+1)-th level of the tree (illustrated in the second row of the scheme in the figure) which is not a direct ancestor of the node originating the new schedule. Its parent (i.e. node i) will shift ahead and advertise the new talk interval information during the m-th communication period. For reasons similar to the talk interval reduction, a pause period is introduced in the subtree rooted at nodes i, i.e. the nodes below the n-th level of the tree which are not direct ancestors of node k (which originated the new schedule). Assuming that (i) clocks of nodes are properly synchronized, and (ii) direct and reverse beacons never get lost, it can be shown that the following properties hold.

Property 1 (Schedule agreement). Child nodes wake up at the instant, and for the duration, enforced by their parent, even when talk intervals change.

Property 2 (Non overlapping schedules). For any two nodes i and j such that j is a child of i, the talk intervals i and j are not overlapped.

Property 3 (Adjacent schedules). In steady state conditions, the talk intervals shared by any node with its children and its parent, respectively, are contiguous.

C. *Schedule robustness Beacon Protection*

Beacon messages are critical for correctness of the protocol. When a node misses a direct beacon containing the new parameters, it cannot schedule its activity for the next communication period. In addition, the node cannot send direct beacons to its children until it re-acquires the correct schedule information. As a consequence, the loss of coordination propagates along the routing tree to its descendants. Direct beacons may get lost, for example, due to communication errors or collisions with other beacons or regular messages transmitted by interfering nodes. As direct beacons are sent through broadcast frames, they cannot be re-transmitted by the underlying MAC protocol. Instead, reverse beacons are unicast messages and, thus, they are retransmitted by the MAC protocol if not received correctly.

To add robustness to the direct beacon transmission and prevent collisions, the last part of the talk interval – referred to as *Beacon Period* – is reserved for the direct beacon transmission only. Child nodes must refrain from initiating regular message transmissions during the Beacon Period. In addition, the transmission of the direct beacon is initiated with a random back off delay. Finally, two back-to-back copies of the direct beacon are transmitted.

D. *Beacon Loss Compensation*

The Beacon Protection mechanism increases the probability that a direct beacon is successfully received by child nodes, but it does not solve the problem of direct-beacon losses. Therefore, we also devised the following mechanism to compensate the negative effects that derive from missing a direct beacon. Since talk intervals typically remain constant for a number of communication periods, when a node misses a direct beacon, it uses the current schedule parameters also in the next communication period. However, if the node misses the direct beacon even in the subsequent communication period, it remains awake until it re-acquires a new direct beacon.

Obviously, this heuristic produces a correct schedule if the parent node has not changed the talk interval in the meantime, which is true in almost all cases. Otherwise, it produces a non-optimal behaviour of the node (and its descendants as well) for a limited number of communication periods. The actual effect of a wrong prediction is different, depending on whether the talk interval has been increased or decreased. If a parent has reduced its talk interval, the corresponding child node wakes up earlier than the correct instant and we can now have overlapping schedules.

This results in energy wasting and useless message transmission that can potentially interfere with transmissions from other nodes. However, the child node remains awake until the end of the communication period and, very likely, receives a fresh direct beacon. On the other hand, if the talk interval has been increased, according to old schedule parameters, the child node wakes up at the right time but would go to sleep earlier than the correct instant.

However, since it missed the direct beacon in the previous communication period, it does not go to sleep until it receives a fresh direct beacon. Thus, it is very likely that it receives the new direct beacon almost immediately. If this is not the case, it will remain active until a new direct beacon is received.

III. LOAD BALANCING ALGORITHM

In a wsn, with a decentralized and heterogeneous structure, some nodes may have different capabilities of processing and batteries, imbalances of load can occur. Indeed, a more powerful node in term of processing capacity can become idle, because it has finished its work quickly while the others, less powerful, are occupied most of the time, consuming more energy. Powerful nodes capacity can be exploited by overloaded nodes if a fraction of their load is shared with them. If the difference between the heaviest loaded and the lightest loaded nodes is minimized, the average work execution time can be reduced, the energy of the nodes will be better exploited and the nodes lifetime can be extended. It is what contributes to the stability of the network topology that plays a principal role in different problems like: routing, scheduling, resource reservation etc. Load balancing is certainly one of the solutions for increasing the efficiency of applications and the network life time.

Load Balancing algorithms are designed essentially to distribute equally the load on nodes and maximize their utilization while minimizing the total task execution time.

This issue has been of considerable interest in the network research community when it comes to wired and wireless networks. It aims to guarantee that no node is under loaded or overloaded. It looks at setting up a uniform load on all nodes. Then, it is expanded in order to take into account new environments and new applications (large scale applications, multimedia applications, etc.). Compared to the wired networks, the mobile environments introduce new highly variable parameters such as limited resources, wireless link communication and mobility.

IV. IMPLEMENTATION AND EVALUATION

In this section, the implementation of the proposed schemes is given first. Then, the evaluated results on the proposed schemes are given.

A.*Implementation*

To evaluate the performance of ASLEEP, we implemented it by using the ns2 simulation tool.

B.Simulation setup

In both protocols of our analysis we referred to a network scenario consisting of 30-50 nodes randomly deployed over a 50x50 m2 area(as per existing authour's preferrence), with the sink placed at the center of the sensing area. Each node in the network generates a fixed number of messages per communication period, independent of its position on the routing tree. This scenario corresponds to a random deployment of sensor nodes over a given area for periodic reporting of sensed data, which is a typical case in monitoring applications. In such applications, data of interest (e.g., temperature, vibrations) are sensed and reported periodically to the sink node – data messages are typically short e.g., 10-20 bytes [11]. The sensing/communication period depends on the specific application.

TABLE 1. SIMULATION PARAMETERS

Parameter	Value	Parameter	Value
Communication Period (CP)	30 s	Average Error-Burst Size	5.7 ms
Message rate	1 msg/CP	Average Error-free Burst Size	46.2 ms
Message size	20 bytes	Observation window (L)	10 CPs
MAC frame size	40 bytes	TI time slot (q)	100 ms
Transmission Range	15 m	Beacon Period	60 ms
Carrier Sensing Range	30 m	TI decrease time threshold (L_{down})	5 CPs
Message Error/Loss Rate	10%	TI decrease threshold (g_{down})	2q (200 ms)

C.Analysis in dynamic conditions

To investigate the behaviour of ASLEEP in dynamic conditions we considered two different kinds of variation in the operating conditions.

• *Traffic pattern variation*. Sensor nodes start with a given message generation rate. Then, after some time, they increase significantly their message rate and, finally, they switch back to the original rate. This scenario may occur when sensors are requested to report an event with better fidelity (i.e., using a higher sampling rate or including additional physical quantities) for a limited time.

• *Topology variation*. These experiments start with an initial configuration where only one half of the nodes deployed in the sensing area report data. After some time, also the remaining nodes start reporting data. This scenario may occur when additional nodes are required to report data so as to observe the sensed phenomenon with increased spatial resolution.

The following performance indices are measured:

• Talk interval. Plotting the talk interval duration over time provides a graphical representation of the ability of the protocol to adapt to changing operating conditions.

• Duty-cycle, denotes the fraction of time a sensor node is active within a communication period .

• Transient time duration, defined as the number of communication periods from when the variation occurs to when the new talk interval stabilizes. We considered a talk interval as stable when it remains constant for more than L communication periods. This metric gives a measure of how quickly the protocol adapts to the new operating conditions.

V .RESULTS

Since the analysis in dynamic conditions is aimed at investigating how the protocol reacts to changes in the traffic pattern and network topology, we did not consider the effects of message errors/losses in this part. This allow us to better understand the behavior of the protocol.

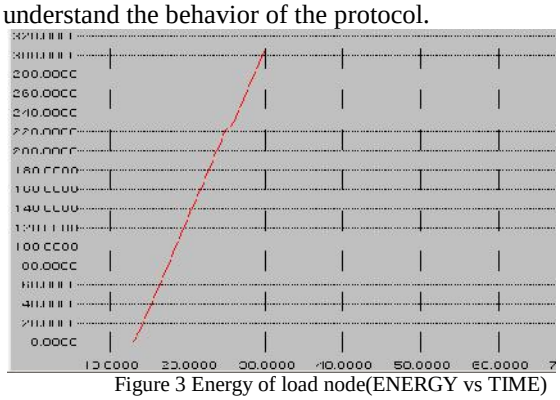

Figure 3 Energy of load node(ENERGY vs TIME)

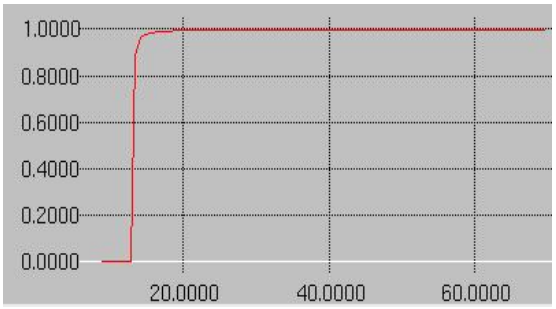

Figure 4 PDR of Alterate node (PDR vs TIME)

REFERENCES

[1] Adreas Merentitis, Nektarios Kranitis, Antonis Paschalis, and Dimitris Gizopoulos," Low Energy Online Self-Test of Embedded Processors in Dependable WSN Nodes"(2012) IEEE TRANSACTIONS ON DEPENDABLE AND SECURE COMPUTING,VOL. 9, NO. 1

[2] Akyildiz I.F., Su W., Sankarasubramaniam Y., and E. Cayirci,(2002) "Wireless Sensor Networks: a Survey", Computer Networks, Vol.38, No: 4.

[3] Anastasi G., Conti M., Castronuovo M., Di Francesco M., "Experimental Evaluation of an Adaptive Staggered Sleep Protocol for Wireless Sensor Networks"(2008), Proc. IEEE WoWMoM, International Workshop on Experimental Activities in Wireless Networks and Systems

[4] Anastasi G.,Conti M., Di Francesco M., "An Adaptive Sleep Strategy for Energy Conservation in Wireless Sensor Networks"(2009),

Technical Report DII-TR http://info.iet.unipi.it/~anastasi/papers/DII-TR-2009-03.pdf
[5] Chaudhary D.D., Pranav Pawar and Waghmare L.M.,"Comparison and Performance Evaluation of Wireless Sensor Network with different Routing Protocols" (2011) ,IPCSIT vol.6
[6] FENGYUAN REN, JIAO ZHANG, TAO HE, CHUANG LIN, and DAS S.K.,(2011),"Energy-Balanced Routing Protocol for Data Gathering in Wireless Sensor Networks" IEEE TRANSACTIONS ON PARALLEL AND DISTRIBUTED SYSTEMS, VOL. 22, NO. 12,
[7] Ganesan D., Cerpa A., Ye, Yu Y., Zhao J., Estrin D., (2004) "Networking Issues in Wireless Sensor Networks", Journal of Parallel and Distributed Computing, Vol. 64, pp. 799-814.
[8] Giuseppe Anastasi , Marco Conti, Mario Di Francesco: "Extending the Lifetime of Wireless Sensor Networks through Adaptive Sleep"(2010), - IEEE Transactions on Industrustrial Informatics.
[9] ISMAIL AHMEDY, ASRI NGADI, SYARIL NIZAM OMAR and JUNAID CHAUDHRY (2011) "A review on wireless sensor networks routing protocol: Challenge in energy perspective" Scientific Research and Essays Vol. 6(26).
[10] Jong-Shin Chen, Neng-Chung Wang , San-Heui Jhuang , (2010) "Efficient Cluster Head Selection Methods for Wireless Sensor Networks" JOURNAL OF NETWORKS, VOL. 5, NO. 8
[11] Kansal A., Hsu J., Zahedi S., Srivastava M., ",(2007) "Power Management in Energy Harvesting Sensor Networks,ACM Transactions on Embedded Computing Systems, Vol. 6, N. 4,.
[12] Kenan Xu, Hossam Hassanein, Glen Takahara, and Quanhong Wang, (2010) " Relay Node Deployment Strategies in Heterogeneous Wireless Sensor Networks" -IEEE TRANSACTIONS ON MOBILE COMPUTING, VOL. 9, NO. 2
[13] Kobi Cohen and Amir Leshem, (2010) "A Time-Varying Opportunistic Approach to Lifetime Maximization of Wireless Sensor Networks", IEEE TRANSACTIONS ON SIGNAL PROCESSING, VOL. 58, NO. 10
[14] Mirza D., Owrang M., Schurgers C., (2005) "Energy-efficient Wakeup Scheduling for Maximizing Lifetime of IEEE 802.15.4 Networks", Proc. Int'l Conference on Wireless Internet , Budapest - Hungary.
[15] Mohamed K. Watfa, Haitham AlHassanieh, and Samir Selman, (2011) "Multi-Hop Wireless Energy Transfer in WSNs",IEEE COMMUNICATIONS LETTERS, VOL. 15,NO. 12
[16] Wanqing Tu, (2012)" Efficient Resource Utilization for Multi-Flow Wireless Multicasting Transmissions", - IEEE JOURNAL ON SELECTED AREAS IN COMMUNICATIONS, VOL. 30, NO. 7
[17] Wei Ye,,and Fernando,(2008)"Robust Optimization Models for Energy-Limited-Wireless Sensor Networks"-IEEE TRANSACTIONS ON WIRELESS COMMUNICATIONS, VOL. 7, NO. 6

Arun Thangavel pursing Master of Engineering in Applied Electronics at K.S.R College of Engineering. He presented a paper in an International conference at Karunya University. His research interests include wireless sensor network, network lifetime and energy.

B.Yuvarani received B.E degree in Electrical and Electronics Engineering in VMKV in 2001. She received M.E degree in Power Electronics and Drives in Sona College of Technology in 2010. Her area of interest includes Power Electronics and Drives.

Cloud Computing: A Review

Miss Shraddha Mehta, Miss Mital Upahaya, Miss Mita Rathod

Abstract -- **Cloud computing is the next generation in computation. Cloud computing is a recent trend in IT that moves computing and data away from desktop and portable PCs into large data centers. It implies a service oriented architecture through offering software's and platforms as services, reduced information technology overhead for the end-user, great flexibility, reduced total cost of ownership, on demand services,security,Efficiency and Bandwidth etc..**

Keyword– Cloud Computing, Virtualization, On Demand Service, Hypervisor, Virtual Machine.

I. INTRODUCTION

Computing is the next natural step in the evolution of on-demand information technology services and products. When plugging an electric appliance into an outlet, we care neither how electric power is generated nor how it gets to that outlet it comes because of the cloud computing. Cloud Computing use the hardware and software are available easily and access in the internet

In Computing, to be considered fully virtualized, must allow computers to be built from distributed components such as processing, storage, data, and software resources. Cloud Computing use the (API) accessibility to software that enables machines to interact with cloud software. Cloud Computing has the facility of on-demand Self-service and it provides flexibility, reliability, efficiency , security and many more.

It provides On-demand delivery of computing power; consumers pay providers based on usage (pay as-you-go) similarly as public utility services like water, gas, electricity and telephony. It has main three types of service model like SAAS(Software as a service),PAAS(Platform as a service) and IAAS(Infrastructure-as a service).

II.SERVIEC MODEL

It has main three Types or Personalities

- Software-as-a-Service (SaaS): A wide range of application services delivered via various business models normally available as public offering.
- Platform-as-a-Service(PaaS):Application Development platforms provides authoring and runtime environment.
- Infrastructure-as-a-Service (IaaS): It also known as elastic compute clouds, enable virtual hardware for various uses.

Miss Shraddha Mehta, Miss Mital Upahaya and Miss Mita Rathod are with Department of Computer Engineering, RK University, Rajkot

III. VIRTUALIZATION

Virtual means "not a real" Virtualization is way to run multiple operating systems and user applications on the same hardware E.g., run both Windows and Linux on the same laptop. Virtualization means the separation of a service request from the underlying physical delivery of that service. It is used to dynamically partition and share the available physical resources such as CPU, storage, memory and I/O devices.

It has mainly three types of virtualization:

- Memory virtualization

Process feels like it has its own address space, It Created by MMU and configured by OS

- Storage virtualization

Logical view of disks "connected" to a machine, It has External pool of storage

- CPU/Machine virtualization

Each process feels like it has its own CPU .It Created by OS preemption and scheduler.

IV. USES OF VIRTUALIZATION

- Server consolidation

It is Run a web server and a mail server on the same physical server

- Easier development

It Develop critical operating system components (file system, disk driver) without affecting computer stability.

- QA

It is Testing a network product (e.g., a firewall) may require tens of computers and Try testing thoroughly a product at each pre-release milestone.

- Cloud computing

It has Amazon sells computing power and You pay for e.g., 2 CPU cores for 3 hours plus 10GB of network traffic.

V.HYPERVISOR

Hypervisor also known as Virtual Machine Monitor Software emulating hardware to operating systems. First developed for Servers and Mainframes by IBM. Due to plentiful hardware not widely used, but fundamental method of virtualization

- Types of Hypervisor

It has mainly two Types:

1. Native Hypervisor

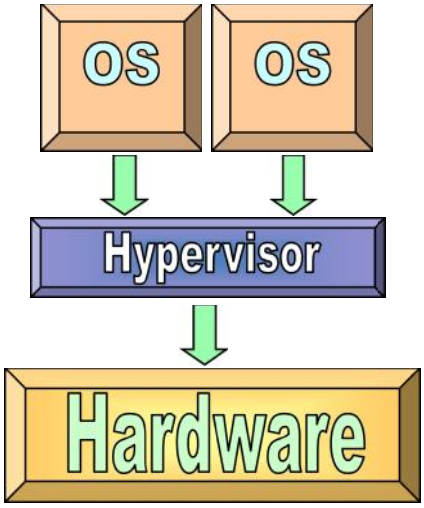

Fig 1.1 Native Hypervisor

Hypervisor directly on top of hardware and it Emulates hardware to operating systems and it isDifficult to implement

2. Hosted Hypervisor

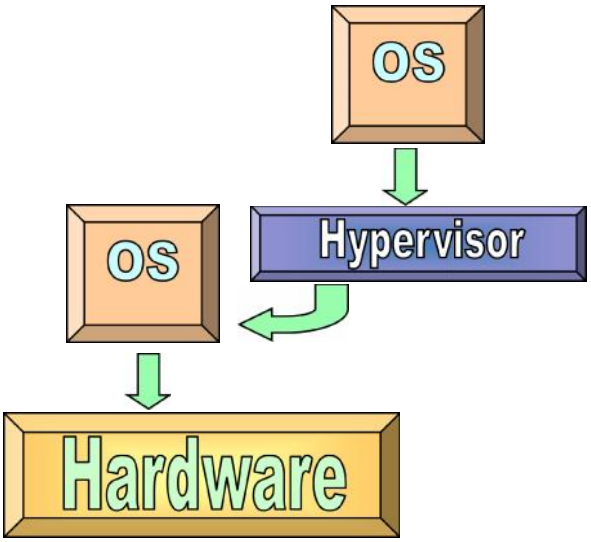

Fig 1.2 Hosted Hypervisor

It is Runs under host operating system and it isEasier to implement..It isLess efficient.

VI.VIRTUAL MACHINE

A virtual machine is a tightly isolated software container that can run its own operating systems and applications as if it were a physical computer. Behaves exactly like a physical computer and contains it own virtual CPU, RAM hard disk and network interface card (NIC)VM thinks it is a ”real” computer.VM is composed of software and contains no hardware. So it offers a number of distinct advantages over physical hardware .

VII.VIRTUAL MACHINE MONITOR

It Resides as a layer below the operating system and Presents a hardware interface to an OS It has Multiplexes resources between several virtual machines (VMs) and Performance Isolates VMs from each other .

VIII.PITFALLS OF VIRTUALLZATION

- Detection/Discover

You can't manage what you can't see!.Unprepared for the complexity of what VMs exist and which are active or inactive. To overcome these challenges, discovery tools need to extend to the virtual world by identifying Virtual Machine Disk Format (.vmdk) files and how many exist within the environment. This will identify both active and inactive VM’s.

- Correlation

Difficulty in understanding which VMs are on which hosts and identifying which functions are supported by each VM.It mapping guest to host relationships and grouping the VM’s application is a best practice when implementing virtualization.

- Configuration management

It ensuring VMs are configured properly is crucial in preventing performance and Complexities in VM provisioning and offline VM patching.A Technical Controls configuration management database (CMDB) will provide the current state of a VM, allowing a technician to update the configuration by auditing and making changes to the template.

- Additional security considerations

If a host is vulnerable, all guest VMs and the business applications are also at risk and Leave more impact than the same exploit on a single physical server .It use an application that dynamically maps guest-to-host relationships and tracks guest VM’s as they move from host to host.

- VM identity management issues

Virtualization introduces complexities for separation of duties and Identify roles and put them through the same processes you leverage for physical devices including change management, release management and hardening guidelines.

- VM network configuration control

With multiple OS sharing a single IP address, network access control becomes much more complex in a virtual network.and IP sweeps will not pick these up.

- Identifying and controlling VM proliferation

VM's can pop up and move to any location in an instant.To manage this potential issue, establish and enforce a process for Virtual Machine deployment.

- VM host capacity planning

Virtualization can make understanding what applications are running and how many resources are being leveraged much more difficult. To better deal with this issue, organizations must track how many guest to host relationships exist and the configuration of the VM's.

- Intellectual property

Virtualization makes it more difficult to know who has what information. Verifying encrypted data and historical information guest VMs, can help manage and secure intellectual property.

X.CONCLUSION

Cloud Computing is an internet computing model where data isstored on servers that are on the Internet and temporarily cached on the clients' computing devices such as: desktop computers, laptops, hand-held mobile devices, etc. Cloud computing involves the supply of on-demand IT computing functions and utilities that are delivered from third party platforms as a service. On-demand services and components include: software-as-a-service, platform-as-a-service, and storage-as-a-service.

REFERENCES

[1] Y. Huang, H. Su, W. Sun, J. M. Zhang, C. J. Guo, M. J. Xu, B. Z. Jiang, S. X. Yang, and J. Zhu, "Framework for building a low-cost,scalable, and secured platform for Web-delivered business services," IBM Journal of Research and Development, vol. 54, no. 6, pp.535-548, November 2010.

[2] ABIResearch.http://www.abiresearch.com/. 2010.

[3] R. Buyya, C. S. Yeo, S. Venugopal, J. Broberg, and I. Brandic, "Cloud computing and emerging IT platforms: Vision, hype, and reality for delivering computing as the 5th utility," Journal on Future Generation Computer Systems, vol. 25, no. 6, pp. 599 - 616, June 2009.

[4] Michael Armbrust, Armando Fox, Rean Griffith, Anthony D. Joseph, Randy H. Katz, Andrew Konwinski, Gunho Lee, David A. Patterson, Ariel Rabkin, Ion Stoica, and Matei Zaharia. Above the clouds:A berkeley view of cloud computing. Technical Report UCB/EECS-2009-28,.

[5] Rajkumar Buyya, Chee Shin Yeo, Srikumar Venugopal, James Broberg, and Ivona Brandic. Cloud computing and emerging it platforms: Vision, hype, and reality for delivering computing as the 5th utility. Future Gener. Comput. Syst., 25(6):599–616, 2009.

[6] Zehua Zhang and Xuejie Zhang. Realization of open cloud computing federation based on mobile agent. In ICIS '09: IEEE International Conference on Intelligent Computing and Intelligent Systems, 2009., volume 3, pages 642–646, 2009.

[7] Rajiv Ranjan and Rajkumar Buyya. Decentralized overlay for federation of enterprise clouds. CoRR, abs/0811.2563, 2008

[8] E.Angel Anna Prathiba and B.Saravanan," HASBE for Access Control by Separate Encryption/Decryption in Cloud Computing", *International Journal of Emerging Trends in Electrical and Electronics (IJETEE) Vol. 2, Issue. 2, pp.* 66-71, *April-2013.*

[9] Mrs. Ashutosh, "Introduction of SOA in Cloud computing for facilitating new services", *International Journal of Emerging Trends in Electrical and Electronics (IJETEE) Vol. 2, Issue. 2, pp.* 59-62, *April-2013.*

Evaluation of Image Quality Assessment by Decoupling Detail Losses and Regression Techniques

SUDHARSAN.D and SUNDARAVADIVEL.P

***Abstract*— Image quality assessment plays a fundamental role in Image processing and communication applications. In my work, two types of spatial distortions, i.e., detail losses and additive impairments, are decoupled and evaluated separately for spatial quality assessment. The detail losses refer to the loss of useful visual information that will affect the content visibility caused by data compression and so on. To assess the performance of image quality metrics (IQMs), some regressions, such as logistic regression and polynomial regression, areused to correlate objective ratings with subjective scores. However, some defects in optimality are shown in these regressions. In this correspondence, monotonic regression (MR) is found to be an effective correlation method in the performance assessment of IQMs. The experimental results have proven that MR performs better than any other regression.**

***Index Terms—Correlation, Image Quality Metrics(IQM), Monotonic Regression(MR),objective ratings*.**

I. INTRODUCTION

Image processing is one of the emerging areas of science and technology. The two principal application areas that stems from digital image processing methods are improvement of pictorial information for human interpretation and processing of image for storage, transmission and representation for autonomous machine perception.

An image may be defined as a two dimensional function *f(x, y)* where *x* and *y* are spatial coordinates, and the amplitude of *f* at any pair of coordinates *(x, y)* is called the intensity or gray level of the image at that point. When *x, y,* and the intensity values of *f* are all finite, discrete quantities, we call the image a digital image. The field of digital image processing refers to processing digital images by means of a digital computer. A digital image is composed of a finite number of elements, each of which has a particular location and value. These elements are called picture elements or pixels. Image processing is a discipline in which both the input and output of a process are images. A digital image is represented by a matrix of values, where each value is a function of the information surrounding the corresponding point in the image. A single element in an image matrix is a picture element or pixel. In a colour system, a pixel includes information for all colour components.

SUDHARSAN.D is a PG Scholar, Dept. of EEE, K.S.R. College of Engineering, Tiruchengode and SUNDARAVADIVEL.P is working as Assistant Professor, Dept. of EEE, K.S.R. College of Engineering, Tiruchengode., Emails: sudharsa21@gmail.com , sundarkmp@gmail.com

Image digitization refers to the process whereby an apparently continuous analog image is recorded as discrete intensity values at equally spaced locations on an*xy*-grid over the image field. This grid is called a raster. Typically the image area is divided into an array of rows and columns in much the same way as a television image. In North and South America and Japan, the television image is composed of 483 lines covering a rectangular area having proportions that are 3 units high by 4 units wide. If each line in such an image is divided into about 640 equal picture elements or pixels, then each pixel will be square if you discard three lines and record a raster of 640 x 480 pixels.

Digital images are composed of pixels(short for picture elements). Each pixel represents the colour (or gray level for black and white photos) at a single point in the image, so a pixel is like a tiny dot of a particular colour. By measuring the colour of an image at a large number of points, we can create a digital approximation of the image from which a copy of the original can be reconstructed. Pixels are a little like grain particles in a conventional photographic image, but arranged in a regular pattern of rows and columns and store information somewhat differently. A digital image is a rectangular array of pixels sometimes called a bitmap.

The process of getting an image to look the same between two or more different media or devices is called colour management and there are many different colour management systems available today. Unfortunately, most are complex, expensive, and not available for a full range of devices. The hue of a colour identifies what is commonly called “colour”. For example, all redshave a similar hue value whether they are light, dark, intense, or pastel.

II. IMAGE QUALITY ASSESSMENT

The need to measure image quality arises in the development of image equipment and in the delivery and storage of image information. The principles presented can be applied to other types of motion video and even still images. The methods of image quality assessment can be divided into two main categories: subjective assessment (which uses human viewers) and objective assessment (which is accomplished by use of electrical measurements). While we believe that assessment of image quality is best accomplished by the human visual system, it is useful to have objective methods available which are repeatable, can be standardized, and can be performed quickly and easily with portable equipment. These objective methods should give

results that correlate closely with results obtained through human perception.

After some investigation of compressed image, it becomes clear that the perceived quality of the image after passing through a given digital compression system is often a function of the input scene. This is particularly true for low bit-rate systems. A scene with little motion and limited spatial detail (such as a head and shoulders shot of a newscaster) may be compressed to 384 Kbits/sec and decompressed with relatively little distortion. Another scene (such as a football game) which contains a large amount of motion as well as spatial detail will appear quite distorted at the same bit rate. Therefore, we directed our efforts toward developing perception-based objective measurements which are extracted from the actual sampled image. These objective measurements quantify the perceivedspatial and temporal distortions in a way that correlates as closely as possible with the response of a human visual system. Each scene was digitized (at 4 times sub-carrier frequency) to producea time sequence of images sampled at 30 frames per second (in time) and 756 x 486 pixels (in space).

Objective measurement of video quality was accomplished in the past through the use of static video test scenes such as resolution charts, colour bars, multi-burst patterns, etc., and by measuring the signal to noise ratio of the video signal These objective methods address the spatial and colour aspects of the video imagery as well as overall signal distortions present in traditional analog systems. With the development of digital compression technology, a large number of new video services have become available. The savings in transmission and/or storage bandwidth made possible with digital compression technology depends upon the amount of information present in the original (uncompressed) video signal, as well as how much quality the user is willing to sacrifice.

Compression is achieved through the use of a codec: a compression –decompression algorithm that looks for redundancy in data files. For example, XXXYYYY could be reduced to 3X4Y. In this example, the compression is considered “lossless” because the file can be decompressed and restored to the original format without any loss of data. Video compression, however, is considered “lossy” because it results in a loss of data. When compressing video, codec’s look for redundancy in areas where the human eye or ear cannot distinguish between differences. Since the human eye is less sensitive to colour differences than to brightness, the colour information (chrominance) is separated from the brightness information (luminance). The codec then averages the chrominance data for adjacent pixels, which reduces the volume of data. The luminance data is not changed. Normally, individuals cannot perceive the differences caused by the lossy compression. However, when the image is enlarged, the data loss is obvious, and it will look blocky.

III. PERFORMANCE OF IQA ALGORITHMS

The performance of several publicly available objective IQA models was evaluated on our database. Many popular IQA algorithms are licensed and sold for profit and are not freely available.

Peak Signal to Noise Ratio is a simple function of the Mean Squared Error between the reference and test videos and provides a baseline for objective IQA algorithm performance.

Structural Similarity is a popular method for quality assessment of still images that was extended to video. The SSIM index was applied frame-by-frame on the luminance component of the video and the overall SSIM index for the video was computed as the average of the frame level quality scores. Mat lab and Lab view implementations of SSIM are freely available for download.

Multi-Scale SSIMis an extension of the SSIM paradigm, also proposed for still images that have been shown to outperform the SSIM index and many other still image quality assessment algorithms. We extended the MS-SSIM index to video by applying it frame-by-frame on the luminance component of the video and the overall MS-SSIM index for the video was computed as the average of the frame level quality scores. A Mat lab implementation of MS-SSIM is freely available for download.

Speed SSIMis the name we give to the IQA that uses the SSIM index in conjunction with statistical models of visual speed perception. Using models of visual speed perception was shown to improve the performance of both PSNR and SSIM Weevaluated the performance of this framework with the SSIM index, which was shown to perform better than using the same framework with PSNR.A software implementation of this index was obtained from the authors.

Visual Signal to Noise Ratio *(VSNR)* is a quality assessment algorithm proposed for still image andis freely available for download. We applied VSNR frame-by-frame on the luminance component of the video and the overall VSNR index for the video was computed as the average of the frame level VSNR scores.

Image Quality Metric*(IQM)* is an IQA algorithm developed at the National Telecommunications and Information Administration (NTIA). Due to its excellent performance in the VQEG Phase 2 validation tests, and as the IQM methods were adopted by the American National Standards Institute (ANSI) as a national standard, International Telecommunications Union RecommendationsIQM are freely available for download for research purposes.

IV. REGRESSION TECHNIQUES

To assess the performance of image quality metrics (IQMs), aScheme first proposed by Video Quality Expert

Group (VQEG) is widely adopted by researchers. The scheme is designed for theobjective measurement evaluation problem and can be applied for the assessment of image/video quality metric. It can be described by the following three steps:
Step 1. Metric computation
Rate a set of images by IQM, while mean opinion scores (MOSs)of these images are measured by human observers beforehand.
Step 2. Correlation (or regression)
Correlate the outputs of IQM with MOS via a predicting function(this process can be also called regression). Then, the predictedMOS is obtained by calculating the IQM ratings through the regressionfunction.
Step 3. Index computation
Compute the performance indexes between the MOS and the predicted

In this scheme, most of the research effort is devoted to step 1 inwhich the images are produced. The images are judged by human observersand rated to produce the MOS data. The IQMs are defined, implemented,and applied to the images. However, steps 2 and 3 havereceived less attention and could be improved. In particular, in step 2,a single standard optimal regression procedure has not been adopted and as a consequence, in step 3, the output index measure is not unique.This correspondence proposes a regression procedure that is optimaland produces a unique and maximum index measure.

As examples of the several regression procedures in use for the IQM research, VQEG recommended some nonlinear regressions for correlation, such as logistic regression (LR) and monotonic polynomial regression (MPR). Some other researchers also proposed their ownregression functions based on these. However, no matter which kind ofregression function is applied in step 2, they all face the same problems, i.e., regression is not optimal, whereas some regressions have a large computational burden. Moreover, the nonoptimal regression causes the problem that performance indexes may vary when only the regression function changes.

In this correspondence, we focus on step 2 (correlation or regression process) in the performance assessment of the IQM. As a result, we find monotonic regression (MR) to be an improvement for step 2, which is the correlation process. This correspondence is detailed as follows:
This section briefly discusses the principle of the correlation method with which VQEG is concerned and gives a detail introduction of the LR and the MPR. The experimental results and the advantages are discussed below, whereas the three commonly used correlation methods (LR, MPR, and MR) are tested on a certain database for comparison.In order to make ourpaper easier to understand, some additional materials are given in theappendixes.

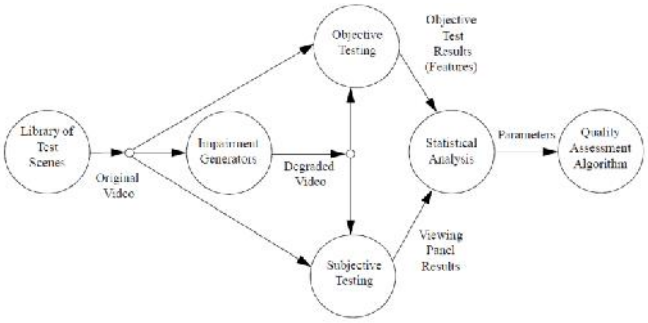

*Fig 1.*Development Process for Image Quality Assessment Algorithm

This stage of the development process utilized joint statistical analysis of the subjective and objective data sets. This step identifies a subset of the candidate objective measurements that provides useful and unique video quality information. The best measurement was selected by exhaustive search. Additional measurements were selected to reduce the remaining objective- subjective error by the largest amount. Selected measurements complement each other. For instance, a temporal distortion measure was selected to reduce the objective-subjective error remaining from a previous selection of a spatial distortion measure. When combined in a simple linear model, this subset of measurements provides predicted scores that correlate well with the true.

This stage of the development process utilized joint statistical analysis of the subjective and objective data sets. This step identifies a subset of the candidate objective measurements that provides useful and unique video quality information. The best measurement was selected by exhaustive search. Additional measurements were selected to reduce the remaining objective- subjective error by the largest amount. Selected measurements complement each other. For instance, a temporal distortion measure was selected to reduce the objective-subjective error remaining from a previous selection of a spatial distortion measure. When combined in a simple linear model, this subset of measurements provides predicted scores that correlate well with the true.

Fig 2. Input image

The input image is shown above. We can add any type of noise parameters to the given input image and get various types of results. By adding some parameters like Blur, Gaussiannoise, jpeg we getting the result as distorted images is to be shown below. The results are

Fig 3. Jpeg compression

V. SIMULATION RESULTS

By demonstration the superiority of Monotonic Regression using actual data, the Correlation Coefficient of several representative Image Quality Metrics are computed on CSIQ Image Quality Assessment Database by Logistic Regression, Monotonic Polynomial Regression, and Monotonic Regression Usually, metric rating is directly regressed with MOS in correlation, but for some metric, such asSSIM. The predictive performance computed by Monotonic Regression is the highest.

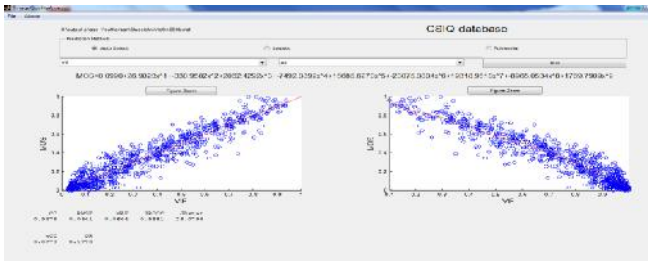

Fig 4. Output for Visual Information fidelity

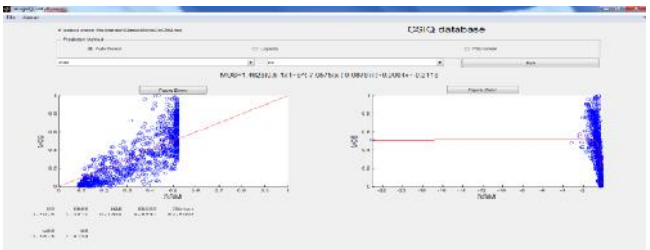

Fig 5. Output for Structural Similarity

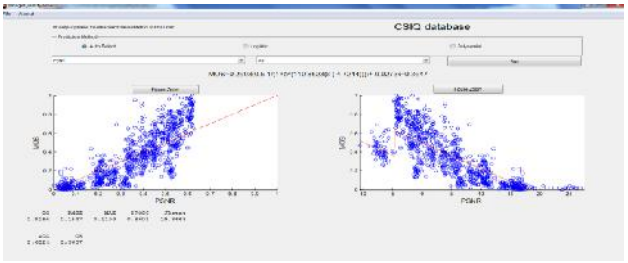

Fig 6. Output for Peak Signal Noise Ratio

Table 1 comparison of IQM parameters for Monotonic Regression

parameters	CC	RMSE	MAE	WCC
PSNR	0.816	0.154	0.119	0.682
SSIM	0.807	0.167	0.134	0.687
VSNR	0.806	0.163	0.124	0.697
VIF	0.947	0.084	0.064	0.877

VI. RESULTS AND DISCUSSION

To demonstrate the theoretical superiority of MR using actual data, the CC of several representative IQMs are computed on LIVE Image Quality Assessment Database (LIVE) by LR, MPR, and MR. Usually, metric rating is directly regressed with MOS in correlation, but for some metric, such as SSIM , VIF , the rating has to be transformed before correlation. The transform helps find a “better regression” by mapping ratings to a suitable space, as some metrics cannot exhibit real predictive performance under the common coordinate system. Here, better regression means that the metric will show higher predictive performance comparedwith others.

VIICONCLUSION

The quality metrics for image was successfully found out for different parameters like peak signal to noise ratio, correlation coefficient for various conditions like adding noise likeBlur, Gaussians noises. Thus the experimental superiority of Monotonic Regression using actual data, the Correlation Coefficient of several representative Image Quality Metrics are computed on Image Quality Assessment Database by Logistic Regression, Monotonic Polynomial Regression and Monotonic Regression. Usually, metric rating is directly regressed with Mean Opinion Scores in correlation, but for some metric, such as Structural Similarity. The predictive performance computed by Monotonic Regression is the highest.

In this correspondence, I have studied correlation methods in the Image Quality Metrics performance assessment and proved Monotonic Regression as an effective way of Mean Opinion Scores correlation. The experimental results have confirmed that Monotonic Regression is more appropriate and suitable than conventional methods. I believe Monotonic Regression might substitute other correlation methods in the Image Quality Metrics performance assessment in the future.

REFERENCES

[1]. Bosch. M, Fengqing Zhu and Delp. E.J.(2011), "Segmentation based video compression using texture and Motion Models" IEEE of Journal volume 5,Issue 7, Digital object Identifier,pp.321-334.

[2]. Hemami. S. S and Reibman. A. R.(2010), "No-reference image and video quality estimation: Applications and human-motivated design," Signal Process.-Image Commun., vol. 25, no. 7, pp. 469–481,

[3]. Homin Kwon, Hagyong Han, Sungmok Lee, Wontae Choi andBongsoonKang(2010) "Newvideo enhancement pre-processor using the region-of-interest for the videoconferencing"Consumer Electronics, IEEE Transactions on Volume 56,pp. 321-343.

[4]. Leung, S.O., Chan, K.L. and Fung, P.W. (2010), "Compression techniques for still image and motion video"IEEE region conference ,vol 34,pp. 342-354.

[5]. Li.S, Zhang .F, Ma .L. andKnag. K.N,(2011), "Image quality assessment by separately evaluating detail losses and additive impairments," IEEETrans. Multimedia, vol. 13, no. 5, pp. 935–949.

[6]. Narwaria. M and Lin W. S,(2010) "Objective image quality assessment based on support vector regression," IEEE Trans. Neural Netw., vol. 21, no. 3,pp. 515–519.

[7]. Pei-KueiTsung, Li-Fu Ding, Wei-Yin Chen, Tzu-Der Chuang, Yu-Han Chen, Pai-Heng Hsiao, Shao-Yi Chien and Liang-Gee Chen (2010)"Video encoder design for high-definition 3D video communication systems" Communications magazine , volume 48 ,pp. 432-443.

[8]. Pinson .M.H. and Wolf.S.(2011), "A new standardized method for objectively measuring video quality," IEEE Trans. Broadcasting, vol. 50, no. 3, pp.312–322, .

[9]. Winkler, S.(2012) "Analysis of Public Image and Video Databases for Quality Assessment"IEEE Journal of volume 6,pp. 543-545.

[10] Xiangyu Lin, Hanjie Ma, Lei LuoandYaowu Chen(2012) "No-reference video quality assessment in the compressed domain" Consumer Electronics, IEEE Transactions on Volume: 58, pp. 534-545.

[11] Xu Dong (2010), "pre-processing for video compression," Consumer electronics, International conference on Digital object identifier,vol.31, pp. 521-534.

[12] Zeng .K and Wang.Z (2010), "Quality-aware video based on robust embeddingof intra- and interframe reduced-reference features," in Proc. IEEE Int.Conf. Image Process, pp. 3229–3232.

[13] Z. Wang, A. C. Bovik, H. R. Sheikh, and E. P. Simoncelli, "Image quality assessment: From error visibility to structural similarity," *IEEETrans. Image Process.*, vol. 13, no. 4, pp. 600–612, Apr. 2004.

[14] H. R. Sheikh, M. Farooq, and A. C. Bovik, "A statistical evaluation of recent full reference image quality assessment algorithms," *IEEETrans. Image Process.*, vol. 15, no. 11, pp. 3441–3452, Nov. 2006.

[15] D. P. Bertsekas, *Nonlinear Programming*, 2nd ed. elmont, MA:Athena Scientific, 1999.

[16] R. Barlow, D. Barholomew, J. Bremner, and H. Brunk, *Statistical InferenceUnder Order Restrictions*. New York: Wiley, 1972.

Hard Disk Duplication

K.Venkateswarlu and P charanarur

Abstract— In this paper, we have proposed a survey on Hard disk Duplication. Hard disk duplication means it copying or recovery or booting the hard disk. Hard disk duplication mostly used for to restore lost or damaged data, or to move wanted data into a new disk, though other reasons also exist. Hard disk duplication can be done in two ways one is disk cloning and other one is disk imaging. In this survey mainly we compare different disk image and clone tools [1].

***Keywords*—Disk cloning, system Backup, Disk cloning tools, File and folder Backup, Partition and drive Backup.**

I. INTRODUCTION

This Disk cloning is the process of copying the contents of one computer hard disk to another disk such that drive 2 is identical to drive 1 although it is possible to clone different sized drives. Disk image is used for recovery or backup the data or booting the disk. Disk image is mostly used in computer forensics. Some tools can perform both disk clone and drive image. Disk imaging as defined by Jim Bates, Technical Director of Computer Forensics Ltd, refers to "An image of the whole disk was copied. This was regardless of any software on the disk and the important point was that the complete content of the disk was copied including the location of the data. Disk imaging takes sector-by-sector copy usually for forensic purposes and as such it will contain some mechanism (internal verification) to prove that the copy is exact and has not been altered. It does not necessarily need the same geometry as the original as long as arrangements are made to simulate the geometry if it becomes necessary to boot into the acquired image."[3].

II. HARD DISK DUPLICATION COMMON USES

There are a number of notable uses for disk cloning software. These include:

A. Reboot and restore: A technique in which the disk of a computer is automatically wiped and restored from a "clean", master image, which should be in full working order and should have been swept for viruses. This is used by some cybercafés and some training and educational institutes, and helps ensure that even if a user does misconfigure something, downloads inappropriate content or programs, or infects a computer with a virus, the computer will be restored to a clean, working state. The reboot and restore process can either take place irregularly when a computer shows signs of malfunctioning, on a regular basis (e.g., nightly) or even, in some cases, every time a user logs off, which is the safest approach (although that does involve some downtime).

K.Venkateswarlu is working as Associate Professor&HOD and P charanarur is working as Assistant professor, both are with Dept. of E C E MRRITS, Udayagiri, A.P. India, Emails: Kaliki59@gmail.com, panem.charan@gmail.com

B. Provisioning new computers: Provisioning with a standard set of software so that a new user is ready to go straight away with a complete application suite and does not have to waste time installing individual applications. This is often done by original equipment manufacturers and larger companies.

C. Hard drive upgrade: An individual user may use disk copying (cloning) to upgrade to a new, usually larger, hard disk.

D. Full system backup: A user may create a comprehensive backup of their operating system and installed software.

System recovery: An OEM can provide media that can restore a computer to its original factory software configuration.

III. DISK CLONE HISTORY

Before Windows 95, some computer manufacturers used hardware disk copying machines to copy software. This had the disadvantages of copying not just the used data on the disk, but also unused sectors, as the hardware used was not aware of the structures on the disks. A larger hard disk could not be copied to a smaller one, and copying a smaller one to a larger left the remaining space on the new disk unused. The two disks required identical geometries.

Other manufacturers and companies partitioned and formatted disks manually, then used file copy utilities or archiving utilities, such as tar or zip to copy files. It is not sufficient simply to copy all files from one disk to another, because there are special boot files or boot tracks which must be specifically placed for an operating system to run, so additional manual steps were required.

Windows 95 compounded the problems because it was larger than earlier popular operating systems, and thus took more time to install. The long filenames added to the FAT file system by Microsoft in Windows 95 were not supported by most copy programs, and the introduction of the FAT32 file system in 1997 caused problems for others. The growth of the personal computer market at this time also made a more efficient solution desirable.

Ghost was introduced in 1996 by Binary Research. It initially supported only FAT file systems directly, but it could copy but not resize other file systems by performing a sector copy on them. Ghost added support for the NTFS file system later that year, and also provided a program to change the Security Identifier (SID) which made Windows NT systems distinguishable from each other. Support for the ext2 file system was added in 1999.

Competitors to Ghost soon arose, and a features war has carried on to the present day. Many disk cloning programs

now offer features which go beyond simple disk cloning, such as asset management and user settings migration. On UNIX based computer systems, dd was more commonplace due to the lack of file system support in Ghost.

IV. SOME OF DISK CLONING TOOLS

A. Platform independent

1. Norton Ghost (Home and SMB Edition), Symantec Ghost Solution Suite (Enterprise Edition)
2. Kleo Bare Metal Backup for Servers
3. PING (Part image Is Not Ghost)
4. R-Drive Image

B. Windows

5. ACA System Restore - not a real disk cloning tool
6. Active@ Disk Image[citation needed]
7. Altiris - Deployment Solutions
8. Apricorn - EZ Gig software & data transfer kits, e.g., packaged with Crucial SSD upgrades
9. Clonezilla Freeware hard disk clone tool.
10. Drive Image XML Backup Software Runtime Software [1]
11. Ease US Todo Backup [2]
12. HD Clone [3]
13. Macrium Reflect
14. Microsoft Image Backup which is part of Windows 7 - does not support compression

C. Linux

15. UDP Cast - a utility to clone multiple PCs at once using multicast
16. Mondo Rescue
17. Part Image (SystemRescueCD)
18. Trinity Rescue Kit
19. FOG
20. ntfsclone - a utility in the package of ntfsprogs
21. partclone[3]
22. TeraByte Image for Linux
23. Redo Backup and Recovery
24. dd (Unix)

D. AmigaOS

25. Nibbler
26. QuickNibble
27. ZCopier
28. XCopy/Cachet
29. FastCopier
30. Disk Avenger
31. Tetra Copier
32. Cyclone
33. Maverick
34. D-Copy
35. Safe II

V. DISK IMAGE

A disk image file (or simply a disk image) is an exact binary copy of an entire disk or drive. Disk image files contain ALL the data stored on the source drive including not only its files and folders but also its boot sectors, file allocation tables, volume attributes and any other system-specific data. Actually, a disk image is not a collection of files or folders but is an exact duplicate of the raw data of the original disk, sector by sector.

Since disk images contain the raw disk data, it is possible to create an image of a disk written in an unknown format or even under an unknown operating system. File formats of disk images usually depend on the type of the source drive. For example, ISO files are CD images; IMG (or IMA) files usually are images of hard, floppy and/or removable disks; and XDF files are always floppy disk images.

Disk images are widely used by CD recording software for transferring and storing complete CD contents. A lot of CD recording programs use their own formats for disk images. Some of these formats are plain ISO image files renamed with another extension.

VI. DISK IMAGE USES

Some operating systems such as Linux[1] and Mac OS X[2] have virtual drive functionality built-in(such as the loop device), while others such as Microsoft Windows require additional software. Virtual drives are typically read-only, being used to mount existing disk images which are not modifiable by the drive. However some software provides virtual CD/DVD drives which can produce new disk images; this type of virtual drive goes by a variety of names, including "virtual burner".

VII. COMPARISON OF TOOLS

Disk Digger: Disk Digger has two modes of operation which you can select every time you scan a disk. These modes are called "dig deep" and "dig deeper."

Digging Deep: The "dig deep" mode makes Disk Digger "undelete" files from the file system on your disk. Under most file systems, when you delete a file, it doesn't actually get wiped clean from the disk. Instead, the file system will simply mark the file as deleted, and no longer show you the file when you browse the contents of the disk. Disk Digger scans the file system for such deleted files, exposes them to you, and allows you to bring them back as ordinary files again

After a file is deleted, the file system is completely free to overwrite the contents of the deleted file with new data. From the point of view of the file system, the deleted file is now as good as free space, ready for the taking. The next file that is saved by the file system may just be written on top of the deleted one. If that happens, the deleted file will truly be lost forever.

So, a general rule would be something like this: The undelete process is effective only for files that have been deleted very recently. Or, more precisely: The probability of successfully recovering a file is inversely proportional to the amount of time elapsed after deleting it[4].

Digging Deeper: The "dig deeper" mode causes Disk Digger to become a powerful data carver, and carve out whatever files it can find on the disk, independent of the file system. Data carving refers to physically scanning every single sector on the disk, and looking for traces of known file types.

Advantage: The main advantage is that it's independent of the file system that's on the disk, so the disk can be formatted as FAT, NTFS, HFS, ext2, or anything else; it doesn't matter. Disk Digger scans "underneath" the file system, which gives it an additional advantage of being able to scan any free space on the disk outside of the file system, which the "dig deep" mode cannot do.

Disadvantages: The main disadvantage of digging deeper is the time it takes to complete the scan. If you're scanning a memory card or USB drive, it shouldn't be too bad, but if you're scanning an entire hard drive, be prepared for a several-hour job. Of course the burden of the time spent on the scan is subjective, and depends on the value of the files you're trying to recover.

Another disadvantage of this mode is that only a limited number of file types can be recovered. Since we're not aware of the file system, we have no way of knowing what types of files are present, so the only things we have to go on are the actual bytes that we see on the disk. This means that Disk Digger has to be aware of the structure of the types of files we need to recover, and search for patterns of bytes specific to each file format. Fortunately, Disk Digger supports a fairly wide variety of file types which should cover most cases.

The only other disadvantage of this approach is that it's not possible to recover files that have been fragmented by the file system. Since it's not aware of the file system, Disk Digger has no way of knowing whether or not a certain file has been fragmented. So, technically, when digging deeper, Disk Digger will only recover the first fragment of a file. Most files consist of a single fragment anyway, but in some cases, the file system will choose to split a file into two or more fragments. A rule of thumb is: the larger a file is, the more likely it is that it's been fragmented.

Platform: Disk Digger will run on Windows 7 (32 and 64-bit), Windows Vista (32 and 64-bit), and Windows XP.

VIII. NTFS WALKER

NTFS Walker is a portable application that contains its own NTFS drivers that allow it to “walk through” the entire file structure, bypassing the need for the Windows operating system.

The ability to recover deleted files from an NTFS file system is something any good consultant should have in their back pocket. This also applies to the ability to recover files from a machine that has been rendered unbootable. There are plenty of tools available for that task, but few of them are as simple as the free tool NTFS Walker.

NTFS Walker is a portable application (it can be used from a thumb drive) that contains its own NTFS drivers that allow it to “walk through” the entire file structure, bypassing the need for the Windows operating system. Once NTFS Walker has read your system it will then allow you to view every record on the file system’s Master File Table. And when you view a record you can actually get very detailed information about the file to be recovered [5].

Supported operating systems: Windows XP, Vista and Windows 7

IX. FILE & FOLDER BACKUP

This is the simplest form of backup there is, and basically just makes a copy of files. These kind of basic backups are suitable when your documents or data are the most important thing, but you don’t care about your operating system or the applications installed on it. As you have a fine control over what to backup, the size of your backup is determined by your data only. However, once you’ve taken a full back up, you can run “incremental backups” subsequently, which only backs up the files that have changed. This saves space and time, while still giving you an up to date copy of files should the worst happen.

X. PARTITION & DRIVE BACKUP

This can save a copy of your entire computer, including the operating system. It’s the best choice if your computer is your primary work machine and getting it up and running again quickly is important, or if you have a lot of applications installed that you don’t want to lose. With a full partition and drive backup, you can simply change the broken drive and restore everything back to it in a few hours. Of course, these kind of backups will take longer to perform, and they include everything on that partition, so they tend to grow large. The screen shots of back up are shown below.

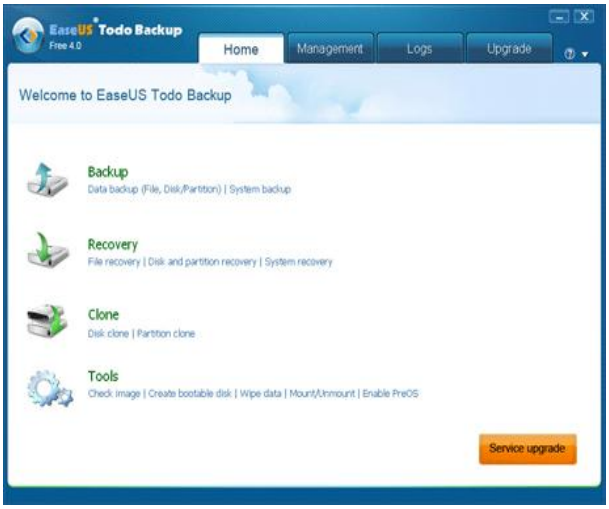

Fig. 1 Todo Backup

XI. RECOVERY FEATURES

Disaster Recovery:

Restore important files from backed up image and perform disaster recovery just by simple clicks. It ensures quick recovery from system crash, a personal error, hardware or software failure, virus attack or hacker's intrusive destruction, etc.

Bootable disk: double insurance:

This freeware provides Linux based bootable disk to enable you to survive system disaster easily.

XII. DRIVE IMAGE XML(C)

Image creation uses Microsoft's Volume Shadow Services (VSS), allowing you to create safe "hot images" even from drives currently in use. . Images are stored in XML files, allowing you to process them with 3rd party tools. Never again be stuck with a useless backup! Restore images to drives without having to reboot. Drive Image XML is now faster than ever, offering two different compression levels.

Features:

1. Backup logical drives and partitions to image files.
2. Browse images, view and extract files.
3. Restore images to the same or a different drive.
4. Copy directly from drive to drive.
5. Schedule automatic backups.
6. Run Drive Image from WinPE boot CD-ROM.

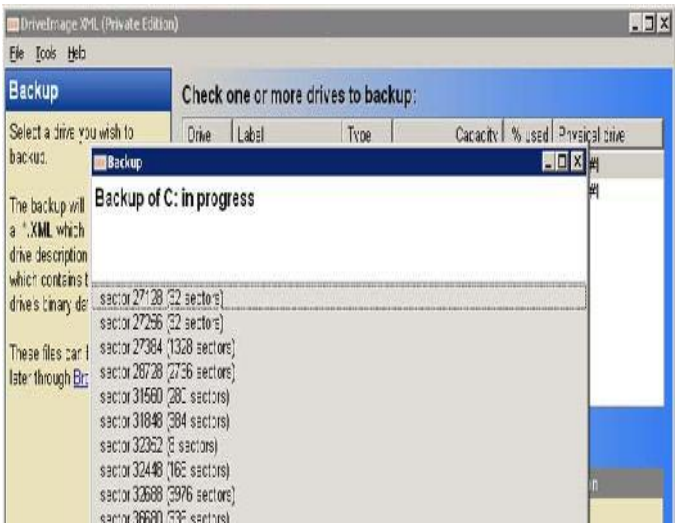

Fig.2 Drive image xml

CONCLUSIONS

ACKNOWLEDGMENT

The authors would like to thank everyone, whoever remained a great source of help and inspirations in this humble presentation. The authors would like to thank K.L. University management for providing necessary facilities to carry out this work.

REFERENCES

[1] 2http://www.wilderssecurity.com/showthread.php?t=238515
[2] 3 http://en.wikipedia.org/wiki/Disk_image
[3] http://www.undisker.com/products/undisker/disk-images.html
[4] 5NTFSWalkerDownload.com,http://download.cnet.com/NTFSWalker/3000-2094_4-75218525.html#ixzz1qQpICV9L
[5] A http://www.easeus-backup.com/review/easeus-todo-backup-free.htm
[6] B http://www.easeus-backup.com/review/easeus-todo-backup-free.htm
[7] C http://www.runtime.org/driveimage-xml.htm

Robust Automatic Face, Gender and Age Recognition Using ABIFGAR Algorithm

Mr.R.Jeganlal' ,Prof.V.Gopi and Ms.S.Rajeswari

Abstract- The face recognition system attains good accuracy in personal identification when they are provided with a large set of training sets. In this paper, we proposed Advanced Biometric Identification on Face, Gender and Age Recognition (ABIFGAR)algorithm for face recognition that yields good results when only small training set is available and it works even with a raining set as small as one image per person. The process is divided into three phases: Pre-processing, Feature Extraction and Classification. The geometric features from a facial image are obtained based on the symmetry of human faces and the variation of gray levels, the positions of eyes, nose and mouth are located by applying the Canny edge operator. The gender and age are classified based on shape and texture information using Posteriori Class Probability and Artificial Neural Network respectively. It is observed that the face recognition is 100%, the gender and age classification is around 98% and 94% respectively.

Index Terms- Posteriori Class Probability and Artificial Neural Network, Canny edge operator

I. INTRODUCTION

Gender recognition is a fundamental task for human beings, as many social functions critically depend on the correct gender perception. Automatic gender classification has many important applications, for example, intelligent user interface, visual surveillance,collecting demographic statistics for marketing, etc. Human faces provide important visual information for gender perception.Gender classification from face images has received much research interest in the last two decades. In the early 1990s various neural network techniques were employed to recognize gender by frontal faces (Golomb et al.,1991; Brunelli and Poggio, 1992), for example, Golomb et al.(1991) trained a fully connected two-layer neural network, SEXNET,which achieves the recognition accuracy of 91.9% on 90 face images. Recent years have witnessed many advances (Yang et al., 2006);

R.Jeganlal Dept.of ECE, PSN College of Engineering and Technology(Autonomous),Tirunelveli, rjeganlal@gmail.com

Prof.V.Gopi *DEAN Dept. of ECE, PSN College of Engineering and Technology(Autonomous), Tvl, kaniyavicky@yahoo.co.in*

Ms.S.Rajeswari *Asst.Prof, Dept. of ECE, PSN College of Engineering and Technology(Autonomous),Tvl, rajee.eswari2006@gmail.com*

we summarize recent studies in Table 1. Moghaddam and Yang (2002) used raw image pixels with nonlinear SVMs for gender classification on thumbnail faces; their experiments on the FERET database (1,755 faces) demonstrated SVMs are superior to other classifiers, achieving the accuracy of 96.6%.In BenAbdelkader and Griffin (2005), local region matching and holistic features were exploited with Linear Discriminant Analysis (LDA) and SVM for gender recognition. On the 12,964 frontal faces from multiple databases (including FERET and PIE), local regionbased SVM achieved the performance of 94.2%. Lapedriza et al. (2006) compared facial features from internal zone (eyes, nose,and mouth) and external zone (hair, chin, and ears). Their experiments on the FRGC database show that the external face zone contributes useful information for gender classification. Baluja and Rowley (2007) introduced an efficient gender recognition system by boosting pixel comparisons in face images. On the FERET database,their approach matches SVM with 500 comparison operations Mäkinen and Raisamo (2008).systematically evaluated different face alignment and gender recognition methods on the FERET database. More recently face appearance and motion cues are combined for gender recognition in videos (Hadid and Pietikäinen, 2009).A common problem of the above studies is that face images acquired under controlled conditions (e.g., the FERET database)are considered, which usually are frontal, occlusion-free, with clean background, consistent lighting, and limited facial expressions.However, in real-world applications, gender classification needs to be performed on real-life face images captured in unconstrained scenarios; see Fig. 1 for examples of real-life faces. As can be observed, there are significant appearance variations on real-life faces, which include facial expressions, illumination changes, head pose variations, occlusion or make-up, poor image quality, and so on. Therefore, gender recognition in real-life faces is much more challenging compared to the case for faces captured in constrained environments. Few studies in the literature have addressed this problem. Shakhnarovich et al. (2002) made an early attempt by collecting over 3,500 face images from the web. On this difficult data set, using Harr-like features, they obtained the performance of 79.0% (Adaboost) and 75.5% (SVM). Recently Gao and Ai (2009) adopted the probabilistic boosting tree with Harr-like features, and obtained the accuracy of 95.51% on 10,100 real-life faces. However, the data sets used in these studies are not public available;therefore, it is difficult for benchmark in research community. Kumar et al. (2008, 2009) recently investigated face verification on real-world images, where many binary ''attribute'' classifiers (including gender) were trained.

They reported the performance of 81.22% on gender classification; however, as they mainly focused on face verification, they did not fully study gender recognition on real-life faces. In this paper, we use a recently built public database, the Labeled Faces in the Wild (LFW) to investigate gender classification on real-world face images. The public database used in this study enables future benchmark and evaluation.

Fig.1. Examples of real-life faces.

The paper is structured as follows. Section 1 describes local binary patterns. In Section 2, learning LBPH bin using Adaboost is discussed. Section 3 presents extensive experiments. Finally Section 4 concludes the paper.

II. RELATED WORK

The image of a person's face exhibits many variations which may affect the ability of a computer vision system to recognize the gender. We can categorize these variations as being caused by the human or the image capture process.Human factors are due to the characteristics of a person, such as age, ethnicity and facial expressions (neutral, smiling, closed eyes etc.), and the accessories being worn (such as eye glasses and hat). Factors due to the image capture process are the person's head pose, lighting or illumination, and image quality (blurring, noise, low resolution).Head pose refers to the orientation of the head relative to the view of the image capturing device. The human head is limited to three degrees of freedom, as described by the pitch, roll and yaw angles [1].The impact of age and ethnicity on the accuracy of gender classification has been observed. Benabdelkader and Griffin [2], after testing their classifier with a set of 12,964 face images, found that a disproportionately large number of elderly females and young males were misclassified. In empirical studies by Guo et al. [3] using several classification method on a large face database, it was found that gender classification accuracy was significantly affected by age, with adult faces having higher accuracies than young or senior faces. In [4], when a generic gender classifier trained for all ethnicities was tested on a specific ethnicity, the result was not as good as a classifier trained specifically for that ethnicity. Studies have shown that a human can easily differentiate between a male and female (above 95% accuracy from faces [5]). However, it is a challenging task for computer vision. Nevertheless, such attribute classification problems have not been as well studied compared to the more popular problem of individual recognition. In this paper, we survey the methods used for human gender recognition in images and videos using computer vision techniques. In the detection phase, given an image, the human subject or face region is detected and the image is cropped. This will be followed by some preprocessing, for example to normalize against variations in scale and illumination. A widely used method for face detection is by Viola and Jones [6], which has an OpenCV implementation. The benchmark for human detection is based on using Histogram of Oriented Gradients (HOG) [7]. In the case of gait analysis, many methods use a binary silhouette of the human which is extracted using background subtraction. In feature extraction, representative descriptors of the image are found and selection of the most discriminative features may be made. In some cases when the number of features is too high, dimension reduction can be applied. As this step is perhaps the most important to achieve high recognition accuracy, we will provide a more detailed review in later sections. Lastly, the classifier is trained and validated with a dataset. Gender recognition is a within-object classification problem [8]. The subject is to be classified as either male or female, therefore a binary classifier is used. Examples of classifiers that have been widely used to perform gender recognition are Support Vector Machine (SVM), Adaboost,neural networks and Bayesian classifier. From our survey, SVM is the most widely used face gender classifier (usually using a non-linear kernel such as the radial basis function), followed by boosting approaches such as Adaboost. Nearest neighbor classifier and Markov models are also popular for gait-based gender classifiers.

III.METHODOLOGY

1. LOCAL BINARY PATTERNS

The original LBP operator (Ojala et al., 2002) labels the pixels of an image by thresholding neighborhood of each pixel with the center value and considering the results as a binary number.Formally, given a pixel at (xc,yc), the resulting LBP can be expressed in the decimal form as where n runs over the 8 neighbors of the central pixel, ic and in are the gray-level values of the central pixel and the surrounding pixel,and s(x) is 1 if xP0 and 0 otherwise.Ojala et al. (2002) later made two extensions of the original operator. Firstly, the operator was extended to use neighborhood of different sizes, to capture dominant features at different scales.Using circular neighborhoods and bilinearly interpolating the pixel values allow any radius and number of pixels in the neighborhood.The notation (P,R) denotes a neighborhood of P equally spaced sampling points on a circle of radius of R. Secondly, they proposed to use a small subset of the 2P patterns, produced by the operator LBP(P,R), to describe the texture of images. These patterns, called uniform patterns, contain at most two bitwise transitions from 0 to 1 or vice versa when considered as a circular binary string. For example, 00000000, 001110000 and 11100001 are uniform patterns.It was observed that most of the texture information was contained in the

uniform patterns. Labeling the patterns which have more than 2 transitions with a single label yields an LBP operator,denoted LBP(P,R,u2), which produces much less patterns without losing too much information.After labeling an image with a LBP operator, a histogram of the labeled image can be used as texture descriptor. Each face image can be seen as a composition of micro-patterns which can be effectively described by LBP. In the existing studies (Ahonen et al.,2004), to consider the shape information, face images are divided into non-overlapping sub-regions (as shown in Fig. 2); the LBP histograms extracted from sub-regions are concatenated into a single,spatially enhanced feature histogram The extracted feature histogram describes the local texture and global shape of face images.The limitations of the above LBP-based facial representation arethat dividing the face into a grid of sub-regions is somewhat arbitrary,as sub-regions are not necessary well aligned with facial features,and that the resulting facial representation suffers from fixedsize and position of sub-regions. In Zhang et al. (2004), Sun et al.(2006), Adaboost was used to learn the discriminative sub-regions (in term of LBP histogram) from a large pool of sub-regions generated by shifting and scaling a sub-window over face images. In these studies, the Chi square distance between corresponding LBP histograms of the sample image and the template is used to construct the weak classifier.

2. LEARNING LBP-HISTOGRAM BINS

In the existing work, the LBP histograms are always extracted from local regions, and used as a whole for the regional description.However, not all bins in the LBP histogram are discriminative for facial representation. Here we propose to learn discriminative LBP-Histogram (LBPH) bins for better gender classification.Adaboost (Freund and Schapire, 1997; Schapire and Singer,1999) provides a simple yet effective approach for stagewise learning of a nonlinear classification function. Here we adopt Adaboost to learn the discriminative LBPH bins. Adaboost learns a small number of weak classifiers whose performance is just better than random guessing, and boosts them iteratively into a strong classifier of higher accuracy. The process of Adaboost maintains a distribution on the training samples. At each iteration, a weak classifier which minimizes the weighted error rate is selected, and the distribution is updated to increase the weights of the misclassified samples and reduce the importance of the others. Similar to Viola and Jones (2001), the weak classifier hj(x) consists of a feature fj which corresponds to a single LBPH bin, a threshold hj and a parity pj indicating the direction of the inequality sign:

3. EXPERIMENTS

We conduct experiments on the LFW database (Huang et al., 2007). LFW is a database for studying the problem of unconstrained face recognition, which contains 13,233 color face photographs of 5,749 subjects collected from the web. All the faces were detected by the Viola-Jones face detector (Viola and Jones, 2004), and the images were centered using detected faces and scaled to the size of 250x250 pixels. We manually labeled the ground truth regarding gender for each face. The faces that are not (near) frontal, as well as those for which it is difficult to establish the ground truth, were not considered (see Fig. 3 for some examples). In our experiments, we chose 7,443 face images (2,943 females and 4,500 males); see Fig. 1 for some examples. All experimental results were obtained using the 5-fold cross-validation. We partitioned the data set into five subsets of similar size, keeping the same ratio between female and male. The images of a particular subject appear only in one subset. As illustrated in Fig. 4, all images were aligned with commercial face alignment software (Wolf et al., 2009); the grayscale faces of 127x91 pixels were cropped from aligned images for use.

IV. RESULTS

To improve computation efficiency, we adopted a coarse to fine feature selection scheme: We first run Adaboost to select LBPH bins from each single scale LBP(8,R,u2), then applied Adaboost to the selected LBPH bins at different scales to obtain the final feature selection results. We plot in Fig. 2 the recognition performance of the boosted strong classifiers as a function of the number of features selected. We can see that the boosted strong classifier of multiscale LBP provides better performance than that of each single scale, achieving the recognition rate of 94.40%.

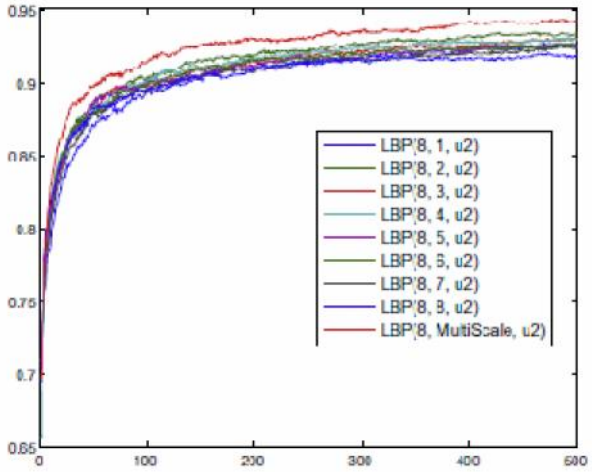

.

Fig.2.Classification Performance of boosted strong classifiers.

As observed in Table 2, the boosted LBP features also produce smaller standard variation. We see in Table 1 there is notable bias towards males in all experiments, as observed in existing studies (Shakhnarovich et al., 2002). This might be due to the unbalanced training data.

Approach			Recognition rates (%)		
Feature	Dimension	Classifier	Female	Male	Overall
Raw pixels	2,944	SVM	86.89	94.13	91.27 ± 1.67
Standard LBP	2,478	SVM	89.78	95.73	93.58 ± 1.50
Boosted LBP	500	Adaboost	91.98	95.98	94.40 ± 0.86
Boosted LBP	500	SVM	92.02	96.64	94.81 ± 1.10

Table 1.Experimental results of Gender classifications

VI CONCLUSION

In this paper, we investigate gender classification on real-life faces acquired in unconstrained conditions, a challenging but relatively understudied problem. We learn discriminative LBP-Histogram bins as compact facial representation for gender classification. By adopting SVM with the selected LBPH bins, we obtain the classification rate of 94.81% on the LFW database

ACKNOWLEDGEMENT

We wish to express our sincere thanks to all the staff member of E.C.E Department, PSN Colleg of Engineering and Technology for their help and cooperation.

REFERENCES

[1]. *E. Murphy-Chutorian and M. M. Trivedi*, "Head pose estimation in computer vision: A survey," Pattern Analysis and Machine Intelligence, IEEE Transactions on, vol. 31, no.4, pp. 607–626, 2009.

[2]. *C. Benabdelkader and P. Griffin*, "A Local Region-based Approach to Gender Classification From Face Images," in Computer Vision and Pattern Recognition-Workshops, 2005.CVPR Workshops. IEEE Computer Society Conference on, 2005, p. 52.

[3]. *G. Guo, C. R. Dyer, Y. Fu, and T. S. Huang*, "Is gender recognition affected by age?," in Computer Vision Workshops (ICCV Workshops), 2009 IEEE 12th International Conference on, 2009, pp. 2032–2039.

First Author Mr. R.Jeganlal pursuing his M.E Degree from PSN college of engineering & Technology.

Second Author Prof.V.Gopi is working as Professor in ECE Department,PSN College of Engineering and Technology.

Third Author Ms.S.Rajeswari is working as Assistant Professor in ECE Department,PSN College of Engineering and Technology.

Prolonged Network Lifetime and Data Wholeness By Clusters Using B-Ct Algorithm

M.Keerthika and Dr.P.S.Periasamy

Abstract-The unique characteristics of cost and rapid deployment of sensor networks feigns exciting applications in the areas of communication and in industrial automation, which makes the wireless sensor network, an integral part of our life. The key challenge in the design of WSN is being the power consumption of the entire network thereby prolonging the network lifetime. This is possibly being achieved by introducing the cluster head multicast routing communication. The existing methods lacks in minimizing the power consumption of data transmission from source to destination due to network overhead. Thus, the cluster head is built to overcome the deficiencies of existing works.The basic concept of cluster head is to perform filtering of raw data collected from its clusters and transmitting the filtered packets to the destination. This paper deals in performing the concept in two different topologies which abruptly reduces the network overhead and achieves in the reduction of total power consumption of WSN. Further, the implemented algorithm is validated through simulations and has proven its mere performance and scalability.

Index terms: Mobile sinks, wireless sensor networks, information retrieval, clustering, sensor islands, rendezvous nodes.

1 INTRODUCTION

A Wireless Sensor Network (WSN) is formed from a large number of tiny nodes deployed in a particular region of wireless networks. Each sensor node has its own availabilities with it. The specifications of these nodes vary, depending on the requirements and the application. Further the nodes has its advantage of using minimal power and memory. With those specifications the wireless sensor networks use the sensor nodes in various application. However, at the same time, WSNs pose a variety of challenges and difficulties. The typical WSN consists of two main components: sensors and sink. The main purpose of sensor is to sense , process and to collect the data from its sources. The sink, or base station (BS), is the place where the gathered data is received and then delivered to the user.Providing Quality of Service (QoS) support in WSNs for improving their timing and reliability performance under severe energy constraints has attracted recent research works. The standardization efforts of the IEEE task have contributed to solve this problem by the definition of the IEEE 802.15.4 protocol are cheap and its widely used in Wireless Personal Area Networks (WPANs). In fact, this protocol shows great potential for flexibly fitting different requirements of WSN applications by adequately setting its parameters (low duty cycles, guaranteed time slots (GTS)).

M.Keerthika is studying M.E Communication Systems, K.S.R. College of Engineering, Tiruchengode. And Dr.P.S.Periasamy is working as Proff & Head, Department of ECE, K.S.R College of Engineering, Tiruchengode. Keerthi.mks@gmail.com,periasamy.ps@gmail.com.

A PAN composed of multiple devices that have to transmit data to the PAN coordinator through single or multiple hops. We assume that the application requires periodic data at the PAN coordinator each node, upon reception of a query coming from the PAN coordinator, generates a packet and attempts to access the channel to transmit it.

Therefore, each node has only one packet per query to be transmitted. If the node does not succeed in accessing the channel before the reception of the next query, the packet is lost, and a new one is generated in the mode in which the beacon is enabled, the IEEE 802.15.4 protocol uses slotted CSMA/CA as a Medium Access Protocol (MAC). Even though the IEEE 802.15.4 protocol provides the GTS allocation mechanism for real-time flows, the allocation must be preceded by an allocation request message. However, with its original specification, the CSMA/CA which is slotted has no QoS support for such time-sensitive events, including GTS allocation requests, alarms, PAN management commands, etc., which may result in unfairness and in the reduction of network lifetime, particularly in high load conditions.

II. TECHNICAL OVERVIEW

Zigbee is cheap, low-power, wireless mesh network. First, it allows the technology to be widely used in various applications such as monitoring and deploying the sensors. Second, it allows low power-usage with longer life which employs only smaller batteries. Third, the given wireless mesh standard provides high reliability and wide range. It has not possess the capability of power network which is used along with other necessary elements. In other words, Zigbee protocol has its purpose not to support power line networking but intended to support for various smart applications. e.g. Penn Energy, which has its intent to require them to interoperate again via the open AN standards.

III.PROTOCOLS

The protocols build on recent algorithmic research (Ad-hoc On-demand Distance Vector, neuRFon) to automatically construct a low-speed ad-hoc network of nodes. In large wireless sensor networks, it has its group of clusters. Which can also group into a mesh or a single cluster. The beacn and non- beacon modes are supported by current profiles of the ZigBee protocol .

In unslotted CSMA/CA mechanisms it uses non-beacon interval mode . In such network zigbee has its robust power requirement out of which some met its power requirements whereas some needs external stimulus.The light switch being the best example. The lamp which uses ZigBee node will receive continous power supply, since it is connected to the given mains supply, while a power light

battery will be in asleep mode when it is thrown. It then wakes up to receive the data, acknowledge it and then goes to sleep mode again. Such a network is used in lamp node and zigbee found its requirements in all such traits accordingly.

The beacon-enabled network uses special network nodes called ZigBee Routers which transmit periodic beacons in which other nodes confirm its presence. Nodes may swing between its duty cycle and battery life. Beacon intervals has its range from 15.36 milliseconds to 15.36 ms * 214 = 251.65824 seconds at 250 kbit/s, from 24 milliseconds to 24 ms * 214 = 393.216 seconds at 40 kbit/s and from 48 milliseconds to 48 ms * 214 = 786.432 seconds at 20 kbit/s. However, long beacon intervals with low duty cycle requires less power. In general, the ZigBee protocols use less power and as this being used in two different mode such as beacon and non-beacon, the power requirements is used accordingly. In beacon mode the node is active only at the time of transmitting and receiving data and in the remaining time, the nodes fall asleep. Whereas, in non-beacon mode the nodes should be active all the time through the entire network.

The general access mode is "carrier sense, multiple access/collision avoidance" (CSMA/CA). That is, the nodes talk as in the same way as persons do. It has its expectations in three ways such as time scheduling, message acknowledgement and not to use CSMA.. Finally, Guaranteed Time Slots used by devices in Beacon Oriented networks has low latency which by definition do not use CSMA indispensable in system such as IVC to have the ability of selectively revoke the group memberships of the compromised vehicles by updating keys or releasing Certificate Revocation Lists (CRLs).

IV. CLUSTERING TECHNIQUE

The network is sectioned into a set of subnetworks, each of which is called a cluster. Ineach cluster, one node represents the others and is called the cluster head (CH). Since theCH is responsible for all of the events inside its clusterin which according to essential algorithm it moves to another node and form its CH when the probability is high. One of the notable protocolsthat follows this technique is LEACH and EDACH.Since LEACH in WSN is introduced first. TheLEACH (Low-Energy Adaptive Clustering Hierarchy) protocol, which is presented by Heinzelmanet al., is a well-known protocol that follows the clustering scheme. LEACH assumes thatthe nodes inside the fixed network , and that the base station is away from them. All nodes in the network are homogenous and energy constrained. However, in LEACHprotocol, some nodes consume more energy than others, which leads, over time, to somenodes being disconnected from its network. The main reason to use the LEACH protocol is to divide the network into a number of sub-networks called clusters.

Each clusterconsists of a fixed number of nodes in which the nodes vote and select its representative, theCH. Each sensor inside the cluster should send its data to the CH, which is responsible to deliver the data to its sink. As mentioned above, this process can lead the CH tohandle the most significant tasks inside the cluster, which means the CH loses its energy faster than the other nodes. LEACH is a Time Division Multiple Access (TDMA) –based protocol which gives time slots for each node to exchange data between its member nodes and their CH. The TDMA with round algorithm measures the probability of nodes becoming CH. The rounds are the corner stones of the LEACH protocol and algorithm. Each round is composed generally oftwo phases: setup phase and a steady-state phase. During the setup phase, the cluster is elected by creating the clusters. The second phase is responsible for distributing the timeslots among the network nodes.

V. BACK - BONE CLUSTER PROTOCOL

In the proposed protocol, the public buses which is mounted by circulating within urban environments on fixed trajectories and in its near-periodic schedule. We assumption that sensors are deployed in urban areas in which the proximity to public transportation vehicle routes in different area. Also, an adequate number of nodes are emplyed as RNs gives energy depletion and less throghput. Finally, separate clusters are grouped under SN.

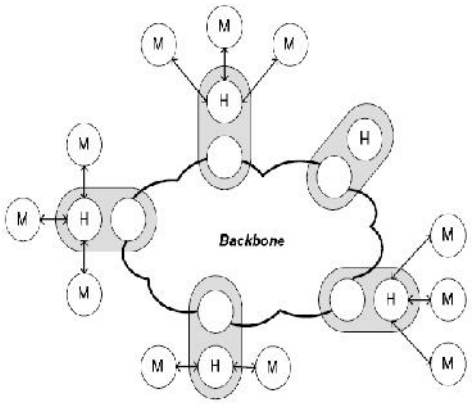

The structure of a protocol node in the B-CT protocol is shown in Figure 2. The node has its backbone protocol in which cluster members do not join the backbone overlay topology. The B-CT node exploits a property of the overlay node design that permits a multiple internal overlay nodes contain in a overlay node. Virtual adapter is used to communicate via internet protocol, called a dummy adapter, and protocol messages from the internal protocol nodes are multiplexed on a encapsulation header. The Muliplexing protocol (MUX) is also performed by encapsulation header.

The B-CT protocol has only a single exchange of protocol messages, whose purpose is to assign a backbone logical address LABBone to a cluster member.

A cluster head send its request to the cluster members.In HyperCast, application data is forwarded in spanning trees that are embedded in the overlay topology. Each node forwards data to one or more of its neighbours in the overlay topology. A multicast message is forwarded downstream in a rooted tree that has the sender of the multicast message as the root. A unicast message is forwarded upstream in a rooted tree that has the destination of the message as the root. In HyperCast, each node can locally compute its upstream neighbour (parent) and its downstream neighbours (children) with respect to a given root note. In the B-CT protocol, the computation must consider neighbours in a cluster topology as well as in the backbone topology. If a B-CT that contains a CT node that

is a cluster member, the situation is simple since a node has only one neighbour, i.e., its cluster head. Let us now look at a B-CT node that contains a cluster head.

The neighbourhood of this node is the union of the neighbours in the cluster and the backbone network. When this node calculates the downstream neighbours in the overlay network and it identifies the cluster network. If so, the neighbours in the downstream are all other cluster members and all downstream neighbours in a spanning tree that has the local node as the root. If the root is not one of its cluster members, then the downstream nodes consists of its downstream neighbours with respect to the given root in the backbone and all cluster members. An upstream neighbour uses any one of its cluster members(if the root is in its cluster), and in the backbone network (if the root node is not one of its cluster members).Thus, the overhead of multihop data relaying to the edge RNs is minimized. Given that the communication cost is several orders of magnitude higher than the computation cost in-cluster data aggregation can achieve significant energy savings. Also, we assume that each node has a fixed number of transmission power levels. Finally, we assume theunit disk model, which is the most common assumption in sensor network literature. The underlying assumption in this model is that nodes which are closer than a certain distance (transmission range R)can always communicate. However, in practice a message sent by a node is received by the receiver with only certain probability even if the distance of the two nodes is smaller than the transmission range. It will describe how our protocol can be adapted so that it can still work on the top of a morerealistic physical layer.

VI. SIMULATION RESULTS

Distribution of traffic

graph 1, pstree as a function of N1, for different values of N, D, and SO, having set BO = 5, is shown. There exists an optimum value of N1 maximizing pstree , and this value obviously increases by increasing N and is approximately equal to √N; therefore, it is independent of D and SO. This means that, once we fix N, there exists an optimum split between level one and level two nodes, maximizing the probability of success traffic are shown.

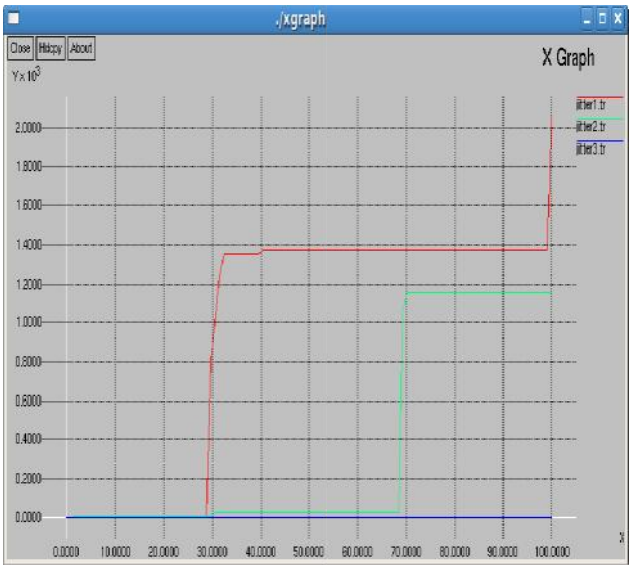

Throughput

In graph 2, results related to the two topologies, showing the success probability as a function of N for different values of SO and BO by setting D = 5, are compared. For a fair comparison, the success probability is computed by fixing the same value of TB and, therefore, by giving to nodes the same time to transmit the data to thecoordinator.

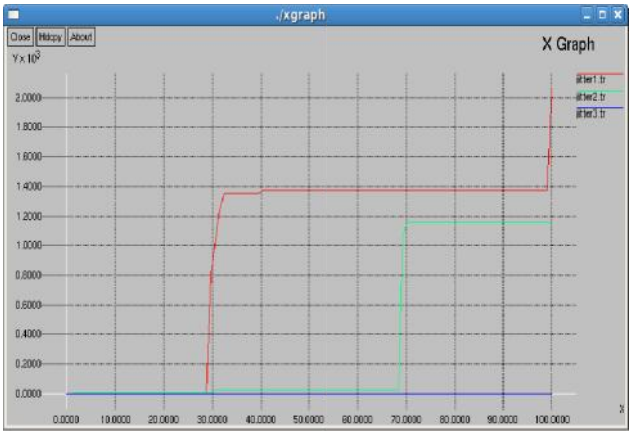

To this aim, we set SO = BO for the star topology y, and we compare the case “star” with SO = BO = 1 with the case “tree,” with BO = 1 and SO = 0, whereas the case “star” with SO = BO > 1 (note that the cases SO = BO = 2, 3, etc., bring the same ps) are compared with the cases “tree” with BO > 1, whatever SO is. In the “tree” case, N1 is set to the optimum value maximizing pstreeobtained. As we can see, when BO = 1, the “star” is preferable since in the “tree” only one router has a part of the superframe allocated; therefore, many packets of level two nodes are lost. For BO > 1, instead, the “tree” outperforms the “star.” The difference between the “star” and the “tree” obviously increases by increasing BO and SO, resulting in an increase in pframe and ps, respectively.

Probability of success changes when different loads

The average delays obtained in case of star and tree-based topologies as a function of N are shown. The curves are obtained by setting D = 5 and N1 = 3 in the case of trees. The delays increase by increasing N since the probability of finding the channel busy and delaying the transmission gets larger. A horizontal asymptote is also

present due to the maximum delay that a packet may suffer, which is equal to the superframe duration TA in the "star" case and to TB + TA in the "tree" case. As expected, the delays are larger for trees since packets coming from level two nodes need two super frames to reach the coordinator. Also note that by increasing BO, delays get significantly larger. The curves "tree" with SO=0, BO=3 and "tree" with SO = 1 and BO = 3 overlapped since TB assumes the same value and the delays of level one nodes are approximately the same (in fact, the curves "star" with SO =BO = 0 and SO = BO = 1 are also approximately the same).By comparing Figs. 11 and 12, we can finally deduce that the choice of the topology depends on the application requirements.

VII. CONCLUSIONS

This paper introduced backbone clustering protocol that proposes the use of urban buses to carry MSs that retrieve information from isolated parts of WSNs. The connectivity objective is to employ MSs to collect data from isolated urban sensor islands and also through prolonged lifetime of selected peripheral RNs which lie within the range of passing MSs and used to cache and deliver sensory data derived from remote source nodes. High data throughput is assured by regulating the number of RNs for allowing sufficient time to deliver their buffered data and preventing data losses.

Unlike other approaches, B-CT moves the processing and datatransmission burden away from the vital periphery nodes (RNs) and enables balanced energy consumption across the WSN through building cluster structures that exploit the high redundancy of data collected from neighbor nodes and minimize intercluster data overhead.

While comparing the performance of those three protocols,will get an minimum power consumption from the B-CT protocol.The performance gain of Backbone cluster over alternative approaches has been validated by extensive simulation tests.

REFERENCES

[1] Charalampos Konstantopoulos,Grammati Pantzi ou, DamianousGavalas, Aristides Mpitziopoulos, and Basillis Mamalis, "A Rendezvous Based Approach Enabling EnergyEfficient Sensory Data Collection with Mobile Sinks"., vol. 23, NO .5, MAY 2012.

[2] E. Hamida and G. Chelius, "Strategies for Data Dissemination to Mobile Sinks in Wireless Sensor Networks," IEEE Wireless Comm., vol. 15, no. 6, pp. 31-37, Dec. 2008.

[3] S. Olariu and I. Stojmenovic, "Design Guidelines for Maximizing Lifetime and Avoiding Energy Holes in Sensor Networks with Uniform Distribution and Uniform Reporting," Proc. IEEE INFOCOM, 2006.

[4] X. Li, A. Nayak, and I. Stojmenovic, "Sink Mobility in WirelesSensor Networks," Wireless Sensor and Actuator Networks, A. Nayak, I. Stojmenovic, eds., Wiley, 2010.

[5] B. Mamalis, D. Gavalas, C. Konstantopoulos, and G. Pantziou, "Clustering in Wireless Sensor Networks," RFID and Sensor Networks: Architectures, Protocols, Security and Integrations, Y. Zhang, L.T. Yang, J. Chen, eds., pp. 324-353, CRC Press, 2009.

[6] G. Chen, C. Li, M. Ye, and J. Wu., "An Unequal Cluster-Based Routing Protocol in Wireless Sensor Networks," Wireless Networks, vol. 15, pp. 193-207, 2007.

[7] S. Soro and W.B. Heinzelman, "Prolonging the Lifetime of Wireless Sensor Networks via Unequal Clustering," Proc. 19thIEEE Int'l Parallel and Distributed Processing Symp., 2005.

[8] J. Luo and J-P.Hubaux, "Joint Mobility and Routing for Lifetime Elongation in Wireless Sensor Networks," Proc. IEEE INFOCOM, 2005.

[9] M. Demirbas, O. Soysal, and A. Tosun, "Data Salmon: A Greedy Mobile Basestation Protocol for Efficient Data Collection in Wireless Sensor Networks," Proc. Int'l Conf. DistributeComputing in Sensor Systems (DCOSS '07), pp. 267-280, 2007.

Keerthika.M -Received B.E degree in Electronics and communication Engineering in Sengunthar college of engineering.She is pursing Master of Engineering in Communication Systems at K. S. R. College of Engineering. She presented a paper in an International conference at Magna Engineering College.and she is presented many papers in national level conferences, Her research interests include wireless sensor network, network security, and Digital image processing.

Dr.P.S.Periasamy- received B.E degree in Electrical and Electronics Engineering in Government college of engineering,Salem,University of Madras.and completed his M.E in Applied Electronics in Government College of Technology,Coimbatore,bharathiyar university,Tamilnadu.and he is presently working as a Proff & Head in K. S. R. College of Engineering.He published seven papers in international journal and two papers in national journal,his area of interest is Digital Image Processing,computr ntworks and signal processing,He pulished many papers in internatinal and national conferences.He is a life member of ISTE,IETE,BES,and CSI.

Performance Evaluation of WDM RoF Link at various data rates

Kumari Kalpna, Reena Joshi and Kanu Gopal

Abstract: ***The objective of this paper is to investigate the performance evaluation of WDM RoF link. In this paper, WDM Radio over Fiber (RoF) system is introduced, which is one of the enabling technologies for 3G and beyond. The performance evaluation of WDM Radio over Fiber transmission system (RoF), based on various performance metrics such as Q-factor, BER and eye opening has been made at various data rates. The integration of the two systems is responding to the demands for high data rate applications and reasonable mobility for broadband communication. This work deals with the modeling, realization and characterization of WDM RoF systems providing data rates within the 100 to 3000 Mbps range. It has been investigated that system provides optimum results at data rate of 500 Mbps.***

Keywords: **WDM RoF, Q-Factor, BER, eye opening and jitter.**

I. INTRODUCTION

With the development of wireless communication system, the bandwidth requirements of the radio signal rapidly increased to realize multi-gigabit/s broadband wireless access. In order to avoid the congestion at low frequency band, the carrier frequency is required to move toward a higher frequency band and wave length division multiplexing radio-over-fiber (WDM RoF) is the most preferred option. WDM RoF systems are attractive for broadband wireless access networks supporting broadband multimedia wireless services [1]. This paper is organized as follow: In Section II WDM RoF link is modeled to verify our proposed scheme. In section III & IV, the simulation results are evaluated and the tolerances of the proposed system are discussed. Finally, a conclusion is given in Section V.

II. SYSTEM MODEL

The System model of 8 Channel WDM RoF System is as shown in fig. 1. The system has been designed and optimized using simulation tool Optsim 5.1, a photonic system simulation tool by RSoft, USA. Central station (CS) transmits optical intermediate frequency (IF) and local oscillator (LO) signals to the remote node where amplification and wavelength conversion takes place. At central station each data channel transmits 100Mbps to 3000Mbps data which is DPSK-encoded over 2.5GHz IF [2].

Kumari Kalpna, Reena Joshi and Kanu Gopal are with College of Engineering & Management, Kapurthala, Email: Er.katoch@gmail.com, er.reena7@gmail.com, kanugopal34@gmail.com

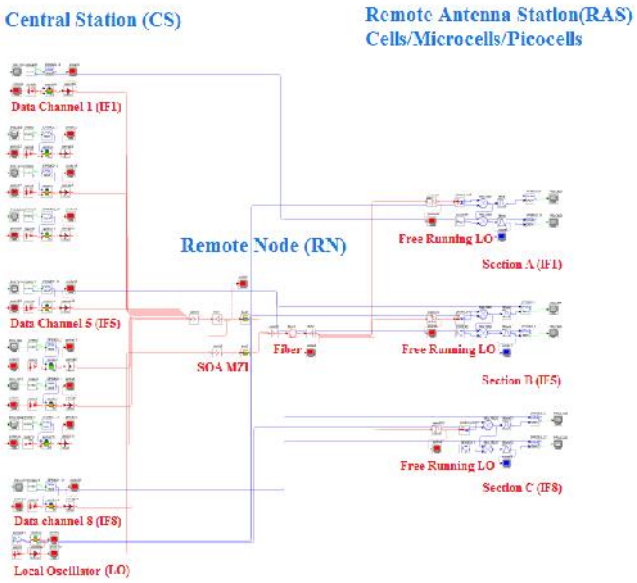

Fig.1 Simulation model for WDM RoF link

Central station transmits this IF to remote node where wavelength conversions take place using SOA-MZI. The modulated signals are transmitted to remote antenna stations (RAS) covering each cell. In this model DPSK-encoded multiple data channels in the wavelength range of 1545.80 nm to 1552.20 nm and local oscillator frequency of 25 GHz is transmitted over a common optical fibre for simultaneous wavelength conversions, while keeping crosstalk penalties at minimum [3].

III. PERFORMANCE EVALUATION OF WDM ROF LINK AT VARIOUS DATA RATES

The Performance of the modeled WDM RoF link is evaluated on the basis of Eye opening, BER and Q Value at Output Section A, B and C for data rates from 100 Mbps to 3000 Mbps. The output has been obtained on the sample basis from higher wavelength channel, central wavelength channel and lower wavelength channel in order to check the optimal functioning of the system over entire wavelength range. A pseudo random sequence length of bits taken one bit per symbol is used to obtain realistic output values at the receiver. The electroscope gives eye diagram, Q factor, Bit error rate (BER) and eye pattern [5]. To observe the impact of data rates upon system performance, simulation results are obtained for different data rates varying from 100 Mbps to 3000 Mbps. BER of the order of e-14 and Q value more than 16 dB has been reported at 500 Mbps, which results in an optimal value for the modeled system. Simulation results obtained reveal that with increase in data rate impact of dispersion become dominant resulting in high BER and poor Q value.

IV. RESULTS AND DISCUSSIONS

The eye patterns of received signal corresponding to λ=1552.20 nm, λ=1549 nm and λ=1545.80 nm are shown in figure 2- 4.

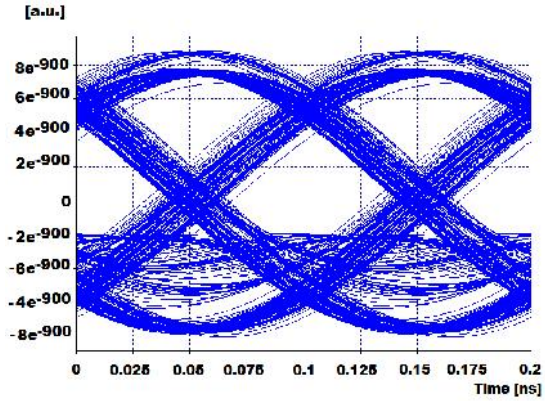

Fig. 2.Eye patterns of received signal at (a) ^{a}=1552.20 nm

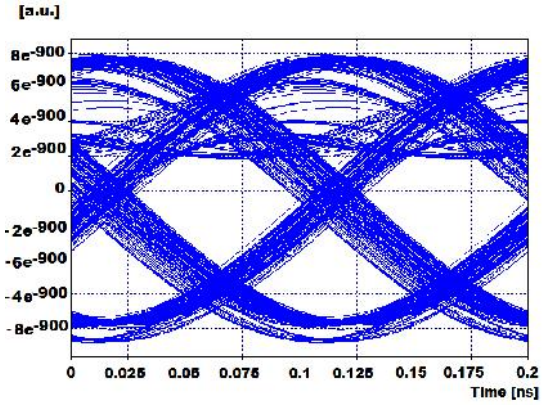

Fig. 3.Eye patterns of received signal at (a) ^{a}=1549 nm

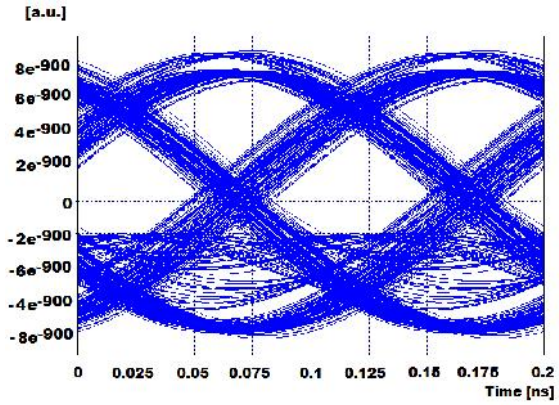

Fig. 4.Eye patterns of received signal at (a) ^{a}=1545.80 nm

The discrete eye opening, Q value reported more than 16 dB and BER of less than e-14 indicates the error free transmission and robustness of the modeled system [7].

V. CONCLUSION

It is observed that the optimal BER of e-14 and Q value of 16 dB has been reported at data rate of 500 Mbps. At data rates beyond 500 Mbps eye tends to close and BER increases beyond the threshold value indicating that the modeled system is suitable for data rate upto 500 Mbps. Hence the system is suitable for high capacity remote antenna applications.

REFERENCES

[1] Hidenori Taga, "Long Distance Transmission Experiments Using the WDM Technology" Journal of Lightwave Technology, Vol. 14, No. 6, 1996.

[2] Anthony Ngoma, "Radio-over-Fiber Technology for Broadband Wireless Communication Systems" Master thesis submitted to the Department of Electrical Engineering at Technical University, Eindhoven, 2005.

[3] Hong Bong Kim, "Radio over Fiber based Network Architecture", Ph.D. thesis in Department of Electronics and Information Technology University of Berlin, 2005.

[4] Reza Abdolee, Razali Ngah, Vida Vakilian and Tharek A.Rahman, "Application of Radio-over-Fiber (RoF) in mobile communication" Proceeding of Asia-Pacific Conference on Applied Electromagnetic, Melaka, Malaysia, 2007.

[5] Pardeep Kaur and R.S.Kaler, "Radio over Fiber Networks", Proceedings of National Conference on Challenges and Opportunities in Information Technology (COIT-2007) RIMT-IET, Mandi Gobindgarh, 2007.

[6] Vishal Sharma, Amarpal Singh and Ajay K. Sharma, "Simulative investigation of nonlinear distortion in single-and two-tone RoF systems using direct-and external-modulation techniques" International Journal for Light and Electron Optics, Optik, Vol. 121, Issue 17, pp.1545-1549, 2008.

[7] Vishal Sharma, Amarpal Singh and Ajay K. Sharma, "Challenges to radio over fiber (RoF) technology and its mitigation schemes – A review" Volume 123, Issue 4, pp. 338-342, 2012.

Software Testing By Using Knowledge Based Approach

Amrita Singh and Er.Anil Pandey

Abstract: Knowledge Management concept for accessing the true and optimal result in the field of software testing. In this paper, we propose knowledge based approach for rectifying the error and give the result as much correct. First we go for testing categories and its approach for testing quality software. Intelligent means optimal result for help of best testing method. Testing is a process centered on the goal of finding defects in a system. There are numbers of method are present to test software. But a rule-based approach, the domain knowledge is represented by a set of production rules and less depends to tester. Data is represented by a set of facts. And predication is based on condition satisfaction.

Keywords: Knowledge, Knowledge management, Rule based, Software testing.

I. INTRODUCTION

Software engineering is deligent knowledge work. Management of knowledge in software engineering has received consideration. Knowledge is one of the organization's most important values, affecting its combativeness. One way to acquire organization's knowledge and make it available to all their associates is through the use of knowledge management system. Knowledge classification survey makes an important contribution to advancing knowledge in both science and engineering.

The knowledge management as a set of activities, Technique and tools are supporting the creation and transfer of software engineering (SE) knowledge management organization.

Effective knowledge management of the testing process is the key to improve the quality of software testing. Knowledge management has different features in software testing. One of the most important research questions is how to effectively integrate the knowledge management with the software testing process so that the knowledge assets can be spread and reused in software testing organizations [1].

In this paper, the current state of knowledge management in rule based was analyzed and the major existing problems were identified; rule based methods was proposed towards a knowledge Management system in rule based was designed and implemented. Knowledge management is the process of capturing and making use of an organization's collective expertise anywhere in the business [2].

Amrita Singh and Er.Anil Pandey are with Computer Science and Engineering, Invertis University Bareilly, Emails: amritas054@gmail.com, anil.p@invertis.org

The importance of knowledge management that has become a hot spot in international manages fields. In order to enhance its competitive power, many enterprises have initiatively taken knowledge management into their core business process, which drives the development of consultation business whose new business scope is knowledge management, and then a lot of software tools and systems about knowledge management have been developed by IT enterprise [3].

Knowledge management is an approach to discovering, capturing, and reusing both tacit (in people's heads) and explicit (digital- or paper-based) knowledge as well as the cultural and technological means of enabling the knowledge management process to be successful [5]. The knowledge management (KM) cornerstone is improving productivity by effective knowledge sharing and transfer [6]. The rule based system, knowledge is represented in the form of (If condition Then conclusion < action >) production rules [7].

Knowledge Management is one of the hottest topics today in both the industry world and information research world. In our daily life, we deal with huge amount of data and information. Data and information is not knowledge until we know how to dig the value out of it. This is the reason we need knowledge management. Unfortunately, there's no universal definition of knowledge management, just as there's no agreement as to what constitutes knowledge in the first place. We chose the following definition for knowledge management for its simplicity and broad context. Knowledge Management (KM) refers to a multi-disciplined approach to achieving organizational objectives by making the best use of knowledge. Knowledge management focuses on processes such as acquiring, creating and sharing knowledge and the cultural and technical foundations that support them.

A knowledge management system facilitates creation, access and reuse of knowledge, and its main goals are to promote knowledge growth, communication, preservation and sharing [8]. The knowledge management approach using software testing involves the process of detecting software discrepancies so that they can be corrected before they are installed into a live environment supporting operational business units [9].

II. KNOWLEDGE BASED APPROACH IN SOFTWARE TESTING

Software testing process normally involved black box and white box of testing. Black Box Testing is conducted on the

application by test engineers or by domain experts to check whether the application is working according to customer requirements.

White box testing method is conducted by developer in a technical perception where as black box testing is conducted by test engineers with end-user perception. Programmers will conduct white box testing in a positive perception whereas tester will conduct black box testing with a negative perception where there is a more chance of finding more defects .The more defects you identify results in a quality system.

White box testing will not cover non functional areas. As functional requirements are also very important for production system those are covered in black box testing.

White Box Testing conducted on the source code by developers to check does the source code is working as expected or not is called white box testing.

As the source code is visible, finding and rectifying the problems is easy for developers. The defects that are identified in white box testing are very economical to resolve. To reduce the defects as early as possible white box testing is helpful. Software testing by using knowledge based approach is:

A. Test Cases

Test case is a set of conditions or variables under which a tester will determine whether a system under test satisfies requirements or works correctly. The process of developing test cases can also help find problems in the requirements or design of an application a test case has components that describes an input, action or event and an expected response, to determine if a feature of an application is working correctly.

Testing an application's or program's working is not black-and-white. A program may work in one situation or condition, but may fail in another. It is up to the software tester, to ensure that a program works correctly in all possible conditions.

Example: Imagine a program which adds two numbers. The program must accept two numerical inputs, perform the addition and display the output. But certain conditions exist, which can hamper the functioning of the program. Like if one input is zero. The program should correctly display the output, which is the number itself. What if one number is negative? Then the program should perform subtraction and correctly assign a positive or negative sign to the answer.

Test cases, at root level, are used to measure how a program handles errors or tricky situations such as if one input is incorrect or if both inputs are incorrect. They are also expected to expose hidden logical errors in the program's code that have gone undetected.

1. Traffic Signal

1. Verify if the traffic lights are having three lights,

(Green, Yellow, Red)

2. Verify that the lights turn on in a sequence

3. Verify that lights turn on in a sequence based on time specified,

(Greenlight min, Yellowloght10sec, Redlight1min)

4. Verify that only one light glow at a time

5. Verify if the speed of the traffic light can be accelerated as time specified based on the traffic

2. *Rule Based*

The people cross the road safely when the traffic light is green, and must stop when the traffic light is red.

IF “traffic light” is green

THEN action is go

IF “traffic light” is red

THEN action is stop

These statements represent the IF-THEN form are called production rules.

B. Knowledge Management (KM)

Knowledge management is based on the idea that an organisation’s most valuable resource is the knowledge of its people. Therefore, the extent to which an organisation performs well, will depend, among other things, on how effectively its people can create new knowledge, share knowledge around the organisation, and use that knowledge to best effect.

Knowledge management is a process that emphasises generating, capturing and sharing information know how and integrating these into business practices and decision making for greater organizational benefit.

C. Knowledge Based System (KBS)

Knowledge-based systems also process data and rules to output information and make decisions. In addition, they also process expert knowledge to output answers, recommendations, and expert advice. The Knowledge management system (KMS) can be implemented by using two components which are involved Knowledge management system (KMS) functionality and its related infrastructure through rule based system .The knowledge management system from the information technological point of view [1], knowledge is an entity differentiated from the information object in that there is an element of expert review and distillation where knowledge is concerned.

III. RULE BASED TESTING METHOD

The rule-based test pattern generation system fig1.The reaching input RI (n) is input signals. Test data generation

rules are used by a rule interpreter to generate new test cases. A simulator executes these test cases. The simulator records coverage statistics for the test inputs. The rule interpreter analyzes the execution results and generates additional test cases. This cycle continues until the amount of requested coverage is achieved or until a user specified number of test cases have been generated and executed. The coverage metric in the rule-based approach is branch coverage.

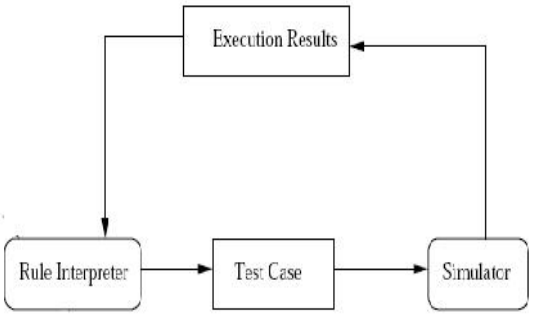

Fig1. Rule based Test Case Generation

A. Test Case Generation Process

The test generation process terms are test pattern, Test case, and branch point.

Test pattern: A test case R = $\{r_1, r_2 \ldots r_z\}$, each r_x $(1 \le x \le n)$ input bit $x_y \in \{0, 1\}$.

Test Case: test case R = $\{r_1, r_2 \ldots r_n\}$, each r_x $(1 \le y \le z)$ input pattern. For example, R = $\{r_1, r_2\}$ = {(0, 1), (0, 0)} is a test case.

Branch Point: let N be the number of nodes in the diagram for n €N, n is a branch point if there is than one outgoing arc.

R reaches p. Given a branch point p and a test case

R =$\{r_1, r_2 \ldots r_m\}$, R reaches p if p is not covered by

$R_{1 \ldots} r_{m-1}$, but covered by r_m,

The test generation processes are:

1. Generate an initial test case R_0= $\{r_{01}, r_{02} \ldots r_{0n}\}$,

$(n \ge 1)$ by some technique .Set x = 0.

2. Simulate the Rule –based Test case Generation model with R_0 and collect branch coverage statistics, include branch coverage for each r_{0y} $(1 \le y \le n)$.

3. While (x < max and coverage <100%), for a branch Point p_z which is not covered yet:

(i) Determine a subsequence Q_m $\{r_x1, r_{x2} \ldots r_{xm}\}$ of R_x = $\{r_{x1}, r_{x2} \ldots, r_{xm}\}$ (m<n) such that Q_m reaches p_k. Let Qm_{-1} = $\{r_{x1}, r_{x2} \ldots r_{xm-1}\}$.
(ii) Usingg test generation rules, generate additional input Patterns Qm' = $\{r'_{xm} \ldots r_{xm'}\}$, (m' > m)
(iii) The new test sequence concatenates patterns in Qm': $R_{x+1} = Q_{m-1}$
(iv) Simulate Rx_{+1}
(v) Increment x

We assume that there is an initial test sequence of input patterns (1) that has been simulated and for which we have step-by-step coverage information (2). As long as the coverage is not complete, and as long as a userdefined number of generation steps have not been exceeded, we do the following: first we determine a branch point we want to cover. Then we determine the subsequence that reaches the branch point (3i). Is more likely to execute the uncovered branch? The simulator executes this new test sequence and records coverage information.

B. Test Data Generation Rules

Test data generation rule consists of two parts: the precondition and the test generation effect. The precondition of a rule describes situations in which the rule could be applied. The test generation effect describes how to generate new test sequences. Three types of rules:
1. Rules with preconditions that apply to any statement
2. Rules for specific types of statements
3. Rules that do not have preconditions and apply to all statements P is an uncovered branch point which we want to cover.p' refers to a branch point that directly dominates p, $p' >_d p$. r_m is the last test pattern in R that reaches p.

Test Case Generation Rules 1:

Precondition: │RI (P) │is less than a given number max
Test generation effect: Generate combinations of values for RI (p). Rule 2 to Rule 7 will not be executed.
Rule 1 is applicable when the length of RI (p) is small.
For example, if │RI (p) │ is 2, only four new test patterns (00, 01, 10, 11) will be generated that contain all the possible values. We do not have to consider the statement type and possible relationships among RI (p).Thus it makes generation easy and fast. However this rule is not 1024 test cases will be produced.

For IF/ELSIF and WHILE statements are the new patterns are generated depending on whether or not the condition contains constants.
1 .p contains constants:

Test Case Generation Rules 2:

Precondition: the statement represented by p is IF, ELSIF or WHILE and p contains constants.
Test generation effect: EACH constant c contained in p, do:
EVERY u € RI (p) that │u│=│c│, set the value of u = c, > c and < c in r_m, in two ways:
(i) Set each u one at a time.

(ii) Set all us at once.

The rule, for a given constant contained in p, which reaching input u € RI (p) has the same dimensionality as the constant. Then we set these reaching inputs to the value of the constant, a value greater than the constant and a value smaller than the constant to form $r_{'m}$ .There can be more than one such u, this should be done in two ways:

(i) Setting one u at a time.

(ii) Setting all us at once, either all equal to c, all greater than c or all smaller than c. For example, in Fig. 2 (I), both e and h have the same dimensionality as constant c =0101. Given r_m = 00011011, we first generate test patterns by changing the value of e without changing h. This produces 01011011 (set e equal to c), 01101011 (e > c), 01001011(e < c) (Fig. 2 (II). Then we change the value of h without changing e. This produces 00010101, 00010110 and 00010100. Finally, we change e and h together which produces 01010101, 01100110 and 01000100. For the other constant"1010" the same steps are executed.

2. P may or may not contain constants:

Test Case Generation Rules 3:

Precondition: the statement represented by P is IF, ELSIF or WHILE and it may or may not contain constants

Test generation effect:

(i) For each u € RI (p), set u to the NOT value of u in r_m to form r'_m in two ways:

(a) Set each u one at a time.

(b) Set all us at once.

(ii) Let u_1, u_2…, u_n be the reaching inputs such that u_x € RI (p), $1 \le x \le n$

(a) Generate combination of reaching inputs of 2, 3 and 4 inputs u_x at a time. The combination has the following format:

= all pairs: $\{u_x, u_y\}$, $1 \le x, y \le n$ and $x \ne y$.

= all triplets: $\{u_x, u_y, u_t\}$, $1 \le x, y, t \le n$ and $x \ne y \ne t$. = all quadruplets: $\{u_x, u_y, u_t, u_k\}$, $1 \le x, y, t, k \in n$ and $x \ne y \ne t \ne k$

(b) Set all u in each combination to the value 0 one at a time whiles other u in the same combination to the value1. Same example shown above, with Rule 2 (i), 11101011 is generated by replacing e with $\bar{e}$ in r_m without changing h (Fig. 2 (III). 00010100 is generated by setting h without changing e. 11100100 are generated by changing both e and h. With Rule 2 (ii), a combination of length 2 {e, f} is generated. If |R (p) |>2, different combinations will be generated which produce more test patterns.

The main idea of Rule 2 and Rule 3 is to set those reaching inputs based on the constants contained in the branch point p .We set the reaching inputs with values equal to, less than and greater than the constants repectively. Some reaching inputs cannot be set to the constants because their length does not match that of any constant, or because the branch condition does not contain a constant. In this case, we replace them with their logical NOT value in r_m. We do not know the relationships between reaching inputs. To consider relationships, we change values for combinations of two, three, and four input signals. Combinations of more than four result in too many new patterns and test cases.

Test Case Generation Rule 4 and 5 apply to CASE statements.

Test Case Generation Rules 4:

Precondition: the statement represented by p is WHEN and the constant used in p is c.

Test generation effect:

A.each u € RI (p) such that |u| = |c|, set u = c to form $r_{m'}$ in two ways:

(i) Set each u one at a time.

(ii) Set all us at once.

B. for each reaching input u € RI (p) that |u|>|c| set every sequential |c| bits of u to the value one at a time.

The idea of this rule is to set the reaching inputs with the constant used in the WHEN statement. The examples are shown in Fig. 2 (IV) and (V). Given r_m = 101011, in step (1), we determine |sel| = |01|, so the value of is changed to 01 without changing en Then 011011 is generated. In step (2), |en|=4>|01|, so we set the 1st and 2nd bit of en to 01 and then set the 2nd and 3rd to 01 and so on. Thus we generate 100111, 101011 and 101001.

Test Case Generation Rules 5:

Precondition: the statement represented by p WHEN OTHERS.

Test generation effect:

(a) determine all constants c that do NOT occur in any P' € DOM (p) (dominators of p).

(b) For every such c, perform Rule 5.

The idea of Rule 4 is to set the reaching inputs to constants that do not appear in WHEN statements.

Those WHEN statements are must be the dominators of p.

Test Case Generation Rules 6:

Precondition: None.

Test generation effect:

(a) The Generate two special test patterns: r_1 with all '1's, with all '0's.

(b) For each u € RI (p), set u = 0 in r_1 one signal at a time.

(c) For each u € RI (p), set u = 1 r_2 in one signal at a time.

This rule generates new test cases based on two special test cases: all '1's and all '0's. Then we set every reaching input to '0' in the all '1' test case and to '1' in the all '0' test case. An example is shown in Fig. 2 (VII).(s_1 , s_2 ,s_3) is the input vector, but for a given branch point p, assume RI(p) = $\{s_1, s_2\}$ }.First the rule requires the two special test patterns r_1 = 111111111 and r_2 = 000000000Then we set s_1, s_2 to '0' one at a time in r_1 and 000111111 and 111001111 are generated. Similarly, we set s_1, s_2 to '1' one at a time in r_2. This generated 111000000 and 000110000.

Test Case Generation Rules 7:

Test generation effect:

For each newly generated test pattern r, generate another new test pattern r' = $\bar{r}$ this rule can help to satisfy the signal criterion that every input bit can make a transition from '0' to '1' and then from '1' to'0'.

Input V = e [3:0], f [3:0]

P_k:

If (e>"0101" and <"1010") then
R_m: (00011011)

(I) Simple code for IF statement

e	h
01011011	
01101011	
01001011	
00010101	
00010110	
00010100	
01010101	
01100110	
01000100	
10101011	
10111011	
10011011	
00011010	
00011011	
00011001	
10101010	
10011001	
10001000	

(II) Generated Test Case using Rule 2 for example (i)

e	f
(e) 11101011	
00010100	
11100100←	
(f) 00000000	

(III) Generated Test Case using Rule3 for example (vi)

Input v = sel [1:0], en [3:0]
P_k:
Case sel is
.....

When "01"→ …..

……..

(IV) Simple code for CASE statement

sel	en

(1)011011←

(2)100111

101011

101001

(V) Generated Test Case using Rule 4 for example (iv)

V: a1 [2:0] a2 [1:0] a3 [3:0]

RI: a1, a2

111111111

000000000

000111111

111001111

111000000

000110000

(VI) Rule 7

Fig.2 Test Case Generation Rules

IV. CONCLUSION

In this paper knowledge based propose a new idea and method to solve the problems for us, but software testing has its features. Knowledge based in software testing is very important to improve the quality of software products and the economic benefit. This paper proposes a new test generation method based on specific rules for test pattern generation. The results show that a rule based test generation will yield higher coverage. We plan to investigate further other types of knowledge that could be used to determine more sophisticated rules. In the future plan to the investigate test Generation heuristics that can explore timing characteristics. Test should applied using a variety of test methods other than random pattern generation and the rule based method.

ACKNOWLEDGEMENT

The author of this paper would like to thank our honorable teacher Professor Mr. Zubair Khan (Head of Department Computer Science and Engineering Invertis University Bareilly, U.P) for his great help and precious suggestion about this work.

REFERENCES

[1] Research and Implementation of Knowledge Management Methods in Software Testing Process Liu Xue-Mei1, 3 GU Guochang1 Liu Yong-Po2 Wu Ji2 1 College of Computer Science and Technology, Harbin Engineering University Heilongjiang 1150001 , China; School of Computer Science and Technology Beijing University Aeronautics and

Astronautics, Beijing 100083, China; 3 Beijing City University Beijing, 100083, China

[2] Toward a Practical Solution for Capturing Knowledge for Software Projects: Seija Komi Sirviö and Annukka Mäntyniemi, *VTT Electronics* Veikko Seppänen, *University of Oulu*

[3] Yongpo Liu Ji Wu School of Computer Science and Technology Beihang University Beijing, China liuypo@sei.buaa.edu.cn Xuemei Liu Guochang Gu College of Computer Science and Technology Harbin Engineering University Heilongjiang, China xuemliu@163.com

[4] Anneliese Andrews, Andrew O'Fallon School of Electrical Engineering and Computer Science Washington State University Pullman, WA 99164 aandrews, aofallon @eecs.wsu.edu Tom Chen Department of Electrical and Computer Engineering Colorado State University Fort Collins, CO 80523 chen@engr.colostate.edu

[5] A three-tier knowledge management scheme for Software engineering support and innovation: Richard D. Corbin a, Christopher B. Dunbar b, Qiuming Zhu c,*

[6] Knowledge Management in Practice: The Case Of Agile Software Development Meira Levy Deutche Telekom Laboratories@ Ben Gurion University and Department of Industrial Engineering & Management Ben-Gurion University of the Negev, Israel Orit Hazzan Department of Education in Technology and Science Technion - Israel Institute of Technology

[7] Louardi Bradji, Mahmoud Boufaida LIRE Laboratory, Mentouri University of Constantine Ain El Bey, Constantine, Algeria E-mail: bradjilouardi@yahoo.fr, mboufaida@umc.edu.dz Received July 23, 2011; revised September 12, 2011; accepted September 22, 2011

[8] Knowledge Management in Software Engineering Environments: Ana Candida Cruz Natali Richard De Almeida Falbo Computer Science Department, Federal University of Espírito Santo, Fernando Ferrari Avenue, CEP 29060 900, Vitória - ES – Brazil {anatali,} falbo}@inf.ufes.br

[9] Ted E. Lee Department of Management Information Systems Fogelman College of Business & Econ, The University of Memphis elee@memphis.edu

[10] B.Lakshmana Rao, G.V Konda Reddy and G.Yedukondalu, "Privacy Preserving in Knowledge Discovery and Data Publishing", International Journal of Emerging Trends in Electrical and Electronics (IJETEE – ISSN: 2320-9569) Vol. 3, Issue. 3, May-2013.

Amrita Singh is a pursuing M.Tech in Computer Science and Engineering from Invertis University Bareilly. Her Research interest area is Software Engineering. Email-amritas054@gmail.com

Er. Anil Pandey is an Assistant Professor of Computer Science and Engineering from Invertis University Bareilly. His Research area is Software Engineering. Email-anil.p@invertis.org

Hardware implementation of Airway pressure Monitoring system

Dr. Sunil Kumar Singla

Abstract: Pressure is one of the important parameters to be monitored and controlled in many situations such as in anesthesia ventilator. During the time of acute illness or indisposed state the human body is unable to follow the natural respiration process and thus compelled to undergo some artificial way of respiration. The exact amount of air is required during this respiration process. Thus the controlling and monitoring the airway pressure becomes very important. In this paper hardware implementation of airway pressure monitoring system of a ventilator has been discussed.

Keywords: **About four key words or phrases in alphabetical order, separated by commas.**

I. INTRODUCTION

Pressure is defined as force per unit area exerted by a fluid on the surface of the container. Absolute pressure is the fluid pressure above the reference value of a perfect vacuum or the absolute zero pressure. Gauge pressure represents the value of pressure above the reference value of the atmospheric pressure[1]. Pressure has several units such as centimeter of water, mm of Hg., N/m^2 , psi, etc. The relation between the different units is expressed as :

760 mm of Hg. = 101325 N/m^2 = 14.696 psi = 1041.30 cm of water

In the volume limited ventilators, the airway pressure differs from person to person depending upon the lung compliance and the air way resistance of the individual. Airway pressure is a very important parameter, as by observing its display the anesthesiologist can manually control the air way pressure to reach its maximum level. It also helps in calculating the other ventilatory parameters such as lung compliance and airway resistance.

The other advantages of measuring and displaying airway pressure are that it helps in monitoring the functions such as disconnection in the system, unrecognized leaks in the ventilator circuit etc. A sudden marked reduction in the airway pressure is an indication of leakage in the ventilator circuit. At the same time, a reduction in the airway pressure to the level of atmospheric pressure would indicate the disconnection of the device.

Dr. Sunil Kumar Singla is with Electrical and Instrumentation Engineering Department Thapar University Patiala, Email: sunilksingla2001@gmail.com

II. DESIGN REQUIREMENTS

The various requirements for the design of airway pressure monitoring system are:

Pressure range = 0to +120 cm of water
Response time of sensor = 10 ms
Resolution = 5 cm of water, for graphic display
Time period = 1 to 15 sec.
Display = Graphic
Function = Arbitrary

III. HARDWARE DETAILS OF DISPLAY SYSTEM

The block diagram used to display airway pressure of anesthesia ventilator is shown in Fig. 1. The detail of its various components is given below:

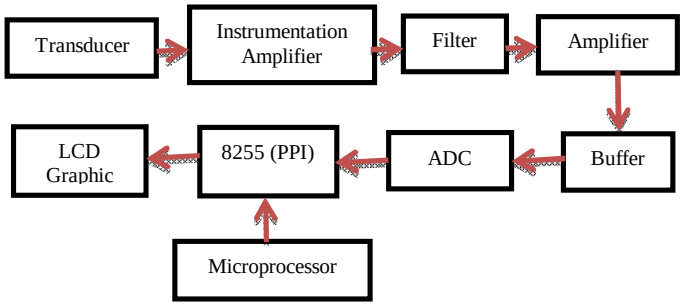

Fig. 1 Block diagram of Airway pressure monitoring system

A. Transducer

Trans

Transducer is the front end device which comes directly in contact with the quantity to be measured [2]. In ventilator display system, the choice of the transducer / sensor to measure the airway pressure, is very critical. Despite being capable of measuring the required pressure in the range of 0 to 1.71 psig or 0 to + 120 cm of water and having the required response time of 10 ms the transducer should have the properties of accuracy, high output, repeatability, long term stability, high input impedance, linearity, negligible hysteresis, temp. compensation, small size, etc.

The transducer should be chosen on the basis of its characteristics of stability, repeatability and response time, although it may give low electric output. One can have other transducers which may give higher output in volts, but they may have less stability of the order of ± 1% of FSO and repeatability of the order of ± 0.5 % of FSO. No doubt we need high output but the compromise cannot be made at the cost of stability and repeatability. Secondly, we can afford to have low electrical signal as it can easily be processed further.

B. Instrumentation amplifier

The output signal obtained from the transducer is of very low magnitude (from 0 to 17 mV). We thus need some amplification for its further processing. In case of precise low-level signal amplification where low noise, low thermal and time drifts, high input impedance and accurate closed loop gain are required the instrumentation amplifier is employed for the purpose of signal amplification [3]. In addition to the above, low power consumption, high common mode rejection ratio and high slew rate are the other features of an instrumentation amplifier. Circuit diagram of an instrumentation amplifier is shown in figure 2. There are two stages in an instrumentation amplifier. The first stage consists of two matched Op-Amps and offers very high input impedance to both the input signals. This stage also allows to set the gain. The input signals are applied to the non- inverting terminals of both the input Op-Amps as shown in Fig. 2. The second stage consists of only one Op-Amp. It is used as a differential amplifier with negative feedback.

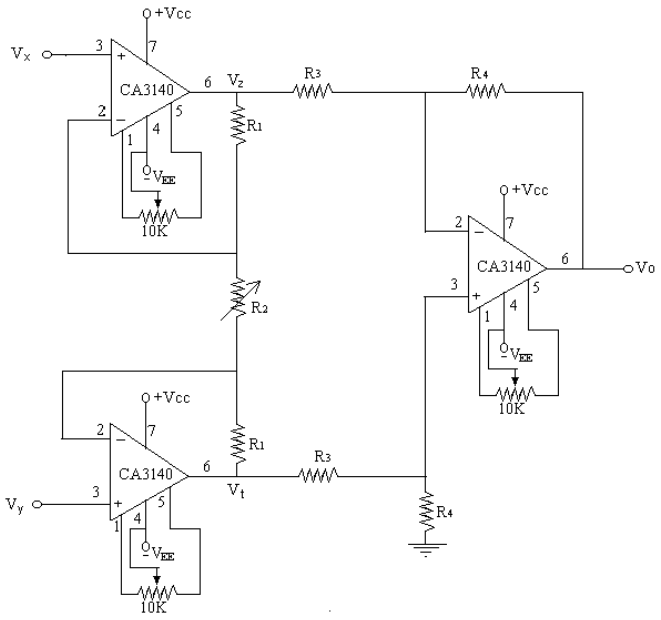

Fig. 2 Circuit diagram of an instrumentation amplifier[3]

The output of the operational amplifier is

$$V_o = \frac{R_4}{R_2}\left[\frac{R_2 + 2R_1}{R_2}\right](V_y - V_x)$$

B.1 Specifications

Input signal = 0-17 mV
Output signal required = 0 – 1.25V
Gain required = output/ input = 73

B.2 Design of instrumentation amplifier

Since we require a gain of 73 ,so

$$\frac{R_4}{R_2}\left[\frac{R_2+2R_1}{R_2}\right] = 73$$

Taking $R_4 = 100K$
& $R_3 = 10K$
We get , $\frac{R_4}{R_3} = 10$

Additional gain of 7.3 is to be provided by $\left[\frac{R_2+2R_1}{R_2}\right]$

Taking $R_1 = 27K$ then
$R_2 = 8.57$ K

But a potentiometer (POT) of 20K has been used in order to have the flexibility in the design to achieve the required gain. In order to remove the offset a 10K POT is placed between pin No. 1 and pin No. 5 of each Op-amp and negative supply for the POT is taken from pin No. 4 is applied as shown in Fig 2.

C. Filter Stage

Filter is a device used to separate out the signals of undesired frequencies and to allow the signal of certain desired frequencies to pass [2]. In the present case time period of signal is 1 to 15 sec, so, maximum frequency of signal = 1 Hz. Thus, a low pass filter is required which will allow the signal of low frequencies to pass. So in this design active low pass filter with cut-off frequency of 20 Hz has been used. Fig. 3 shows the circuit diagram of the filter. The cut-off frequency (f_H) at which the gain of the filter rolls off at the rate of –40 dB / decade is

$$f_H = \frac{1}{2\pi\sqrt{R_1 R_3 C_2 C_3}}$$

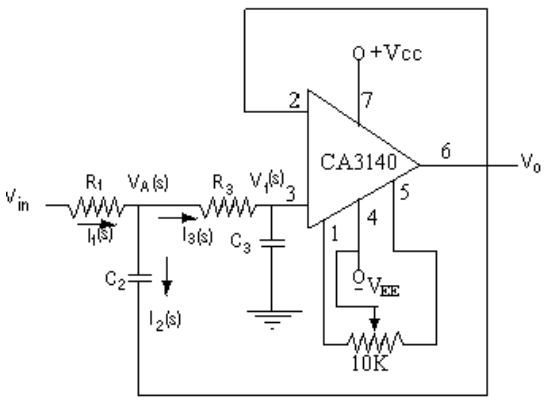

Fig.3 Circuit diagram of the Filter [2]

C.1 Filter design

Higher cut-off frequency f_H = 20 Hz
Taking $R_1 = R_3 = 20$ K
& $C_2 = 2C_3$
Design equation:

$$f_H = \frac{1}{2\pi\sqrt{R_1 R_3 C_2 C_3}}$$

Substituting the values R_1, R_3, C_2 & f_H we get
$C_3 = 0.28\ \mu F$ and $C_2 = 0.56\mu F$

D. Buffer Amplifier

It is a unity gain amplifier also known as voltage follower. The circuit shown in figure 4 has a unity gain and very high input impedance. The input impedance is essentially the input impedance of the operational amplifier itself, which is about 0.5 tetra Ohm for CA3140. The output voltage is equal to the input voltage. In fact, the output voltage tracks the input voltage from positive to negative saturation. Current output is limited to the short circuit current of the operational amplifier and the output impedance is small, typically less than 100 Ohm.

The buffer amplifier is essentially an impedance matching device, which converts a voltage at high impedance to the same voltage at low impedance. The use of unity gain buffer amplifier reduces the loading effect in the measurement system.

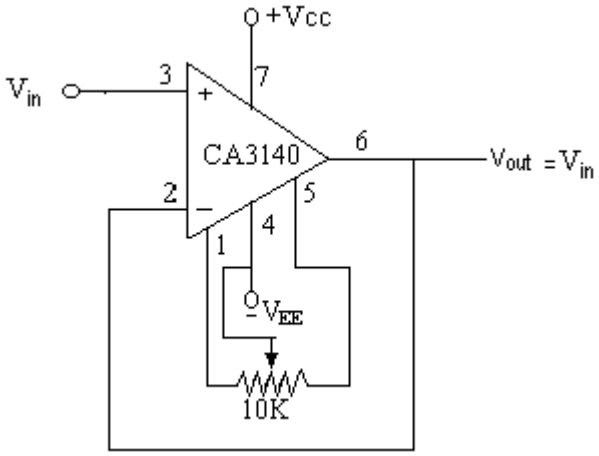

Fig.4 Circuit diagram of buffer amplifier [3]

E. Amplifier stage

The output signal of the instrumentation amplifier is in the range of 0 to 1.25 volts, for the full range of the pressure from 0 to +120 cm of H_2O. In order to have the signal of high magnitude we need to amplify this signal. Since, we are using the ADC 0808, which works satisfactorily in range up to 5 volts, we can amplify the signal by the factor of four. The operational amplifier in the non-inverting mode with feedback registers can be used for this purpose. The circuit diagram of operational amplifier in the non-inverting mode with feedback registers is shown in Fig. 5.

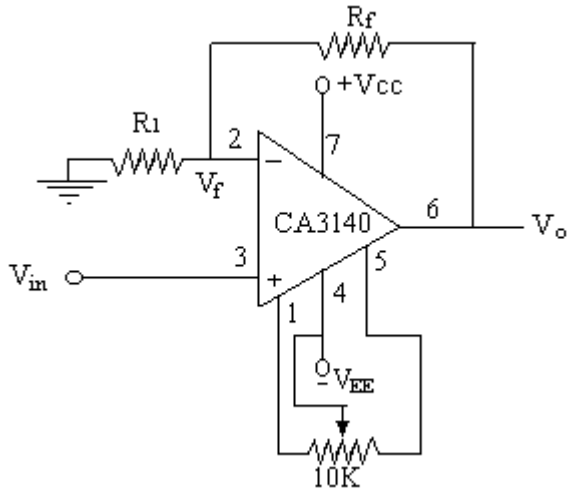

Fig. 5 Circuit diagram of non-inverting amplifier[3]

Output signal required = 5 V
Input signal to amplifier = 1.25 V
Gain required = 4

So $$\left[1 + \frac{R_f}{R_1}\right] = 4$$

Taking R_1 = 10 K
R_f = 30 K

F. Programmable peripheral Interface (8255)

8255 is a programmable input-output device. It can be programmed to transfer data under various conditions from simple input-output to interrupt input-output. The 8255 has 24 input-output pins, which are divided into three ports of 8 pins each named port A, port B, and port C. Port A and port B bits can only be used in a group but the port C bits can be used as individual bits or can be grouped into four bit ports, C_{upper} and C_{lower} [4], [5].

G. Analog to digital converter (ADC)

The ADC 0808 is a 8-bit successive approximation analog to digital converter having 8-channel multiplexer and microprocessor compatible control logic. The 8-channel multiplexer can directly access any of the 8 single-ended analog signals. The ADC 0808 offers high speed, high accuracy, minimal temperature dependence, excellent long term stability and accuracy and consumes minimal power. It is a 28pin module having 8 pins (1 to 5 and 26 to 28) for the 8 channels [4]-[6]. The clock frequency is applied at pin no. 10 The clock frequency may vary from 10 Hz to 1280 kHz. Pin no. 6 is the start of conversion pin. When signal is applied to this pin, conversion starts and at the completion of the conversion pin no. 7 generates the signal giving indication of end of conversion. In order to have continuous conversion the start of conversion pin is connected directly to the end of conversion pin no.7. The pins numbering from 23 to 25 are used for the selection of the input channels. Pin no.

16 is the Ref. (-ve) pin which is connected to the ground. The voltage applied to the Ref. (+ve) pin number 12 is 5 V_{dc} and should be precise.

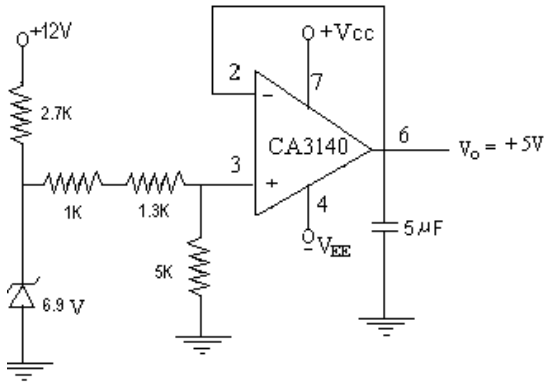

Fig.6 Circuit for obtaining precise reference voltage

The circuit shown in Fig.6 is a voltage stabilizing circuit, which will produce a precise +5V output voltage. The zener diode is of 6.9 V. When a voltage of +12V is applied as shown in the diagram, the voltage appearing at the non-inverting terminal of Op-Amp is +5V.

H. Oriole graphics LCD module

Oriole Graphics LCD module consists of LCD panel with CMOS LSIs for LCD driving. Since these modules have a full dot matrix graphic display, it is possible to display graphic as well as characters [7]. LCD Module 24064S has 240 X 64 dots.

The schematic diagram for interfacing the ADC and OGM LCD with the microprocessor is shown in Fig. 7

.

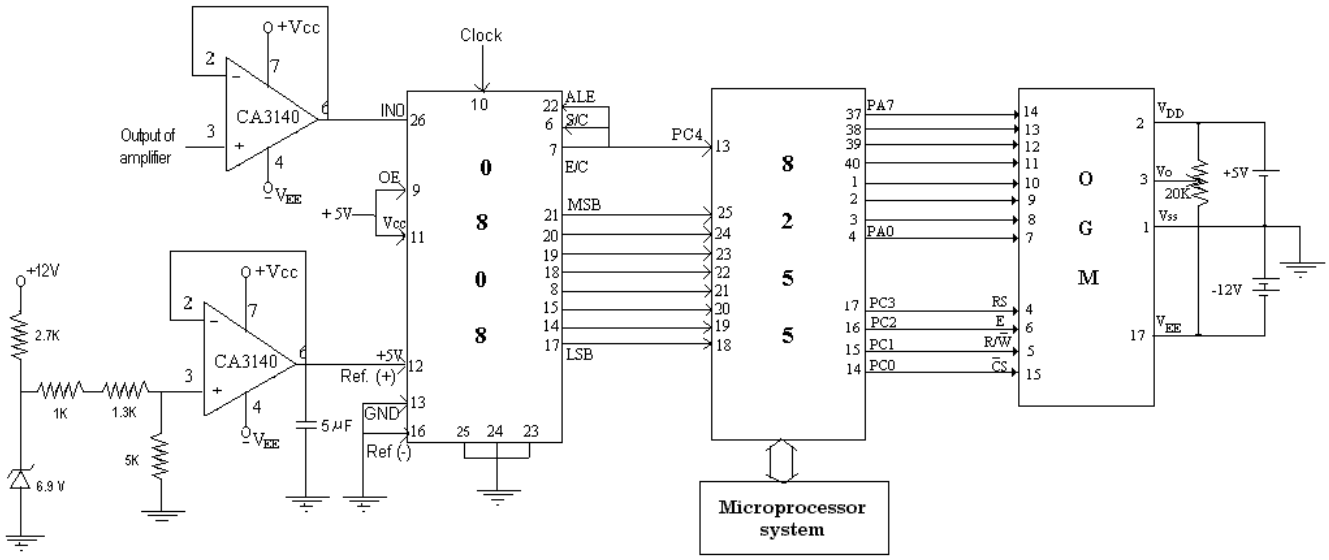

Fig.7 Schematic diagram for interfacing the ADC and OGM LCD with the microprocessor system

IV. CONCLUSION

Airway pressure remains a critical parameter to be monitored during the process of artificial respiration. In this paper a hardware implementation of the airway pressure monitoring system with all its practical aspects has been discussed. The system has been developed for a pressure range of 0 to +120 cm of water with a response time of 10 ms and resolution of 5 cm of water.

REFERENCES

[1]. A K Sawhney, and Puneet Sawhney, Mechanical Measurements, Dhanpat Rai & Sons, New Delhi.

[2]. A K Shanwey, Electrical and electronic instrumentation, Dhanpat Rai & Sons, New Delhi.

[3]. Ramakant A Gayakward, (1995), Op-Amps. and linear integrated circuits, Prentice Hall of India Pvt. Ltd., New Delhi.

[4]. B Ram, (1996), Fundamentals of microprocessor and microcomputers, Dhanpat Rai & Sons, New Delhi.

[5]. Ramesh S Ganokar, Microprocessor architecture programming and applications, Wiley Eastern Ltd.,

[6]. http://www.ti.com/lit/ds/symlink/adc0808-n.pdf

[7]. http://www.docstoc.com/docs/96723106/ProjectReport1doc---Dept-of- EE_-IIT-Bombay

***Dr. Sunil Kumar Singla**: Born on Nov 3, 1976 in India. He did hisgraduation (with honors) in Intrumentation Engg from SLIET,Longowal, India in 1998. He did his post graduation Ininstrumentation and control from NITTTR (formally TTTI)Chandigarh in 2000. He did his Ph.D. in the field of Biometrics from Thapar University Patiala, India in 2011.He has 18 papers in various international and national journals of repute. Dr. Singla has 10 papers in various national and international conferences to his credit. His areas of interest are image processing, biometrics andVirtual Instrumentation.*

A Novel Method of Measuring Soil Moisture

Shrota Sengupta, Partha Protim Neog, Jyoti Goutam Baruah, Jyoti Barman, Bikramjit Goswami

Abstract: This paper is a result of the experimental study of determining soil moisture using a moisture sensor circuit. The technique reviewed here involves the use of a simple oscillator circuit along with a capacitor and application of ANN for automatic detection and optimization. The sensor circuit was calibrated using low and high permittivity material i.e. dry soil and saturated soils respectively. The sensitivity of the circuit was also changed by changing the potentiometer value or capacitance value. The measurements obtained were recorded and used to train the ANN which could then be used to yield the output of the circuit for other input values. This proves to be a novel approach for measuring soil moisture using simple techniques, involving low cost.

Keywords: ANN, moisture sensor, Soil moisture, surface soil moisture.

I. INTRODUCTION

Soil moisture is difficult to define because it means different things in different disciplines. For example, a farmer's concept of soil moisture is different from that of a water resource manager or a weather forecaster. Generally, however, soil moisture is the water that is held in the spaces between soil particles. Surface soil moisture is the water that is in the upper 10 cm of soil, whereas root zone soil moisture is the water that is available to plants, which is generally considered to be in the upper 200 cm of soil[1].

Compared to other components of the hydrologic cycle, the volume of soil moisture is small; nonetheless, it of fundamental importance to many hydrological, biological and biogeochemical processes. Soil moisture information is valuable to a wide range of government agencies and private companies concerned with weather and climate, runoff potential and flood control, soil erosion and slope failure, reservoir management, geotechnical engineering, and water quality. Soil moisture is a key variable in controlling the exchange of water and heat energy between the land surface and the atmosphere through evaporation and plant transpiration. As a result, soil moisture plays an important role in the development of weather patterns and the production of precipitation. Simulations with numerical weather prediction models have shown that improved characterization of surface soil moisture, vegetation, and temperature can lead to significant forecast improvements.

Shrota Sengupta is pursuing B.Tech degree in Electrical and Electronics Engineering, DBCET, Assam. Email: shrota1989@gmail.com
Partha Protim Neog is pursuing B.Tech degree in Electrical and Electronics Engineering, DBCET, Assam. Email: parthappn1991@gmail.com
Jyoti Goutam Baruah is pursuing B.Tech degree in Electrical and Electronics Engineering, DBCET, Assam.
Jyoti Barman is working as assistant professor in Department of Electrical and Electronics Engineering, DBCET, Assam. Email: jyoti.barman@aol.in
Bikramjit Goswami is working as assistant professor in Department of Electrical and Electronics Engineering, DBCET, Assam.)

Soil moisture also strongly affects the amount of precipitation that runs off into nearby streams and rivers. Large-scale dry or wet surface regions have been observed to impart positive feedback on subsequent precipitation patterns, such as in the extreme conditions over the central U.S. during the 1988 drought and the 1993 floods. Soil moisture information can be used for reservoir management, early warning of droughts, irrigation scheduling, and crop yield forecasting.[4]

II. THEORETICAL BACKGROUND

Slope failures due to heavy rainfall occur frequently during the rainy season. Such slope failures are mainly caused by increasing soil mass and decreasing shear strength in the soil as a result of increased water content or groundwater levels. Thus, in addition to measuring the rainfall intensity on the ground surface, measuring the water content underground is also important to predict the possibility of slope failures due to rainfall. Conventional field-monitoring systems usually use a tensiometer or a permittivity soil moisture sensor to monitor the soil's moisture[7].

Moisture may also limit microbial activity in a wide range of environments including salt water, food, wood, biofilms, and soils. Low water availability can inhibit microbial activity by lowering intracellular water potential and thus reducing hydration and activity of enzymes. In solid matrices, low water content may also reduce microbial activity by restricting substrate supply. As pores within solid matrices drain and water films coating surfaces become thinner, diffusion path lengths become more tortuous, and the rate of substrate diffusion to microbial cells declines[8].

Soil Moisture Measurement has a few other applications:

- Irrigation and sprinkler systems.
- Moisture monitoring of bulk foods.
- Rain and weather monitoring.
- Environmental monitoring.
- Water conservation applications.
- Fluid level measurements[2].

The technique used in our experiment is illustrated by the following block diagram, shown in figure1.

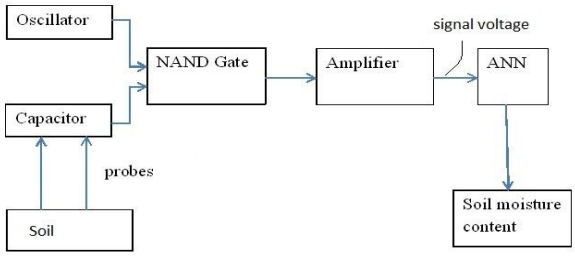

Figure1: Block diagram of soil moisture sensing technique

Here the input from the oscillator and probes via capacitor are fed to the NAND gate which is then given to the amplifier. When the soil moisture is low, the input from the oscillator cannot be diverted to the ground by the capacitor, but is rather fed to the NAND gate. However when moisture content is high, the supply is diverted to the ground. The amplifier further sends the amplified voltage signal to the ANN which then gives the final moisture content.

The circuit diagram used is shown below in figure2.

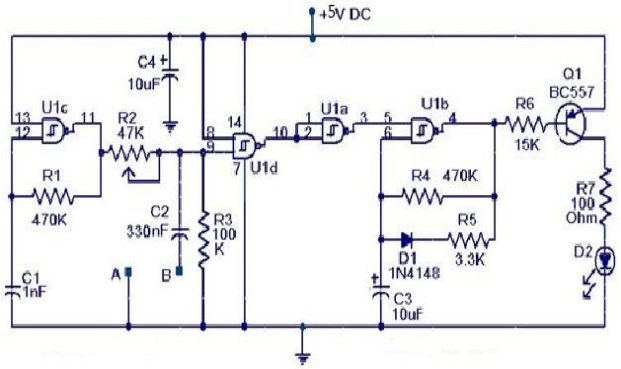

Figure2. Moisture Sensor Circuit.

III. CIRCUIT DESCRIPTION AND PROCEDURE

The U1C(NAND gate) and associated components are wired as an oscillator producing a 2KHz square wave. This square wave is given to one gate input of U1D via a variable potential divider former by R1 and R2.When the resistance across the probes A and B are low that is when soil moisture level is high, the C2 will divert the square wave to ground. The output of U1D will be high. The U1 A inverts this high state to low and so the IC U1B is blocked from producing oscillations. The LED will remain OFF. When there is no moisture across the probes, the C2 cannot bypass the 2KHz signal to the ground and it appears at the gate input of U1D.The output of U1D goes low, and it is inverted to high by U1A.The oscillator wired around U1B is activated and it starts oscillating. These oscillations are amplified by Q1 to drive the LED and LED starts pulsating as an indication of low moisture. Since square wave is used there won't be any oxidation on the probes. The resistor R7 limits the current through LED and ensures a longer battery life.

In order to calibrate the sensor circuit, a few experiments were performed with different sensitivities. The sensitivity of the circuit was varied by changing the values of its potentiometer or capacitor.

The experiment was conducted as follows:

a. A pot was filled with 5kg of completely dry garden soil.
b. The potentiometer of the circuit was set at different values and a supply voltage was given to the circuit.
c. The probes of a CRO were connected across the capacitor C_2.
d. The input probes of the circuit were then inserted in the soil pot and the voltage reading was taken from the CRO.
e. Water of a measured quantity was then added to the pot, mixed well (so as to have uniform moisture) and step(d) was repeated.
f. Steps(e) and (d) were repeated with different quantities of water.

The sensitivity of the set-up was found to be satisfactory after the tests.

IV. RESULTS AND DISCUSSIONS

Experiments were performed on the moisture sensing set-up shown in figure2 with a supply voltage of 4.5V. the resistor(pot) R_2 was set at 34kΩ. When the input probes were kept in air, the voltage across the capacitor was found to be 3.4V. Further the probes were inserted in dry soil. Then measured quantities of water were added to the soil, ranging from (0-84)mL/kg and the corresponding readings were noted as shown below in table1.

Table1

Water(ml/kg)	Output(V)
0(air)	3.4
0(soil)	3.2
1.5	3
6	2.8
12	2.6
18	2.3
24	1.8
30	1.6
36	1.1
42	0.9
54	0.8
66	0.5
78	0.2
84	0

With the data shown in table1 a curve was obtained for soil moisture versus output voltage.

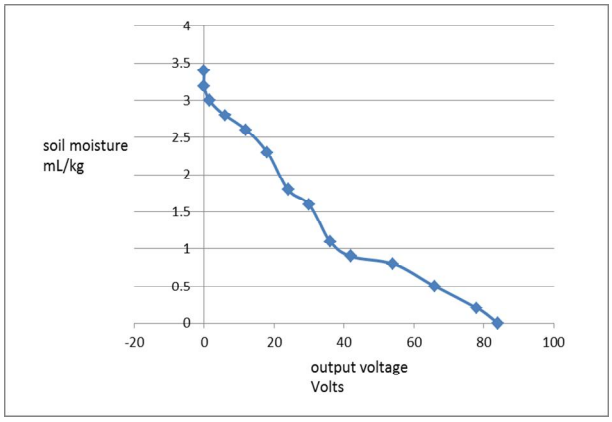

Figure3. Soil moisture versus output voltage plot.

The plot shows an exponential curve which can be defined by the equation(1) shown below.

$$y = -0.0391x + 2.9902 \quad \ldots\ldots(1)$$

Again, with the set-up shown in figure2 another experiment was conducted but with the following modifications:

- Supply voltage=5V
- Resistor(pot)R_2=24kΩ.

Likewise, the probes were inserted in soil and measured quantities of water, ranging from (0-65.7)mL/kg were added to it and the corresponding readings noted as shown below in table2.

Table2

Water(ml/kg)	Output(V)
0	4
4.2	3.5
8.57	3
12.85	2.6
18.57	2.2
27.14	1.5
35.7	1.1
44.29	0.7
52.86	0.4
61.43	0.2
65.7	0

With the data shown in table2 a curve was obtained for soil moisture versus output voltage.

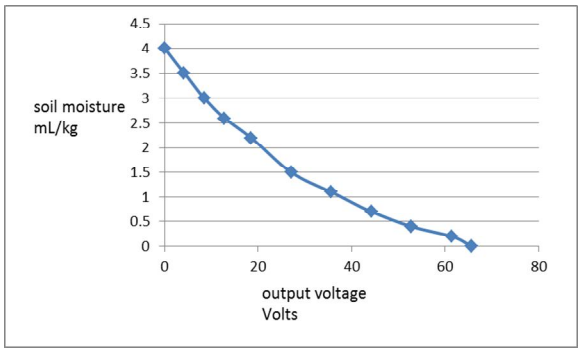

Figure4. Soil moisture versus output voltage plot.

The plot shows an exponential curve which can be defined by the equation(2) shown below.

y = -0.0583x + 3.5001
…….(2)

Again, with the set-up shown in figure2 another experiment was conducted but with the following modifications:

- Resistor(pot)R_2=35kΩ
- Capacitor(C_2)=183nF(approx)

The probes were inserted in soil and measured quantities of water, ranging from (0-64.29)mL/kg were added to it and the corresponding readings noted as shown below in table3.

Table3

Water(ml/kg)	Output(V)
0	4
8.57	3
17.14	2.8
25.7	2.2
34.26	1.2
42.86	0.8
51.43	0.4
60	0.15
64.29	0

With the data shown in table3 a curve was obtained for soil moisture versus output voltage.

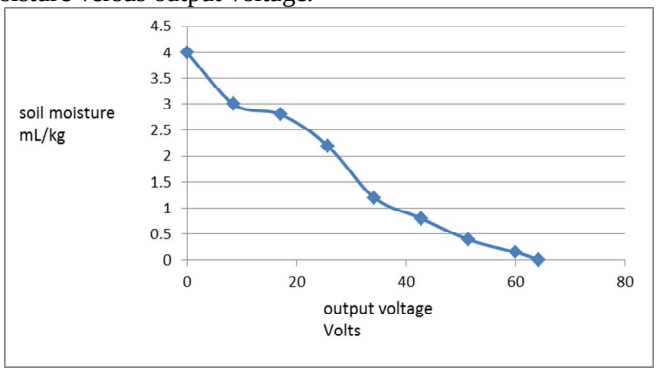

Figure5. Soil moisture versus output voltage plot.

The plot show exponential curve which can be defined by the equation(3) shown below.

. y = -0.0621x + 3.7168 ……..(3)

The voltage output shows the corresponding change in voltage for change in the moisture content of the soil. The more is the moisture level, the lesser the voltage across the capacitor.

The values of the above experiments were fed to the ANN program to train it. Hence the output of the intermediate values could be found out using the program. A few such outputs are shown below:

i. for Voltage=1.3V
water content=211.29mL/kg
ii. for Voltage=2.5V
water content=70.74mL/kg

V. CONCLUSION

The results found in the above experiments could be used in calibrating voltmeters to give the soil moisture content.

This study can be very useful in the following aspects:

- Determine need for irrigation.
- Determine growing conditions for trees, turf and plants anywhere.
- Determine soil moisture percentage for geotechnical and civil engineering purposes[2].

ACKNOWLEDGMENT

This paper could not be written to its fullest without Sri Jyoti Barman of the Department of Electrical and Electronics, who served as our guide, as well as one who encouraged us throughout the time spent studying under him. We are heartily thankful to him. Besides, we would definitely like to thank Sri Bikramjit Goswami, of the same department who boosted us morally and provided us with useful and informative resources.

REFERENCES

[1] Karim, Bin Ismail,"Soil moisture detection using Electrical Capacitance Tomography (ECT) sensor."
[2] "Soil Moisture Measurements",www.eijkelkamp.com.
[3] Collins, J.E. 1987. Soil moisture regimes of rangelands: using datapods to record soil moisture. International Conference on Measurement of Soil and Plant Water Status. Centennial of Utah State University.
[4] Stafford, J.V. 1988. Remote, non-contact and in-situ measurement of soil moisture content: a review. J. Ag. Eng. Res.
[5] Price, R.R., Ximing Huang and L.D. Gaultney. 1990. Development of a soil moisture sensor. Paper No. 90-3555, ASAE, St. Joseph, MI 49058.
[6] Katsuhiko Tanaka, Makoto Shimamura, Asako Togari, Takefumi Suda, Kazuhiro Hirai,Kazunari Sako, Ryoichi Fuakgawa Ritsumeikan University Kusatsu, Japan," Monitoring of Soil Moisture and Groundwater Levels Using Ultrasonic Waves to Predict Slope Failures".
[7] John M. Stark1 and Mary K. Firestone,"Mechanisms for soil moisture effects on activity of nitrifying bacteria", Applied and Environmental Microbiology, Jan. 1995, P. 218–221
[8] K. Tanaka, T. Suda, K. Hirai, K. Sako, and R. Fukagawa,"Monitoring of Soil Moisture and Groundwater Level Using Ultrasonic Waves to Predict Slope Failures," Japan. J. Appl. Phys. (in Press).
[9] S. O. Kasap, D. Lakhanpal, C. Patzer, T. Mandziak, and D. G. Fredlund, Ultrasonics, Vol. 32, 379, 1994.
[10] Y. Taneda, M. Tomita, A. Kawabata, and T. Shiozaki: Transactions of the Japanese Society of Irrigation, Drainage and Reclamation Engineering (Nogyo Doboku Gakkaishi), 46, 1974 (in Japanese).
[11] T. Suzuki, S. Kagawa, and T. Uchimura, "Investigation of moisture contents in slope ground by change in wave velocity," Proc. the 43th
[12] Conf. on Geotechnical Engineering, 2008, 972, 1943 (in Japanese).

Shrota Sengupta was born in Dibrugarh ,India, in 1989. She is currently pursuing the B.Tech degree in Electrical and Electronics Engineering from Don Bosco College of Engineering and Technology.

Her research interests include methods of soil moisture measurement.

Partha Protim Neog was born in Jorhat, India in 1991. He is currently pursuing te B.tech degree in Electrical and Electronics Engineering from Don Bosco college of Engineering and Technology.

His research interests include methods of soil moisture measurements.

Jyoti Goutam Baruah was born in Jorhat, India in 1989. He is currently pursuing te B.tech degree in Electrical and Electronics Engineering from Don Bosco college of Engineering and Technology.

His research interests include methods of soil moisture measurements.

Jyoti Barman was born in Guwahati, India in 1987. He received the B.E degree in Instrumentation Engineering from Assam Engineering College in 2009.

His research interests include study of different sensors, data acquisition System, Wireless sensor network.

Bikramjit Goswami was born in Guwahati, india in 1981. He received the B.E degree in Electrical Engineering from Assam Engineering College in 2003 and the M.Tech degree in Electronics and Communication Technology from Guwahati University in 2012. He is currently pursuing his Ph.D. degree at Assam DonBosco University.

His research interests include development of reconfigurable antenna design using ANN, optical sensing and detaction of bio medical and environmental entities and Microwave remote sensing.

Automatic License Plate Recognition Using Computer Vision for Door Opening

P. Jayalakshmi and Mr. T. Rajesh Kumar

***Abstract* – Sliding window analysis basically used in image processing applications. RUCV technology is used to identify the license plate number of vehicles. It is difficult to detect the alpha numeric characters and numbers from a car image. This paper proposes the system of identifying license plate numbers of Indian cars. It ties to recognize the entry of authorized and unauthorized vehicles. The system can be implemented in apartments for safety purpose. The proposed algorithm consists of three major parts vehicle detection, number plate identification, character recognition, vehicle arrival time. The system is implemented using Mat lab.**

***Index Terms* - Edge detection, Median filter, Template matching.**

I. INTRODUCTION

The growth of technology is increasing day by day to fulfill the human needs. The proposed system is implemented to make human work easier. RUCV is an image processing technology which uses license plate to identify the authorized vehicle license plate number and alpha numeric characters. The objective is to design an efficient automatic authorized vehicle identification system by using the vehicle license plate. The system can be implemented in apartments. The alpha numeric characters are recognized by using template matching. The resulting data is then used to compare template so as to come up with the specific information like the vehicle's owner, license plate number and time of arrival, etc.

Edges typically occur on the boundary between two different regions in an image. Various physical events cause intensity changes such as geometric events and non geometric events. There are several classical edge detection techniques such a Roberts, Prewitt, Sobel and Canny. By using these techniques the longer edges are not accurately detected.

To overcome these issues medfilt2 filter is used to remove the salt and pepper noise. A median filter is more effective than convolution when the goal is to simultaneously reduce noise and preserve edges. Global threshold that can be used to convert the intensity image in to a binary image.

In this paper, several LPR methods have been examined to assess their license plate number and more robust to classify the white and yellow colored plates. Finally it detects the nature the number.

P. Jayalakshmi and Mr. T. Rajesh Kumar are with *Department of Electrical and Electronics Engineering Easwari Engineering College, Chennai, Email:* jayalakshmi3@yahoo.com

II. RELATED WORK

Several approaches have been proposed in literature for vehicle license plate recognition. Most algorithms in literature deal with the recognition problem in two separate stages: license plate detection for finding the location of the plate, and license plate recognition for extracting and recognizing the individual characters.

Rob G. J. Wijnhoven, Member, IEEE and Peter H. N. de with, Fellow [1] have proposed the Automatic garage door opening is typically implemented by use of a radio receiver and transmitter. When arriving in the neighborhood of the garage, the user presses a button on the transmitter and a radio signal is sent to the receiver inside the garage. The receiver then verifies the signal and opens the garage door. Multiple persons can make use of this system by configuring multiple radio transmitters. The use of such a system poses a security issue, which evolves from many possible situations that finally lead to unauthorized access. For example, the radio transmitter can be stolen or lost, the radio code can be captured and reproduced with a specialized receiver, or codes can be tested within a certain neighborhood to find matching locations.

Christos Nikolaos E. Anagnostopoulos [2] have proposed, a new algorithm for vehicle license plate identification is proposed, on the basis of a novel adaptive image segmentation technique (sliding concentric windows) and connected component analysis in conjunction with a character
recognition neural network.

The algorithm was tested with 1334 natural-scene gray-level vehicle images of different backgrounds and ambient illumination. The camera focused in the plate, while the angle of view and the distance from the vehicle varied according to the experimental setup.

S. Chang, L. Chen, Y. Chung and S. Chen [3] have proposed the Automatic license plate recognition (LPR) plays an important role in numerous applications and a number of Techniques have been proposed. However, most of them worked under restricted conditions, such as fixed illumination, limited vehicle speed, designated routes, and stationary backgrounds. In this study, as few constraints as possible on the working environment are considered. The proposed LPR technique consists of two main modules: a license plate locating module and a license number identification module. Christos-Nikolaos E. Anagnostopoulos [4] have proposed the License plate recognition (LPR) algorithms in images or videos are

generally composed of the following three processing steps: 1) extraction of a license plate region; 2) segmentation of the plate characters; and 3) recognition of each character. This task is quite challenging due to the diversity of plate formats and the non uniform outdoor illumination conditions during image acquisition.

Section I of this paper is a background introduction. Section II discusses a brief literature review of License plate recognition. Section III describes the complete system in the form of a block diagram. Section IV describes the experimental results. Concluding remarks and a scope for further research are given in Section VII.

III. PROPOSED SYSTEM

This system consists of edge detection algorithm which is used to find the longer edges in license plate. Fig.1 represents the functional architecture of the proposed system.

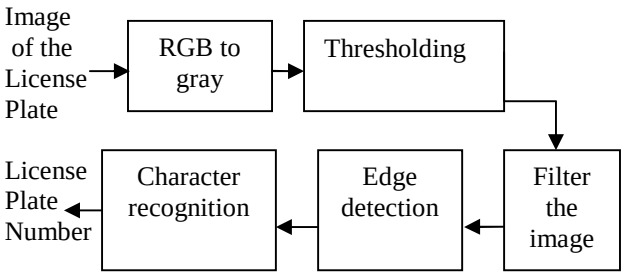

Fig. 1 Functional architecture

First, the image of the license plate is given to the RGB block it convert the RGB image in to gray scale image. Second, the output from the RGB block of gray scale image is given to the median filter block which is used to remove the noise of an image. Third, the filtered image is given to the edge detection block. Finally, recognition of license plate number using templates matching.

A. RGB to gray scale conversion

I = rgb2gray(RGB) converts the true colour image RGB to the gray scale intensity image I. rgb2gray converts RGB images to gray scale by eliminating the hue and saturation information while retaining the luminance.newmap = rgb2gray(map) returns a gray scale colour map equivalent to map.

The input is an RGB image, it can be of class uint8, uint16, single, or double. The output image I is of the same class as the input image. If the input is a colour map, the input and output colour maps are both of class double.

B. Thresholding the image

Level = gray thresh (I) computes a global threshold (level) that can be used to convert an intensity image to a binary image with im2bw. Level is a normalized intensity value that lies in the range [0, 1].The gray thresh function uses Otsu's method, which chooses the threshold to minimize the intra class variance of the black and white pixels. Multidimensional arrays are converted automatically to 2-D arrays using reshape. The gray thresh function ignores any nonzero imaginary part of I. Level EM] = gray thresh (I) returns the effectiveness metric, EM, as the second output argument. The effectiveness metric is a value in the range [0 1] that indicates the effectiveness of the thresholding of the input image. The lower bound is attainable only by images having a single gray level, and the upper bound is attainable only by two-valued images.

C. Filtering the image

Median filtering is a nonlinear operation often used in image processing to reduce "salt and pepper" noise. A median filter is more effective than convolution when the goal is to simultaneously reduce noise and preserve edges. B=medfilt2(A, [m n]) performs median filtering of the matrix A in two dimensions. Each output pixel contains the median value in the m-by-n neighborhood around the corresponding pixel in the input image. medfilt2 pads the image with 0's on the edges, so the median values for the points within [m n]/2 of the edges might appear distorted. B = medfilt2(A) performs median filtering of the matrix A using the default 3-by-3 neighborhood. B = medfilt2(A, 'indexed',...) processes A as an indexed image, padding with 0's if the class of A is uint8, or 1's if the class of A is double.

D. Sobel edge detection

There are several conventional edge detection methods in image processing. They are Prewitt edge detection, Roberts edge detection, Sobel edge detection, Canny edge detection. The Sobel operator performs a 2-D spatial gradient measurement on an image and so emphasizes regions of high spatial frequency that correspond to edges. Typically it is used to find the approximate absolute gradient magnitude at each point in an input grayscale image.
The Sobel operator is slower but its larger convolution kernel smooth's the input image to a greater extent and so makes the operator less sensitive to noise. The operator also generally produces considerably higher output values for similar edges, compared with the Roberts Cross.

E. Character recognition

The vehicle can be classified based on the number plate color. If it is yellow background the number plate can be classified as a commercial vehicle. If it is white background the number plate can be classified as a private vehicle. Fig 2and 3 shows the templates of both number and alpha characters

Fig. 2 Templates for the number character recognition.

Fig. 3 Templates for the alpha numeric character recognition.

F. Stochastic gradient descent (SGD)

In addition to performing linear classification, SVMs can efficiently perform non-linear classification using what is called the kernel trick, implicitly mapping their inputs into high-dimensional feature spaces. Most of these algorithms use either Variants of primal stochastic gradient descent (SGD), Quadratic programming in the dual. In gradient descent, we compute the gradient using the entire training set. A superficially simple alteration of this is to find the gradient with respect to a single randomly chosen example. This technique is called stochastic gradient descent (SGD). By using only a single example we are only getting an approximation to the true gradient; therefore, we are no longer guaranteed to move in the direction of greatest descent. Nonetheless, there are at least two important reasons why stochastic gradient descent is useful for learning problems: It is significantly quicker than gradient descent when n is large, and It can be shown that stochastic gradient descent minimizes the generalization error quicker than gradient descent.

IV. EXPERIMENTS AND RESULTS

In this section experimental results are made to identify the license plate number. The result analysis for different types of Indian license plate are shown in Fig. 4.

(a) Black on yellow

(b) black on white

(c) Extracted number

Fig. 4 Indian license plates.

V. CONCLUSION AND FUTURE WORK

In this paper, we proposed a RUCV system it is used to detect the Indian license plate number. The advantage of this method is to correctly recognize the authorized and unauthorized vehicle license plate number. In licese plate recognition the time consumption is less.

The future work of this paper we use a Wireless communication module which has a code word Embedded on it the code word is not changeable when the user enters the premises he just presses the button on which the Code word is sent to the Recognizer Module. The module then recognizes the number plate from the code word and checks the integrity of the number plate with that of the car and allows access to the car. For additional security, an alarm may be generated as soon as someone with a non-authorized car, but with the same plates appears.

REFERENCES

[1] Rob G. J. Wijnhoven, Member, IEEE and Peter H. N. de With, Fellow, IEEE "Identity verification using computer vision for automatic garage door opening," IEEE Transactions on Consumer Electronics, Vol. 57, No. 2, May 2011

[2] C. N. E. Anagnostopoulos, I. E. Anagnostopoulos, V. Loumos and E. Kayafas, "A License Plate-Recognition Algorithm For Intelligent Transportation System Applications", *IEEE Trans. on Intelligent Transportation Systems*, vol. 7, no. 3, pp. 377-392, Sept. 2006

[3] S. Chang, L. Chen, Y. Chung and S. Chen, "Automatic License Plate Recognition", *IEEE Transactions on Intelligent Transportation Systems*, vol. 5, no. 1, pp. 42-53, Mar. 2004

[4] Christos-Nikolaos E. Anagnostopoulos, *Member, IEEE*, Ioannis E. Anagnostopoulos, *Member, IEEE*, Ioannis D. Psoroulas, Vassili Loumos, *Member, IEEE*, and Eleftherios Kayafas, *Member, IEEE* "License Plate Recognition From Still Images and Video Sequences: A Survey", IEEE Trans. on intelligent Transportation systems, Vol. 9, No. 3, Sep 2008

[5] L. Dlagnekov and S. Belongie, "Recognizing Cars", Technical Report CS2005-083, UCSD CSE, 2005

[6] M. Donoser, C. Arth and H. Bischof, "Detecting, Tracking And Recognizing License Plates", *Lecture Notes in Computer Science, Asian Conference on Computer Vision (ACCV)*, vol. 4844, pp. 447-456, Tokyo, Japan, Nov. 2007

[7] J. J. Weinman, E. Learned-Miller and A. R. Hanson, "Scene Text Recognition Using Similarity And A Lexicon With Sparse Belief Propagation", *IEEE Transactions on Pattern Analysis and Machine Intelligence (PAMI)*, vol. 31, no. 10, pp. 1733-1746, Oct. 2009

[8] G. Csurka, C. R. Dance, L. Fan, J. Willamowski and C. Bray, "Visual Categorization With Bags Of Keypoints", *Proc. European Conference on Computer Vision (ECCV)*, Prague, Czech Republic, May 2004

[9] B. Leibe, A. Leonardis and B. Schiele, "Robust Object Detection With Interleaved Categorization And Segmentation", *International Journal of Computer Vision (IJCV)*, vol. 77, no. 1, pp. 259-289, May 2008

Jayalakshmi P was born in Perambalur, Tamil Nadu. She is currently pursuing the Master degree in Embedded System Technology at Easwari Engineering College under Anna University,Chennai. She received the Bachelor degree in Electronics And Communication Engineering at Srinivasan Engineering College under Anna University, Trichy , in 2011. Her research interests include computer vision with an emphasis on character recognition.

Rajesh kumar T was born in Tirunelveli, Tamil Nadu. . He received his Bachelor degree in Engineering during 1996 from Vinayaka Mission Kirupanandha Variyar Engineering College, Salem under Madras university and Masters degree in Computer Science and Engineering during 2004 from Manonmaniam Sundaranar University, Tirunelveli. He is currently pursuing the Doctoral degree programme under Anna University, Chennai in Faculty of Information and Communication Engineering from July 2011 onwards. His area of interest is Image/Speech Signal Processing and Embedded System. He has thirteen years of teaching experiences in various Engineering Colleges and two years of Industrial experiences. Currently he is working as Assistant Professor (Senior Grade) in Electronics and Communication Engineering Department. His work on authoring a book is in progress for Electronics and Microprocessors and Digital System Design. As far as the Professional memberships are concern, he is a life time member of ISTE and Indian Science Congress, Culcutta. He is an Associate Member in IEEE professional body. Motivating Students with Innovative Ideas in Technical field of Engineering is his axiom.

Hybrid Optimization Technique for Circuit Partitioning Using PSO and Genetic Algorithm

RAJDEEP SINGH, KUMARI KALPNA, DAWINDAR KUMAR MISHRA
rajdeep183@gmail.com, er.katoch@gmail.com, dawindarmishra@gmail.com

Abstract: ***In the partitioning main objective is to minimize the number of cuts. For this PSO algorithm is proposed for the optimization of VLSI interconnection (net list) bipartition. Meanwhile, the corresponding evaluation function and the operators of crossover and mutation are designed. The algorithm is implemented to test various benchmark circuits. Compared with the traditional genetic algorithm (GA) with the same evaluation function and the same genetic operators concerned the hybrid PSO and GA algorithm will give better results.***

Keywords: Partitioning, Particle Swarm optimization, Genetic Algorithm.

I. INTRODUCTION

Circuit partitioning/clustering is an important aspect of VLSI design. It consists of dividing a circuit into parts, each of which can be implemented as a separate component (e.g., a chip) that satisfies certain design constraints [1]. The limited area of a component forces the designer to lay out a circuit on several components. Since crossing components incurs relatively large delay, such a partitioning could greatly degrade the performance of a design if not done properly. There has been a large amount of work done in the area of circuit partitioning and clustering [2] [3]. In circuit partitioning, the circuit is divided into two (bi-partitioning) or more (multi-way partitioning) parts. In circuit clustering, the circuit is built up cluster by cluster. To partition designs of large size bottom-up clustering is often combined with top down partitioning. The classical objective of partitioning is to minimize the cut-size, i.e. number of nets spanning two or more parts .

The different objectives that may be satisfied by partitioning are:

The minimization of the number of cuts: The number of interconnections among partitions has to be minimized. Reducing the interconnections not only reduces the delay but also reduces the interface between the partitions making it easier for independent design and fabrication. It is also called the min cut problem.

To improve the fitness function is the objective of circuit partitioning. Fitness function denotes the improvement in the parameters of the circuit. The more is the fitness function the better is the result of partitioning. Area of each partition is also used as a constraint to reduce the fabrication cost with minimum area or as a balance constraint so that partitions are of almost equal size.

Number of partitions appears as a constraint as more number of partitions may ease the design but increase the cost of fabrication and number of interconnections between partitions .

II. CIRCUIT MINIMIZATION TECHNIQUES

Particle swarm optimization (PSO):

The basic idea of PSO stems from the behavior of birds, in which each particle or bird keeps track of its coordinates in the solution space which are associated with the best solution that is achieved so far by that particle is called as personal best position (p best) and the another best value obtained so far by any particle is called as global best position (g best). Each particle tries to modify its position using the concept of velocity. The salient features of PSO are:

1. PSO method is based on researches on swarms such as fish schooling and bird flocking.
2. It is a history based algorithm such that in each step the particles use their own behavior associated with the previous iterations.
3. It is easy to implement. Therefore the computation time is less.

GA (Genetic Algorithm):

All genetic algorithms work on a population or a collection of several alternative solutions to the given problem. Each individual in the population is called a string or chromosome, in analogy to chromosomes in natural systems. The population size determines the amount of information stored by the GA. The GA population is evolved over a number of generations. All information required for the creation of appearance and behavioral features of a living organism is contained in its chromosomes. GAs are two basic processes from evolution: inheritance, or the passing of features from one generation to the next, and competition, or survival of the fittest, which results in weeding out the bad features from individuals in the population. The objective of the GA is then to find an optimal solution to a problem .Since GA's are heuristic procedures, modeled as function optimizers, they are not guaranteed to find the optimum, but are able to find very good solutions for a wide range of problems [4].A GA based evolutionary approach for circuit partitioning giving a significant improvement in result quality. Comparative evaluation of genetic algorithm and simulated annealing was done with genetic algorithm giving better results [5] .A new hyper-graph partitioning algorithm was proposed.

Hybrid PSO and GA introduction:

Hybridization of evolutionary algorithms with local search has been investigated in many studies [6]. Such a hybrid model is often referred to as a mimetic algorithm. Two global optimization algorithms GA and PSO are combined. Since

PSO and GA both work with a population of solutions combining the searching abilities of both methods seems to be a good approach. Originally PSO works based on social adaptation of knowledge and all individuals are considered to be of the same generation. On the contrary, GA works based on evolution from generation to generation so the changes of individuals in a single generation are not considered [7]. Through GA & PSO have their specific advantage have their specific advantage when solving different algorithm, it is necessary to obtain both their individual feature by combining the two algorithms. The performance of algorithm is described as follow:

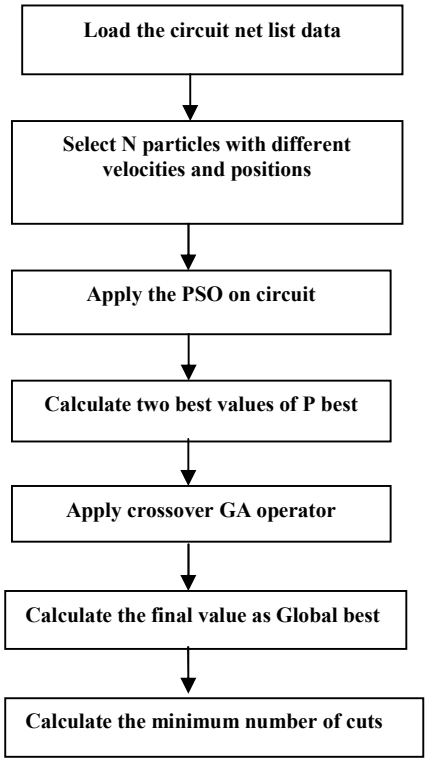

Figure: 1 Flowchart of Hybrid PSO_GA Algorithm

Table 1 Results of partitioning on different Netlists with Hybrid PS0 and Genetic Algorithms with different iterations:

Circuit Series of different net list	Number of Nodes	Number of netlists	Minimum cut
SPP N-65 Series	65	7	10.71
SPP N-70 Series	70	10	16.90
SPP N-75 Series	75	10	13.33
SPP N-80 Series	80	12	15.41
SPP N-85 Series	85	11	20.36
SPP N-90 Series	90	4	15.75
SPP N-95 Series	95	9	14.88

Table: 1 Results of partitioning with Hybrid PS0 and Genetic Algorithms with different iterations

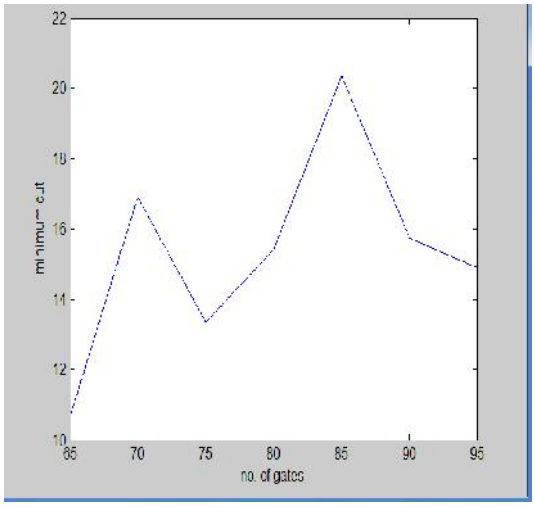

Figure: 2 . No. of Gates Vs. Minimum Cut.

III. RESULTS AND DISCUSSIONS

The Proposed Algorithm is tested on 07 netlists to demonstrate the effect of iteration by using hybrid PSO and GA algorithm on partitioning. The result of partitioning with PSO and GA is given in Table 1, here the number of particles are taken as 5. Fig 2 shows the plot between the no of gates and minimum cuts for the best of first 50 iteration. .

IV. CONCLUSION

In this Paper, Hybrid PSO and GA algorithm is applied to VLSI circuit partitioning problem. It is observed that by increasing in the number of iteration we can decrease the min. cut of the system. By applying the Hybrid PSO and GA algorithms to different netlist, we are getting better results in hybridization. So, by this paper, we have concluded that the

Hybrid PSO and GA method is better than any other optimization technique for minimizing the number of cuts in the different circuit series.

REFERENCES

[1] C.W.Yeh, C.-K.Cheng and T.T.Y. Lin, "Circuit clustering using a stochastic flow injection method," IEEE Trans. Computer-Aided Design, vol. 14, pp. 154–162, 1995.

[2] Naveed Sherwani, "Algorithms for VLSI Physical Design and Automation", third edition, Springer (India) Private Limited.

[3] J. Kennedy, R.C. Eberhart, "Particle Swarm Optimization Proc. IEEE Int. Conf. Neural Networks, Vol. 4, pp. 1942-1948 , 1995.

[4] Y. Shi, R. Eberhart, "A modified particle swarm optimizer", Proc. IEEE Int. Conf. Evol. Comput. Anchorage, AK, 1998, pp. 69-73, 1998.

[5] Kennedy, R.C. Eberhart, Y. Shi, "Comparison between genetic algorithms and particle swarm optimization", Proc. IEEE Int. Conf. Evol.Comput., Anchorage, pp. 611-616, 2001.

[6] Rehab F. Abdel-Kader," Genetically Improved PSO Algorithm for Efficient Data Clustering :Second International Conference on Machine Learning and Computing ,pp 71-75,201

[7] S. Naka , T. Yura, Y. Fukuyama, "A hybrid particle swarm optimization for distribution state estimation", IEEE Trans. on Power Systems, Vol.18, No. 1, pp. 60-68 , 2003.